National Library of Canada
Bibliothèque nationale du Canada

Canadian Theses Service
Service des thèses canadiennes

Ottawa, Canada
K1A 0N4

NOTICE

The quality of this microform is heavily dependent upon the quality of the original thesis submitted for microfilming. Every effort has been made to ensure the highest quality of reproduction possible.

If pages are missing, contact the university which granted the degree.

Some pages may have indistinct print especially if the original pages were typed with a poor typewriter ribbon or if the university sent us an inferior photocopy.

Reproduction in full or in part of this microform is governed by the Canadian Copyright Act, R.S.C. 1970, c. C-30, and subsequent amendments.

AVIS

La qualité de cette microforme dépend grandement de la qualité de la thèse soumise au microfilmage. Nous avons tout fait pour assurer une qualité supérieure de reproduction.

S'il manque des pages, veuillez communiquer avec l'université qui a conféré le grade.

La qualité d'impression de certaines pages peut laisser à désirer, surtout si les pages originales ont été dactylographiées à l'aide d'un ruban usé ou si l'université nous a fait parvenir une photocopie de qualité inférieure.

La reproduction, même partielle, de cette microforme est soumise à la Loi canadienne sur le droit d'auteur, SRC 1970, c. C-30, et ses amendements subséquents.

NL-339 (r. 88/04) c

Canada

National Library of Canada
Bibliothèque nationale du Canada

Canadian Theses Service
Service des thèses canadiennes

Ottawa Canada
K1A 0N4

The author has granted an irrevocable non-exclusive licence allowing the National Library of Canada to reproduce, loan, distribute or sell copies of his/her thesis by any means and in any form or format, making this thesis available to interested persons.

L'auteur a accordé une licence irrévocable et non exclusive permettant à la Bibliothèque nationale du Canada de reproduire, prêter, distribuer ou vendre des copies de sa thèse de quelque manière et sous quelque forme que ce soit pour mettre des exemplaires de cette thèse à la disposition des personnes intéressées.

The author retains ownership of the copyright in his/her thesis. Neither the thesis nor substantial extracts from it may be printed or otherwise reproduced without his/her permission.

L'auteur conserve la propriété du droit d'auteur qui protège sa thèse. Ni la thèse ni des extraits substantiels de celle-ci ne doivent être imprimés ou autrement reproduits sans son autorisation.

ISBN 0-315-55374-X

Canada

THE UNIVERSITY OF ALBERTA

HYDROPROCESSING OF GAS OIL FRACTIONS

by

LYLE TRYTTEN

(C)

A THESIS

SUBMITTED TO THE FACULTY OF GRADUATE STUDIES AND RESEARCH

IN PARTIAL FULFILLMENT OF THE REQUIREMENTS FOR THE DEGREE

OF MASTER OF SCIENCE

DEPARTMENT OF CHEMICAL ENGINEERING

EDMONTON, ALBERTA

FALL, 1989

The University of Alberta

Release Form

NAME OF AUTHOR: **LYLE TRYTTEN**

TITLE OF THESIS: **HYDROPROCESSING OF GAS OIL FRACTIONS**

DEGREE FOR WHICH THESIS WAS PRESENTED: **MASTER OF SCIENCE**

YEAR THIS DEGREE GRANTED: **FALL, 1989**

Permission is hereby granted to THE UNIVERSITY OF ALBERTA LIBRARY to reproduce single copies of this thesis and to lend or sell such copies for private, scholarly, or scientific research purposes only.

The author reserves other publication rights, and neither the thesis nor extensive extracts from it may be printed or otherwise reproduced without the author's written permission.

Signed: Lyle Trytten

Permanent Address:
#64-5215-110 St.
Edmonton, AB
T6H 3K1

DATE: July 7, 1989

THE UNIVERSITY OF ALBERTA

FACULTY OF GRADUATE STUDIES AND RESEARCH

The undersigned certify that they have read, and recommend to the Faculty of Graduate Studies and Research for acceptance, a thesis entitled HYDROPROCESSING OF GAS OIL FRACTIONS submitted by LYLE TRYTTEN in partial fulfillment of the requirements for the degree of MASTER OF SCIENCE.

M. R. Gray, Supervisor

P. J. Crickmore

N. O. Egiebor

E. C. Sanfotd

S. E. Wanke

Date: July 7, 1989

ABSTRACT

A heavy gas oil (SCGO) produced by thermal coking of Athabasca bitumen was fractionated into 6 narrow-boiling cuts of nominal 50°C width and a high-boiling residue. The 7 fractions were characterized using average molecular weight (AMW), density, boiling distribution, elemental analysis (EA) and structural group analysis (a technique for estimating the concentration profile of various structural groups based on data from EA, ^{1}H and ^{13}C NMR spectroscopy, infrared spectroscopy, and basic nitrogen analysis). The average molecular weights of the fractions ranged from 187 for the lightest fraction to 653 for the high–boiling residue. The feedstocks showed increasing contents of sulfur, nitrogen, oxygen, and aromatic carbon with increasing average molecular weight. Density also increased with molecular weight. The fraction of paraffinic carbon and the ratio of atomic hydrogen to carbon decreased with increasing average molecular weight, while the fraction of naphthenic carbon passed through a maximum at AMW = 230.

The six distillate fractions were catalytically hydroprocessed in a 150 mL CSTR with 8 g of a commercial Ni/Mo on γ–Al_2O_3 catalyst. The standard reaction temperature was 400°C for the four lightest fractions and 425°C for the two heavier fractions. The second and fifth fractions were hydroprocessed at two additional temperatures to allow determination of the apparent Arrhenius parameters. The products were characterized in a manner similar to the feedstocks.

Sulfur and nitrogen conversion decreased with increasing feed AMW, as did the reduction in aromatic carbon. Reduction in product AMW and thermal cracking (as evidenced by C–C bond breakage) increased with increasing feed AMW and reaction temperature. The apparent activation energies for hydrodesulfurization (HDS) and hydrodenitrogenation (HDN) increased with increasing feed AMW (HDS: AMW = 214, $E_{a,app}$ = 109 kJ/mol; AMW = 362, $E_{a,app}$ = 149 kJ/mol; HDN: $E_{a,app}$ = 78 kJ/mol and 109 kJ/mol, respectively). A plot of $\log(k_1)$

versus log(feed AMW) at constant temperature was linear for HDS and HDN (catalytic reactions) and non-linear for gas production and pitch conversion (thermal reactions). The estimated effectiveness factor increased with increasing feed AMW for both reactions, and passed through a maximum of 0.69 for HDS and 0.88 for HDN at AMW = 362. The intrinsic rate constants for HDS and HDN decreased throughout the molecular weight range studied. The increase in intrinsic activation energy with increasing feed AMW was not statistically significant.

ACKNOWLEDGEMENTS

I would like to take this opportunity to thank those people who made this degree as enjoyable as it was.

Francesca, for being there when things got hairy.

Dr. Murray Gray, for all the help, encouragement, and guidance.

AOSTRA and NSERC for the funding for this project.

The very able people (Ludmila, Tracy, and Hala) who assisted with the experiments and data analyses.

Dave, Don, Luigi, and Paul for providing a lesson in how to relax.

TABLE OF CONTENTS

Chapter			Page
	List of Tables		ix
	List of Figures		x
	Nomenclature		xi
1.	Introduction		1
2.	Literature Survey		2
	2.1	Background	2
	2.2	General Hydroprocessing	3
	2.3	Hydrodesulfurization	5
	2.4	Hydrodenitrogenation	9
	2.5	Hydrodeoxygenation	10
	2.6	Narrow Boiling Fractions	11
	2.7	Kinetics	13
3.	Analytical Methods		15
	3.1	Elemental Analysis	16
	3.2	NMR Spectroscopy	17
	3.3	Infrared Spectroscopy	17
	3.4	Basic Nitrogen Analysis	20
	3.5	Structural Group Analysis	20
	3.6	Specific Gravity	22
	3.7	Simulated Distillation Analysis	24
	3.8	Refinery Gas Analysis	24
	3.9	Hydrogen Sulphide Determination	26
	3.10	Molecular Weight Estimation	26
	3.11	Diffusivity Estimation	27

4. Description of Equipment and Operating Procedure 32
4.1 Feed Section 32
4.2 Reactor Section 34
4.3 Separation Section 35
4.4 Operating Procedure 35
5. Results and Discussion 38
5.1 Feedstock Properties 38
5.2 Hydroprocessing Products 48
5.3 Kinetics 60
6. Conclusions 78
7. Recommended Future Work 80
8. List of References 81
Appendix A: Reactor Hydroprocessing Data 85
Appendix B: Data from Structural Group Analysis 115
Appendix C: Properties of Feedstocks and Products 136
Appendix D: Kinetic Analysis 147
Appendix E: Factor Analysis 157

LIST OF TABLES

Table		Page
2.1	Representative Kinetics of HDS Reactions	6
2.2	Representative Kinetics of HDN Reactions	6
3.1	Band Assignments for ^{13}C NMR	18
3.2	Band Assignments for ^{1}H NMR	19
3.3	Infrared Spectroscopy Band Assignments	21
3.4	Structural Group Profile for CGOD3	23
3.5	Sample SDA Output	25
3.6	Parameters for the Winn Equation	27
4.1	List of Hydroprocessing Experiments	37
5.1	Boiling Distributions of Feeds	38
5.2	Carbon–Carbon Bond Estimates	56
5.3	Summary of Intrinsic Kinetics	62

LIST OF FIGURES

Figure		Page
2.1	Hydrodesulfurization Pathways for Dibenzothiophene	8
3.1	Deviation Plot for Recorrelated Winn Correlation	28
4.1	Schematic Diagram of Apparatus	33
5.1	Sulfur Distribution in SCGO	40
5.2	Distribution of Nitrogen and Oxygen in SCGO	41
5.3	Distribution of Density in SCGO	42
5.4	Distribution of Carbon Types in SCGO	44
5.5	Distribution of Heteroatom Types in SCGO	46
5.6	Distribution of Molecular Parameters in SCGO	47
5.7	Sulfur and Nitrogen Conversion by Hydroprocessing	49
5.8	Aromatic Carbon Reduction due to Hydroprocessing	51
5.9	Density Reduction due to Hydroprocessing	53
5.10	Reduction in AMW due to Hydroprocessing	54
5.11	Molar C_1 to C_2 Ratio in Effluent Gas	58
5.12	Distribution of Carbon Types in Products	59
5.13	Distribution of Molecular Parameters in Products	61
5.14	Arrhenius Plot for HDS	63
5.15	Arrhenius Plot for HDN	64
5.16	Arrhenius Plot for Gas Formation	66
5.17	Arrhenius Plot for Pitch Conversion	67
5.18	HDS and HDN Rate Constants versus Feed AMW	69
5.19	Thermal Reaction Rate Constants vs. AMW	72
5.20	Intrinsic HDS and HDN Rate Constants versus AMW	74
5.21	Effectiveness Factor versus AMW for HDS and HDN	76
5.22	Thiele Parameter versus Feed AMW for HDS and HDN	77

NOMENCLATURE

Symbol	Definition
a	parameter for equation 3.5
A_r	parameter for equation 2.4
A	pre–exponential factor for Arrhenius equation, [mL/(s·kg catalyst)]
A_d	digitized peak area for IR spectroscopy, [units]
ABS	available carbon–carbon bond sites, [mol bonds/mol oil]
AMW	average molecular weight, [g/mol]
B_r	parameter for equation 2.2
B	IR absorption intensity, [transmittance·wavenumber/(mol·cm)]
C_r	parameter for equation 2.1
C_w	parameter defined by equation 3.13
C	carbon weight fraction
C_4	weight fraction butanes in liquid product
$\mathscr{C}$	concentration, [mol/100 g]
$\mathscr{D}^o$	self–diffusivity, [m^2/s]
$\mathscr{D}_{eff}$	effective diffusivity, [m^2/s]
E_a	intrinsic activation energy, [kJ/mol]
$E_{a,app}$	apparent activation energy, [kJ/mol]
f_i	fraction of whole oil in narrow-boiling fraction
f_{ar}	aromatic carbon fraction
F	digitization factor, [transmittance·wavenumber/units]
H	hydrogen weight fraction
I	parameter defined by equation 5.9, [m^{-2}]
k_r	relative cracking rate constant, as defined by equation 2.4
k	reaction rate constant, [mL/(s·kg catalyst)]
$\hat{k}$	reaction rate constant, [m/s]

k_o	reaction rate constant parameter for equation 2.4
K	parameter defined by equation 3.7
l	IR path length, [cm]
LHSV	liquid hourly space velocity, [mL/h·g catalyst]
M	molecular weight, [g/mol]
n_c	molar carbon to oil ratio, [mol C/mol oil]
n_h	molar hydrogen to oil ratio, [mol H/mol oil]
n_n	molar nitrogen to oil ratio, [mol N/mol oil]
n_o	molar oxygen to oil ratio, [mol O/mol oil]
n_s	molar sulfur to oil ratio, [mol S/mol oil]
N	weight fraction nitrogen
N_a	Avogadro's number, [$6.023*10^{23}$ molecules/mol]
NB	number of carbon–carbon bonds, [mol bonds/mol oil]
$\mathcal{N}$	titrant normality
O	weight fraction oxygen
P_r	liquid product distribution function
Q	oil flowrate, [mL/min]
r	radius, [m]
R	effective catalyst radius, [m]
R_r	rate of reaction, [mg/s·kg catalyst]
RCH	moles of aromatic carbon converted per mole of heteroatoms removed
S	weight fraction sulfur
S_a	specific catalyst surface area, [m^2/kg]
SON	weight fraction heteroatoms
T	temperature, [°C]
T_b	average boiling point, [°C]
T_e	end temperature of narrow boiling fraction, [°C]

$\hat{T}_e$	pseudo–normalized end temperature, [°C]
V	molar carbon bond sites to oil ratio, [mol sites/mol oil]
V_x	molecular volume, [cm³/molecule]
V_{np}	titrant volume at neutralization point, [μL]
W	sample weight, [g]
X	conversion
y	dimensionless temperature, defined by equation 2.3

Greek Symbols

α	parameter for equation 3.5
β	parameter for equation 3.5
ϵ	catalyst porosity
η	effectiveness factor
λ	parameter defined by equation 3.12
μ	viscosity, [Pa·s]
μ_w	"wall" viscosity, [Pa·s]
ρ	density, [kg/m³]
τ	catalyst tortuosity
ϕ	diffusivity parameter for equation 3.8
ϕ	Thiele modulus

Subscripts

1	pseudo–first–order
a	solute molecule
b	solvent molecule
c	catalyst
i	intrinsic
in	reactor inlet (feed)
m	molecule
obs	observed
o	reactor outlet (product)
p	pore
s	Scheibel
t	total (whole oil prediction)
w-c	Wilke–Chang

Chapter 1: INTRODUCTION

Heavy oils and bitumens are two of the chief natural resources of Alberta and Canada. Considerable effort has been focussed world-wide on characterizing oils from the point of view of feedstock properties and the resultant kinetic properties. Much of this effort, however, has been directed at characterizing whole oils, and the principal focus of those studies has been light distillate oils. Less attention has been paid to heavy oil and bitumen, as these oils are more difficult to process and more difficult to characterize.

Bitumens and heavy oils can be distinguished from light oils by their high molecular weight, high contents of sulfur, nitrogen, oxygen, and aromatic carbon, and high metals content. All of these properties adversely affect the processability of the oil, and necessitate more severe processing conditions. Because of these characteristics, some research has been done on characterizing bitumens and heavy oils, but this has been work on whole oil samples of different backgrounds, or histories. Oils with similar physical properties can have very different chemical structures, and thus very different kinetic behaviour. Because of this feature of oils, it can be instructive to examine characteristics of fractions of an oil, to investigate how chemical and kinetic properties vary with molecular weight, while controlling some of the variability caused by examining oils of differing histories.

By fractionating the oil into narrow-boiling fractions, the variation of the physical, chemical, and kinetic properties with changing molecular weight may be examined. In this study, Syncrude Coker Gas Oil (SCGO) was fractionated into 6 narrow-boiling fractions (50°C nominal width) and a high-boiling residue. The six fractions were catalytically hydroprocessed in a pilot scale CSTR, and the feeds and products characterized. The distribution with AMW of the physical and kinetic properties of the SCGO fractions and their hydroprocessing products will be the focus of this thesis.

Chapter 2: LITERATURE SURVEY

There is an extensive amount of literature available concerned with hydroprocessing, hence only a representative fraction of the available literature will be presented. The format for this literature survey will be as follows.

a) Background hydroprocessing research: significant early work dealing with the development of hydroprocessing

b) General hydroprocessing research: representative literature covering general aspects of hydroprocessing and focussing on literature that pertains to this work, *i.e.* heavy gas oils, Ni/Mo catalysts, *etc.*

c) Hydrodesulfurization research: research directed primarily at HDS and dealing with model compounds and whole oils

d) Hydrodenitrogenation research

e) Hydrodeoxygenation research

f) Research on narrow boiling fractions: literature directed at the study of hydroprocessing of narrow boiling fractions

g) Kinetic research: work directed at explaining the observed kinetics for gas oils, and showing what to expect for the feeds used in this study

2.1: Background

Hydrodesulfurization (HDS) and hydrocracking have been described in the literature since the late 1940's. Voorhies and Smith discussed catalytic HDS of cracked cycle stock using an undisclosed sulfur-resistant catalyst in 1949. These researchers found that hydroprocessing under high hydrogen pressure (20.7 MPa) resulted in nearly-complete hydrogenation of aromatics, while a lower hydrogen pressure (5.2 MPa) gave partial saturation of aromatics to form naphthenic compounds. At 370°C, they reached 90% sulfur conversion, mainly from HDS of

aromatic sulfur containing molecules (*i.e.* benzothiophene). Hughes *et al.* (1950) examined the catalytic HDS of high sulfur, heavy petroleum oils using Co/Mo-Al_2O_3 catalysts. At 400°C and 2.1 MPa hydrogen pressure they reported sulfur conversions of up to 88% (by weight). Using silica gel fractionation, they also found that the majority of the sulfur was present in condensed ring aromatic structures, and that these molecules were desulfurized less efficiently than paraffinic and naphthenic sulfur-containing molecules. Van Zjill Langhout *et al.* (1955) examined hydrocracking and HDS at approximately 370°C and a wide range of pressures. Their results showed that increased hydrogen pressure increased desulphurization, while increased weight hourly space velocity decreased the conversion. They also noted a small amount of hydrogenation of aromatics.

2.2: General Aspects of Hydroprocessing

Since the introduction of catalytic hydroprocessing on a large scale in the 1950's, much work has been done on examining different gas oils and distillates, as well as other types of oil. Galiasso *et al.* (1980) investigated six commercial hydrotreating catalysts. Their work showed reaction orders of 2.0 and 1.8 for HDS and 1.4 and 1.0 for hydrodenitrogenation (HDN) using two different catalysts. Apparent activation energies for HDS and HDN were 90 kJ/mol and 137 kJ/mol, respectively, and they found that Ni/Mo catalysts were slightly more active for nitrogen removal and aromatic saturation than Co/Mo catalysts.

Catalytic hydrotreating of a heavy gas oil obtained from Athabasca bitumen was studied by Sambi *et al.* (1982). Their work used a trickle-bed reactor with a Co/Mo catalyst and a variety of operating conditions. Sulfur and nitrogen conversions of up to 93% and 72%, respectively, were reported, and hydrocracking was important at temperatures over 420°C. Hydrogen pressure in the range of 4.1 MPa to 12.4 MPa had a considerable effect on the kinetics at 450°C.

Miki *et al.* (1983) examined the contributions of thermal and catalytic reactions in hydroprocessing heavy oil, and found that the catalyst helped hydrogenate the oil and prevented coking and condensation of aromatic structures. Removal of heteroatoms was shown to be primarily catalytic.

A series of papers by researchers at CANMET (Wilson and Kriz, 1984; Wilson *et al.*, 1985; Fairbridge and Kriz, 1986; Fairbridge and Farnand, 1986) investigated the hydroprocessing of various oils derived from bitumen and coal. Wilson and Kriz (1984) examined high severity hydroprocessing of middle distillate fractions, and found thermodynamic limitations on hydrogenation of the aromatics. Hydrogenation of aromatic compounds was studied by analyzing for chemical classes such as paraffins, cycloparaffins, and various aromatic and hydroaromatic group types (Wilson *et al.*, 1985). Extensive cracking was seen at temperatures above 400°C. The primary aromatic groups in the feed were alkylbenzenes, and the apparent activation energy for hydrogenation decreased from 57 kJ/mol for alkylbenzenes to 39 kJ/mol for benzodicycloparaffins. Hydroprocessing of coal-derived middle distillate (Fisher and Kriz, 1986) showed only 32% conversion of aromatic carbon at very high HDS and HDN, and also showed that sulfur was more reactive than nitrogen. Coal-derived naphtha was hydrotreated by Fairbridge and Farnand (1986), and in this case the rate of reaction of phenolic oxygen was found to be higher than that of sulfur, which in turn was higher than that of nitrogen. Pseudo-first-order kinetics were used to fit all data.

Yui (1989) examined the catalytic hydrotreating of bitumen-derived coker gas oil in pilot and commercial plants, and found orders of reaction of 1 for HDN and 1.5 for HDS. He also found that hydrogen partial pressure had a large effect, as did catalyst wetting in trickle bed reactors. Catalyst wetting problems in trickle bed reactors may account for some deviations from pseudo-first-order kinetics in other experiments where full catalyst wetting was assumed.

Rangwala *et al.* (1984) investigated the hydroprocessing of Syncrude Coker Gas Oil (SCGO) in a continuous stirred tank reactor at a variety of temperatures and flowrates. Their results indicated that Ni/Mo catalysts were more active than Ni/W catalysts for HDS, HDN, and hydrogenation. First order kinetics were found to fit the data well, with conversions below 90% for most runs. Apparent activation energies of 115 kJ/mol for HDN and 125 kJ/mol for HDS were reported, along with apparent activation energies for pitch conversion and gas formation of 135 kJ/mol and 172 kJ/mol, respectively. Further work by this group (Rangwala *et al.*, 1986) with a variety of Ni/Mo catalysts indicated that increasing the Mo content of the catalysts increased activity for HDN, and that operating pressure (>10 MPa) had little effect on the kinetics of HDS, but did affect the HDN kinetics. Irreversible first order kinetics and ideal CSTR behaviour were shown to be valid assumptions, and apparent activation energies of 87 kJ/mol and 80 kJ/mol respectively for HDS and HDN were reported. The apparent activation energies for resid conversion and gas formation were 53 kJ/mol and 180 kJ/mol, respectively. Internal mass transfer resistances did affect the results, especially for HDN. The differences between these values and earlier values were attributed to variations in catalyst activity.

2.3: Hydrodesulfurization

A summary of apparent reaction orders and apparent activation energies for hydrodesulfurization for a variety of feedstocks is shown in Table 2.1.

Katti *et al.* (1984), in examining the HDS of the neutral (*i.e.* non-acidic, non-basic) oils of a heavy distillate from coal liquefaction with a Ni/Mo catalyst, found that the neutral oils were primarily polycyclic aromatic hydrocarbons with a sulfur content of 0.6 weight %. Their research showed first order kinetics for specific sulfur compounds, but fractional order (1<order<2) overall for the oil. It was also shown that 4–methyldibenzothiophene was less active for HDS than other methyl

Table 2.1: Representative Kinetics of Hydrodesulfurization Reactions

Feedstock	Apparent Reaction Order	$E_{a,app}$ kJ/mol	Reference
SCGO	1.0	125	Rangwala *et al.* (1984)
SCGO	1.5	139	Yui (1989)
VGO	2	138	Massagutov *et al.* (1967)
neutral oils	1 – 2		Katti *et al.* (1984)
cracked LGO	2 and 1.8	105	Galiasso *et al.* (1984)
kerosene	2	155	Chu and Wang (1982)
DBT	1	121	Chu and Wang (1982)
DBT	1	123	Broderick & Gates (1981)

Table 2.2: Representative Kinetics of Hydrodenitrogenation Reactions

Feedstock	Apparent Reaction Order	$E_{a,app}$ kJ/mol	Reference
SCGO	1	115	Rangwala *et al.* (1984)
SCGO	1	80	Rangwala *et al.* (1986)
SCGO	1	92	Yui (1989)
cracked LGO	1.4 and 1.0	84	Galiasso *et al.*(1984)
aniline	1	84	Chu and Wang (1982)

-dibenzothiophenes, presumably due to steric hindrances.

Satterfield *et al.* (1980) examined combined HDS and HDN for model compounds, and found that pyridine inhibits the HDS of thiophene, while thiophene enhances HDN of pyridine and piperidine (at high pressures).

The hydrogenolysis and hydrogenation of dibenzothiophene was studied by Broderick and Gates (1981) using a sulfided Co/Mo catalyst. Their work showed that the selectivity for hydrogenolysis (S removal before hydrogenation) versus hydrogenation (aromatic ring hydrogenation before S removal) was dependent on temperature and H_2S concentration. The pathways for hydrogenolysis and hydrogenation are shown in Figure 2.1. The selectivity of the two pathways is a significant variable in any study on hydrodesulfurization, and there is considerable variation between different studies and different conditions. Little is known about what may be expected from a real feedstock with regards to hydrogenation/hydrogenolysis selectivity. A variety of Langmuir-Hinshelwood kinetic equations were fit to the data, and apparent activation energies of 126 kJ/mol and 120 kJ/mol for hydrogenolysis and hydrogenation were calculated.

Massagutov *et al.* (1967) examined the kinetics of HDS of a vacuum gas oil using a Co/Mo catalyst, and found severe diffusion limitations at 400°C (shown by a curved plot of ln(k) vs 1/T). A second order rate equation was fit to the data, and apparent activation energies were calculated at three temperature ranges. The severe diffusion limitations at temperatures over 400°C led to a decrease in the apparent activation energy from 138 kJ/mol (350°C to 380°C) to 22 kJ/mol (410°C to 430°C). As the maximal decrease in the apparent activation energy with diffusion limitations is only 50%, Massagutov *et al.* must also have been seeing some catalyst deactivation to account for the large drop in apparent activation energy.

The kinetics of HDS, HDN, and hydrogenation of polyaromatics were investigated by Chu and Wang (1982) using dibenzothiophene, aniline, and

Hydrogenolysis followed by Hydrogenation

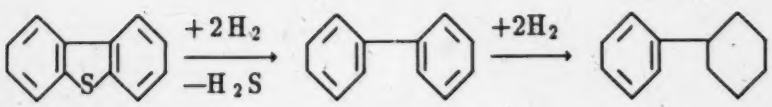

Hydrogenation followed by Hydrogenolysis

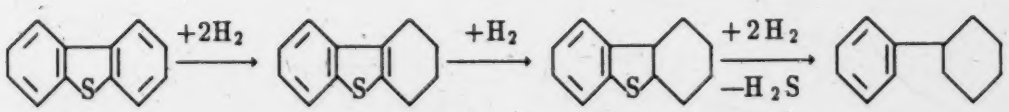

Figure 2.1: Hydrodesulfurization Pathways for Dibenzothiophene

naphthalene. Pseudo-first-order irreversible kinetics were assumed for HDS and HDN, and the data were shown to fit this model well. Kerosene followed pseudo-second-order kinetics, such as seen with a reactive lump/refractory lump model or a distributed kinetics model. The apparent activation energy was 155 kJ/mol. The relative rates of dibenzothiophene desulfurization and kerosene desulfurization did not vary over different catalysts. They also showed that HDS was faster than HDN, which was of the same order of reactivity as polyaromatic hydrogenation, and that aniline denitrogenation and naphthalene hydrogenation were related, in that both reactions require ring saturation, while desulfurization of dibenzothiophene may proceed without ring saturation. The pseudo-first-order rate constants for HDN and hydrogenation of naphthalene were similar.

2.4: Hydrodenitrogenation

A summary of apparent reaction orders and apparent activation energies for hydrodenitrogenation for a variety of feedstocks is shown in Table 2.2.

Furimsky *et al.* (1978) investigated the HDN of basic and non-basic compounds in Athabasca bitumen distillates using promoted Mo catalysts, and found that Ni and Co had comparable promoting activity, and that the promoting activity did not change for metal/molybdenum ratios greater than about 0.6. They also showed that non-basic nitrogen was removed preferentially to basic nitrogen for both coker kerosene and gas oil.

Dorbon *et al.* (1984) investigated the HDN of carbazoles and benzocarbazoles in a coker gas oil, and found that high pressures and moderate temperatures provided better removal of benzocarbazoles than carbazoles, while higher temperatures and moderate hydrogen pressures removed alkyl carbazoles more effectively. Satterfield *et al.* (1985) examined the catalytic HDN of quinoline, and found that both water and hydrogen sulphide increase the rate of denitrogenation.

2.5: Hydrodeoxygenation

The catalytic deoxygenation of a heavy gas oil from thermal hydrocracking of Athabasca bitumen was examined by Furimsky (1978) using promoted Mo catalysts. His work, at 400°C and 13.8 MPa hydrogen, indicated that the preferential pathway for dibenzofuran was hydrogenation to a phenolic compound, followed by HDO, with very little hydrogenation of aromatics. Approximately 50% conversion of the oxygen was obtained.

Lavopa and Satterfield (1987) investigated the catalytic hydrodeoxygenation of dibenzofuran over a Ni/Mo catalyst. They found two parallel pathways, similar to HDS of dibenzothiophene: hydrogenation of one aromatic ring followed by hydrogenolysis of the carbon-oxygen bonds, and hydrogenolysis of the carbon-oxygen bonds followed by hydrogenation of the aromatic rings. Their work showed that the ring hydrogenation pathway was of greater importance than the hydrogenolysis pathway, but that the presence of H_2S depressed catalyst activity for the hydrogenation pathway and increased selectivity for the hydrogenolysis pathway. Both pathways followed pseudo-first-order kinetics, with the intermediate oxygenated products reacting more rapidly than dibenzofuran.

Li *et al.* (1985) investigated the HDO of phenolic compounds in the acidic fractions of a heavy coal distillate, and found that at temperatures above 350°C the rate of direct oxygen removal was greater than that of prior ring hydrogenation. Substituted phenols and naphthols were found to be converted much more rapidly than dibenzofuran, indicating that dibenzofuran deoxygenation would be the determining step in HDO of oils containing both compounds. Individual compounds, as well as overall phenolic oxygen, were found to follow pseudo-first-order kinetics. As well, Li *et al.* hypothesized that compounds containing basic nitrogen may inhibit HDO of phenolic compounds.

2.6: Narrow Boiling Fractions

One of the earliest studies of hydroprocessing of narrow boiling fractions was that of Hoog in 1950. His work consisted of catalytically upgrading a whole oil at 375°C with a Co/Mo catalyst, and also upgrading two narrow boiling fractions of this oil. The whole oil, with a boiling range of 260°C–350°C, contained 1.30 weight % sulfur, while the narrow boiling fractions contained 1.20 weight % sulfur (290°C–300°C) and 1.76 weight % sulfur (330°C–340°C). The light fraction was considerably more reactive for HDS than the heavier fraction, especially at higher flowrates where the sulfur conversion of the heavy fraction declined rapidly. Specifically, at infinite hydrogen dilution (oil partial pressure of 0) the light fraction had a rate constant twice as large as that of the heavy fraction, while at an oil partial pressure of 0.25 MPa, the light fraction was approximately three times as reactive as the heavy fraction. Hoog also noted that there was a maximum sulfur conversion for all fractions with varying gas rates; this conversion corresponded to a 4% sulfur retention for the light fraction and a 7% sulfur retention for the heavier fractions. The proposed explanation was the presence of very refractory compounds, which would be present at a higher level in the heavy fraction than in the light fraction.

Yitzhaki and Aharoni (1988) catalytically upgraded a whole gas oil under a variety of conditions, and fractionated the feed and product oils into narrow boiling fractions (approximately 20°C width). The sulfur contents of the fractions of the feeds and products were determined, and sulfur conversions were calculated assuming that the quantity of each fraction did not change. Pseudo-first-order kinetics were assumed for all fractions, and it was assumed that no change in the boiling ranges occurred. The actual kinetics did not follow pseudo-first-order, although the higher boiling fractions started to approach this behaviour. The light fractions showed definite systematic deviation. This method ignored shifts in

boiling point due to cracking, hydrogenation, and sulfur removal. The inferred rate constants for HDS for gas oil fractions decreased with increasing boiling point, from 3.6 to 1.8 hr^{-1} for fractions with average boiling points ranging from 250°C to 350°C (with a catalyst pellet of 5 mm diameter). A gasoline-gas oil mixture with the same catalyst showed the same behaviour, with HDS rate constants decreasing from 5.1 to 2.7 for the same average boiling point range.

Stangeland (1974) investigated catalytic hydrocracking (*i.e.* emphasis on cracking reactions, not on removal of heteroatoms) by fractionating a feed into 28°C (50°F) boiling fractions, each of which cracked by a first order reaction to form lighter products. Two product-distribution functions were needed to describe the overall product yield: one function for butanes and one for the heavier products. Each feed was characterized solely by its high-end true boiling point (T_e, °C), and the distribution functions and rate constants were calculated as a function of the true boiling point. The effects of the paraffins content and different catalyst types were investigated. Stangeland's model is shown below:

$$[C_4] = C_r \cdot \exp[\,-0.01247\cdot(T_e - 121)\,] \qquad 2.1$$

$$P_r(y) = [y^2 + B_r\cdot(y^3 - y^2)]\cdot(1 - [C_4]) \qquad 2.2$$

$$y = \frac{T_e - 28}{(T_e - 56) - 28} \qquad 2.3$$

In this model, $[C_4]$ is the weight fraction of butanes in the product, y is a normalized temperature, $P_r(y)$ is the liquid product distribution function, and B_r and C_r are adjustable parameters. The relative cracking rate constant (k_r) was modelled by equation 2.4.

$$k_r(\hat{T}_e) = k_o \cdot [\, \hat{T}_e + A_r \cdot (\hat{T}_e^3 - \hat{T}_e) \,] \qquad 2.4$$

where $\hat{T}_e = T_e/556$, $k_o = 1$, and A_r is an adjustable parameter. The normal values for the parameters are: $0 < A < 1$, $-2 < B < 1$, $0 < C < 2$.

2.7: Kinetics

Researchers investigating catalytic hydroprocessing reactions in the past have noted two forms of kinetics for the catalytic reactions (HDS, HDN, HDO): those investigators examining pure compounds, mixtures of model compounds, or oils at low conversion have observed Langmuir-Hinshelwood or pseudo-first-order kinetics for each compound (Chu and Wang, 1982; Lapinas *et al.*, 1987; Sapre and Gates, 1981; Lavopa and Satterfield, 1987; Mann *et al.*, 1987; *etc.*), while researchers working on whole oils at high conversions have noted kinetics of fractional orders from 1 to 2 (Yui, 1989; Man, 1981). Ho and Aris (1987), in a paper on apparent second-order kinetics, showed rigorously that a complex mixture of components with a wide range of reactivities could give rise to kinetics with an apparent order between 1 and 2, although each individual compound reacted according to pseudo-first-order kinetics. This apparent paradox appears because of the large distribution of reactivities seen in complex mixtures, where the low-conversion behaviour is dominated by the more reactive components while the high-conversion behaviour is dominated by the more refractory compounds. The wide boiling ranges of most oils lead to a wide range of reactivities, while high conversion levels ensure that the refractory components will play a significant role in the apparent kinetics. In oils with narrow boiling ranges, or reaction schemes that do not achieve high conversion, however, pseudo-first-order kinetics are observed because only a narrow range of reactivities are significant.

The experiments presented in this thesis are all done on narrow-boiling

fractions at moderate conversion (generally < 90%) and thus pseudo-first-order kinetics may be safely assumed. Previous work on this reactor system with the whole oil (Rangwala *et al.*, 1984; Rangwala *et al.*, 1986) showed that the reactions followed pseudo-first-order kinetics, proving that the assumption of pseudo-first-order kinetics is justified for catalytic reactions for the narrow-boiling fractions.

Chapter 3: ANALYTICAL METHODS

Many techniques are used in analyzing and characterizing gas oils, and these methods can be lumped into two main categories: methods which estimate the physical properties of an oil and methods which reveal some of the chemical structure of the oil. Gas oils are too complex for component by component analysis, so that any method examining the chemical structure of the oil must incorporate some averaging, or lumping, to get an approximation of the actual structure of the oil.

There are several reasons why the characteristics of an oil must be known. To calculate material balances and simple atomic conversions for a hydroprocessing run, the density, boiling distribution, sulfur and nitrogen contents, and effluent gas analyses are all required. To investigate the kinetics more deeply, the viscosity and diffusivity of the feed oil must be estimated, and these estimates require a knowledge of the average sample molecular weight. If the effect of hydroprocessing on the chemical structure of the oil is of interest, then the chemical structure must be estimated in some way. One method for estimating the concentrations of a variety of structural, or functional, groups is structural group analysis (SGA), a method of incorporating data from various analytical sources (elemental analysis, NMR and IR spectroscopy, and basic nitrogen analysis) to estimate the concentration profile of various carbon and heteroatomic group types.

This section will discuss the methods used for elemental analysis, ^{1}H and ^{13}C NMR spectroscopy, infrared spectroscopy, basic nitrogen analysis, specific gravity estimation, simulated distillation analysis (boiling distribution), refinery gas analysis and H_2S determination, molecular weight estimations, and effective diffusivity calculations.

3.1: Elemental Analysis

The carbon and hydrogen contents were calculated by the Microanalytical Laboratory in the Department of Chemistry using a Perkin/Elmer 240 Elemental Analyzer. The carbon and hydrogen measurements were accurate to ± 0.2%.

Nitrogen content was analyzed using an Antek pyro-reactor and digital nitrogen analyzer. The nitrogen in the sample was combusted to NO at 900°C, and then oxidized to NO_2 using a feed stream of ozone. The oxidation to NO_2 released light, and the light release was detected by a photomultiplier tube. Since the release of light is proportional to the total nitrogen content of the oil and the equipment was standardized with samples of known nitrogen concentration, this provided an estimate of the nitrogen concentration accurate to ± 0.02%.

Sulfur content was determined by combustion at 1400°C followed by infrared detection of the SO_2 concentration in a Leco SC–132 Sulfur Determinator. This method was also calibrated with known standards, and was accurate to ± 0.05%.

Oxygen contents were also determined by the Microanalytical Laboratory using the Perkin/Elmer 240 Elemental Analyzer, but the results are much less accurate than those for carbon and hydrogen. Repeat samples were obtained, and an averaging scheme was worked out to agree with both analytical results and the expected trend (as seen for sulfur and nitrogen). The details of this procedure are given in Appendix B.

Once all elemental concentrations were estimated, the values were normalized to 100%. The original and normalized data are given in Appendix B, Tables B1 to B4.

3.2: NMR Spectroscopy

Nuclear Magnetic Resonance (NMR) was used to provide information on the molecular environments of the carbon and hydrogen atoms in the oil. The ^{1}H and ^{13}C NMR analyses were performed on NMR machines in the Department of Chemistry. The ^{1}H NMR spectra were run on a 60 MHz Varian A56/60–A spectrophotometer using the constant wave technique, while the ^{13}C NMR spectra were done by the Spectrophotometry Laboratory on a 200 MHz Bruker WH–200 spectrophotometer. Band assignments for ^{13}C and ^{1}H NMR allow for calculation of the concentrations of different types of carbon and hydrogen, both aliphatic and aromatic. The weight percent of each atom in each band can be obtained by integrating the area of each band and dividing the band area into the total area. Band assignments for the two techniques are based on the work of Khorasheh *et al.* (1987) and Thiel and Gray (1988), and are given in Tables 3.1 and 3.2. Both ^{1}H and ^{13}C NMR spectra were run on samples dissolved in deuterated chloroform with tetramethylsilane (TMS) added as a reference for chemical shifts. The relaxation agent chromium acetonyl acetonate was added to samples for ^{13}C NMR.

The proton and carbon–13 NMR analyses of the feedstocks and products are given in Appendix B, Tables B6 to B9.

3.3: Infrared Spectroscopy

Infrared spectra were collected on a Perkin/Elmer 621 spectrophotometer, using tetrahydrofuran and methylene chloride as solvents. The concentrations of various heteroatomic groups may be calculated from the IR spectra as in equation 3.1 using planimetry to calculate the peak areas.

$$\mathscr{C} = \frac{A_d \cdot F}{10 \cdot B \cdot I \cdot W} \qquad 3.1$$

Table 3.1: Band Assignments for ^{13}C NMR

Band #	Range (ppm)	Carbon Types in Band
1	11 – 15	γ–methyl
2	15 – 18	β–methyl
3&4	18 – 22.5	α–methyl, naphthenic methyl
5&6	22.5 – 37	methylene groups (sub–peaks due to paraffinic methylene
7	37 – 60	methyne groups (sub–peaks due to paraffinic methyne)
8	60 – 85	deuterated chloroform solvent
9	100 – 129.5	aromatic carbon bonded to hydrogen and olefins
10	129.5 – 140	aromatic carbon bonded to carbon
11	140 – 160	aromatic carbon bonded to heteroatoms
12	160 – 185	carbonyl carbon in amides and acids
13	185 – 210	ketones

Table 3.2: Band Assignments for ^1H NMR

Band #	Range (ppm)	Hydrogen Types in Band
1	0.5 – 1.0	γ–methyl
2	1.0 – 2.0	β, naphthenic, alkyl–OH
3	2.0 – 4.5	α, amine, methylene α to sulfoxides, amides, amines, alkyl–OH
4	4.5 – 6.3	olefins
5	6.3 – 8.3	aromatic, amide, phenol
6	8.3 – 9.0	phenanthrene hindered H (9,10 protons)
7	9.0 – 11.0	aldehyde

In equation 3.1, $A_d \cdot F$ is the area in units of transmittance·wavenumber, l is the path length of the cell, W is the sample weight, and B is the absorption intensity. With the path length in cm and the sample weight in g, the units for concentration are mol/100 g. The peak assignments and absorption intensities are detailed in Table 3.3, and follow the work of Jacobson and Gray (1987). The average areas and concentrations of the heteroatomic groups are given in Tables B10 and B11 in Appendix B.

3.4: Basic Nitrogen Analysis

The concentration of basic and very weak basic nitrogen groups was calculated by potentiometric titration of the sample with perchloric acid in dioxane. The samples were dissolved in either benzene+acetonitrile or benzene+acetic anhydride. The method of Buell (1967) was used, with a titrant normality of approximately 0.0585 N. Based on work performed by Jacobson and Gray (1987), all basic nitrogen was assigned to quinoline. The concentration of quinoline can be calculated from the volume of titrant at the neutralization point, V_{np} (μL), the titrant normality, $\mathcal{N}$, and the sample weight, W (g) by equation 3.2.

$$\mathcal{C} = \frac{V_{np} \cdot \mathcal{N}}{W \cdot 10^4} \qquad 3.2$$

The volume of titrant at the neutralization point and the resulting quinoline concentration are tabulated in Tables B12 and B13 in Appendix B.

3.5: Structural Group Analysis

The method for structural group analysis is detailed in Khorasheh (1986) and Khorasheh *et al.* (1987). The data from elemental analysis, NMR spectroscopy, infrared spectroscopy, and basic nitrogen analysis are combined to generate

Table 3.3: Infrared Spectroscopy Band Assignments

Group	Range of Absorbance		Absorption Intensity	
	CH_2Cl_2	THF	CH_2Cl_2	THF
Phenol	3540–3600		5000	
Carbazole	3455–3465		7000	
Carboxylic	1700–1745	1720–1735	12 000	15 000
Ketone	1690–1700	1695–1705	7000	
Amide	1625–1690	1630–1695	15 000	
Sulfoxide	1025–1040		6000	

information about the concentration of various structural groups in the sample. The concentrations of the structural groups is optimized based on quantitative and semiquantitative information and certain constraints; *i.e.* all concentrations must be greater than or equal to 0. The aromatic groups in the profile include benzene, phenanthrene, and biphenyl bridge. The phenanthrene concentration is based on NMR signals from the adjacent 9,10 protons. Biphenyl bridge gives an estimate of condensation of aromatic rings, and formally represents aromatic carbon atoms bound only to other aromatic carbon atoms. Aliphatic carbon groups estimated include paraffinic methyl, methylene, and methyne, naphthenic methyl, methylene, and methyne, α–carbon, and β–methyl. The α–carbon is the concentration of methyl groups adjacent to an aromatic ring and carbon atoms bound directly to both an aromatic ring and paraffinic carbon (*i.e.* the initial carbon of a long chain), while β–methyl is a terminal methyl group one carbon unit removed from an aromatic carbon. The heteroatoms in a sample are represented by the functional groups determined by IR and potentiometric titration, and by balance groups. The balance groups are selected based on the known chemistry of these oils. For example, benzothiophene is used to represent the sulfur which is not in a polar form, and provides a reasonable representation for a gas oil material. The balance for nitrogen is assigned to N–substituted indole, while the oxygen balance is assigned to benzofuran. A sample structural profile is given in Table 3.4. The full structural profiles for feedstocks and products are given in Appendix B, Tables B15 and B16, as is a list of all structural groups used (Table B14).

3.6: Specific Gravity

The specific gravities of the samples were measured using a Digital Precision Density Meter DMA–2, manufactured by the Anton Paar Company. The specific gravity was obtained from the natural frequency of oscillation of a cell filled with

Table 3.4: Structural Group Profile for CGOD3

Structural Group	CGOD3 Concentration (mol/100 g)
Aromatic	
Benzene	0.141
Phenanthrene	0.0
Biphenyl Bridge	0.136
Aliphatic	
α–Carbon	0.753
β–Methyl	0.154
γ–Methyl	0.458
Paraffinic Methylene	0.539
Paraffinic Methyne	0.175
Naphthenic Methyl	0.355
Naphthenic Methylene	0.967
Naphthenic Methyne	1.452
Heteroatomic	
Benzothiophene	0.107
Sulfoxide	0.004
Benzofuran	0.049
Aromatic Hydroxyl	0.003
Aromatic Ketone	0.003
Carboxylic Acid	0.004
Aromatic Amide	0.001
Indole	0.003
Quinoline	0.005
N–Substituted Indole	0.005

the sample at a constant temperature of 23°C. Specific gravity at 15°C can be calculated from the specific gravity at 23°C using equation 3.3.

$$\rho_{15} = \sqrt{\rho_{23} - 0.0011 \cdot (15-23)} \qquad 3.3$$

The specific gravities at 15°C are tabulated in Appendix C, Tables 3 and 4.

3.7: Simulated Distillation Analysis

Simulated distillation analysis (SDA) was used to estimate the boiling distribution of the oil samples. The SDA procedure was similar to the ASTM D2887 method, and has been described previously by Chung (1982) and Man (1981). A gas chromatograph with temperature/time programming capabilities was used to separate the oil according to boiling point. The volumetric response factor was assumed to be unity for all fractions. A sample output from the SDA procedure is shown in Table 3.5. Summaries of SDA runs for the feedstocks and products are given in Tables C5 and C6, Appendix C.

3.8: Refinery Gas Analysis

The reactor effluent gases were analyzed using a Hewlett-Packard 5840A gas chromatograph set up for the analysis of hydrocarbon gases. The refinery gas analysis procedure has been described by Chung (1982). This procedure allowed estimation of the hydrogen, methane, C_2, C_3, C_4, C_5, and C_6 concentrations. The hydrogen was detected by a TCD detector while the hydrocarbons were detected using an FID detector. The method was not able to calculate the concentration of hydrogen sulphide as FID does not respond to hydrogen sulphide. A standard gas mixture from Matheson Gas Products Inc. was used to calibrate the gas chromatograph.

Table 3.5: Sample SDA Output

Sample name cgod3.fed

Date June 10,1988
Sample file was q695ac73.rpt
Baseline file was q6957d58.rpt
The area of rejection was 0.

Retention Time	Run Area	Baseline Area	Corrected Area	Volume	Accumulated Volume	Boiling Point
0.51	62.	28.	34.	0.014	0.014	73.52
1.51	262.	239.	23.	0.010	0.024	85.01
2.51	468.	447.	21.	0.009	0.032	96.51
3.51	637.	594.	43.	0.018	0.050	108.01
4.51	771.	719.	52.	0.022	0.072	119.50
5.51	888.	821.	67.	0.028	0.100	131.00
6.51	992.	918.	74.	0.031	0.130	142.49
7.51	1072.	995.	77.	0.032	0.162	153.99
8.51	1146.	1070.	76.	0.032	0.194	165.48
9.51	1217.	1129.	88.	0.037	0.230	176.98
10.51	1271.	1171.	100.	0.041	0.272	188.47
11.51	1313.	1201.	112.	0.046	0.318	199.97
12.51	1352.	1217.	135.	0.056	0.374	211.47
13.51	1374.	1223.	151.	0.063	0.437	222.96
14.51	1402.	1220.	182.	0.076	0.512	234.46
15.51	1424.	1211.	213.	0.088	0.601	245.95
16.51	1470.	1199.	271.	0.112	0.713	257.45
17.51	1591.	1179.	412.	0.171	0.884	268.94
18.51	2004.	1155.	849.	0.352	1.236	280.44
19.51	3381.	1128.	2253.	0.935	2.171	291.94
20.51	6056.	1099.	4957.	2.056	4.227	303.43
21.51	11656.	1055.	10601.	4.398	8.625	314.93
22.51	18922.	1014.	17908.	7.429	16.055	326.42
23.51	30660.	978.	29682.	12.314	28.368	337.92
24.51	40875.	931.	39944.	16.571	44.939	349.41
25.51	42430.	896.	41534.	17.231	62.170	360.91
26.51	34968.	851.	34117.	14.154	76.324	372.41
27.51	25406.	810.	24596.	10.204	86.528	383.90
28.51	15315.	761.	14554.	6.038	92.565	395.40
29.51	7885.	708.	7177.	2.977	95.543	406.89
30.51	4039.	646.	3393.	1.408	96.950	418.39
31.51	2217.	614.	1603.	0.665	97.615	429.88
32.51	1451.	571.	880.	0.365	97.980	441.38
33.51	1159.	534.	625.	0.259	98.240	452.88
34.51	1034.	488.	546.	0.227	98.466	464.37
35.51	959.	444.	515.	0.214	98.680	475.87
36.51	902.	415.	487.	0.202	98.882	487.36
37.51	855.	382.	473.	0.196	99.078	498.86
38.51	806.	347.	459.	0.190	99.269	510.35
39.51	757.	304.	453.	0.188	99.457	521.85
40.51	676.	262.	414.	0.172	99.628	533.35
41.51	572.	222.	350.	0.145	99.773	544.84
42.51	455.	177.	278.	0.115	99.889	556.34
43.51	341.	155.	186.	0.077	99.966	567.83
44.51	200.	118.	82.	0.034	100.000	579.33

3.9: Hydrogen Sulphide Determination

Hydrogen sulphide concentration in the reactor effluent gases was calculated using the absorption-iodimetric method. The reactor effluent gas was bubbled through 50 mL of 1.0 N NaOH solution for fifteen minutes. The hydrogen sulphide reacted with the caustic to form sodium sulphide according to:

$$2\ NaOH + H_2S \longrightarrow Na_2S + 2\ H_2O \qquad 3.4$$

The resulting solution was acidified with sulphuric acid, then a starch indicator and iodine were added. The excess iodine was back-titrated with sodium thiosulphate.

Once the hydrogen sulphide concentration was calculated, the concentrations of the other reactor gases were normalized to give a total, including hydrogen sulphide, of 100%. The hydrogen sulphide concentration was not changed during normalization. The composition of the reactor effluent gas is given in the reactor data sheets in Appendix A.

3.10: Molecular Weight Estimation

Two techniques were used to estimate molecular weights for the oil samples. The number-average molecular weights (AMW) for the seven feedstocks and four of the products were measured by vapour-pressure osmometry in benzene by the Microanalytical Laboratory. The Winn correlation (Sim and Daubert, 1980), a correlation based on average boiling point and specific gravity, was used to estimate the weight-average molecular weights for all samples but the heaviest feed, which was too heavy to be used for SDA. The form of the Winn correlation is shown in equation 3.5, where the temperature is in K.

$$AMW = a \cdot T_b^{\alpha} \cdot \rho^{\beta} \qquad 3.5$$

The Winn correlation, with the published parameters, could not accurately predict the molecular weights of these samples (as determined by vapour-pressure osmometry). The estimates obtained were systematically high by at least 10%, as shown in Appendix C, Table C7. The parameters for the Winn equation were then estimated based on the 6 available feedstocks and four products. The new and old parameters for the Winn correlation are listed in Table 3.6, with the regression data from the new correlation.

Table 3.6: Parameters for the Winn Equation

Published Parameters	New Parameters
$a = 5.805*10^{-5}$	$a = 2.41*10^{-6} \pm 9*10^{-8}$
$\alpha = 2.3776$	$\alpha = 2.847 \pm 0.30$
$\beta = -0.9371$	$\beta = -2.130 \pm 0.69$

The parameters were estimated by linearizing the Winn equation and fitting it to the available AMW, specific gravity, and average boiling point data by a least–squares technique ($r^2 = 0.986$). A deviation plot (calculated AMW versus measured AMW for the ten points) for the corrected Winn equation is shown in Figure 3.1. The revised equation was used to estimate molecular weights for product materials (*i.e.* interpolating values for chemically similar oils). The deviation between the values from the Winn equation with the published parameters and the values from vapour-pressure osmometry may be due to structural differnces (*i.e.* aromaticity) or to differences between the weight average and the number average.

3.11: Diffusivities

One focus of hydroprocessing studies is on estimating intrinsic kinetics for the hydroprocessing reactions. The data needed for intrinsic kinetic calculations include observed kinetic data, catalyst structure data, and physical property data for the reacting oil. One important property of the oil is the effective diffusivity at

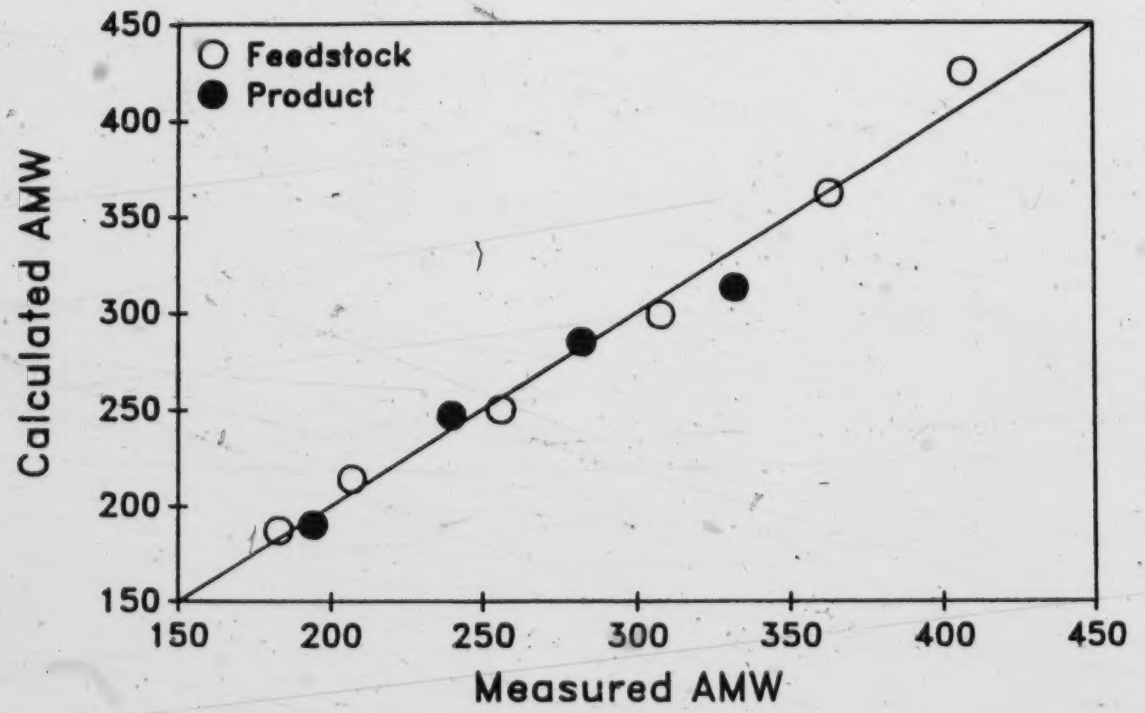

Figure 3.1: Deviation Plot for Recorrelated Winn Equation

reactor conditions, which may be estimated from the molecular diffusivity. The molecular diffusivity may be calculated from the Scheibel (3.6) or Wilke-Chang (3.8) correlations (Perry *et al.*, 1984), which correlate the molecular diffusivity with the molecular weight of the oil, the density and viscosity of the oil at reactor conditions, and the reactor temperature.

$$\mathscr{D}^{0}_{ab} = \frac{K \cdot T}{\mu_b \cdot V_a^{0.333}} \qquad 3.6$$

$$K = 8.2*10^{-8} \cdot \left[1 + \left(3 \cdot \frac{V_b}{V_a}\right)^{0.667} \right] \qquad 3.7$$

$$\mathscr{D}^{0}_{ab} = 7.4*10^{-8} \cdot \frac{(\phi \cdot M_b)^{0.5} \cdot T}{\eta_b \cdot V_a^{0.6}} \qquad 3.8$$

For the special case of unimolecular diffusion (*i.e.* $M_b = M_a$, $V_b = V_a$), these equations can be simplified to the equations 3.9 and 3.10.

$$\mathscr{D}^{0}_{s} = 2.526*10^{-7} \cdot \frac{T}{\mu} \cdot \left(\frac{\rho}{M}\right)^{0.333} \qquad 3.9$$

$$\mathscr{D}^{0}_{w\text{-}c} = 1.17*10^{-9} \cdot \frac{T \cdot \rho^{0.6}}{\mu \cdot M^{0.1}} \qquad 3.10$$

The density and viscosity may be estimated for the oil given the density, average boiling point, and molecular weight at ambient temperature by using the Lee-Kesler correlation for critical properties (Perry *et al.*, 1984) and the principle of corresponding states. These methods for estimating critical properties, density, and viscosity are available in a number of commercial programs for hydrocarbon phase behaviour; HYSIM was used in this study. Although these estimates may deviate as

seen for the Winn equation, the relative values should be correct.

Once the molecular diffusivity has been estimated, the effective diffusivity may be estimated by two methods: one method involves assuming straight pores with molecular size effects (Ternan, 1986) while the other method assumes no molecular size effects but considers cylindrical pores with random orientation (Satterfield, 1980). Ternan's model is of the form:

$$\mathscr{D}_{eff} = \mathscr{D}^{0} \cdot \frac{(1-\lambda)^{2}}{1 + \lambda \cdot C} \qquad 3.11$$

$$\lambda = r_m / r_p \qquad 3.12$$

$$C_w = \mu_w / \mu \qquad 3.13$$

In this equation, r_m is the molecular radius and r_p is the pore radius. The viscosity of the oil in the pore is considered to consist of two terms, a bulk viscosity μ and a "wall" viscosity μ_w. The wall viscosity is used to assign a greater viscosity to molecules near the pore wall due to Van der Waal's interactions between the molecules of the catalyst pellet and the oil molecules near the wall. A correlation for estimating C_w based on solute molecular weight is given in the paper. An average molecular radius may be calculated for large oil molecules by assuming spherical molecules. Given average molecular weight and density at reactor conditions and Avogadro's number ($N_a = 6.023*10^{23}$ molecules/mol), the molecular volume may be calculated by equation 3.14.

$$V_m = \frac{AMW}{\rho \cdot N_a} \qquad 3.14$$

The minimum molecular radius may then be calculated using the spherical

assumption. The pore radius distribution of the catalyst can be used to estimate a weighted-average-pore radius, based on pore volume. Using these data, the effective diffusivity from Ternan's method may be calculated for each feed at reactor conditions. In this study, the range of $\mathscr{D}_{eff}/\mathscr{D}^{o}$ was 0.23 to 0.36.

The standard method of estimating $\mathscr{D}_{eff}$ as described by Satterfield (1980) requires knowledge of only two parameters: the catalyst porosity and the catalyst tortuosity,

$$\mathscr{D}_{eff} = \mathscr{D}^{o} \cdot \epsilon/\tau \qquad 3.15$$

The catalyst porosity may be calculated from the total pore volume and total average catalyst pellet volume. Catalyst tortuosity is a measure of the "twistedness" of the catalyst pores, and cannot be measured directly. Using experimental data from similar runs with catalyst pellets of different sizes, the value of $\mathscr{D}_{eff}/\mathscr{D}^{o}$ may be calculated, and thus the tortuosity. Previous work on SCGO with an identical catalyst (Gray, 1989) has shown that values of $\mathscr{D}_{eff}/\mathscr{D}^{o}$ are in the range of 0.1.

Since the estimates from the tortuosity method are more conservative than those based on the straight pore model of Ternan, the tortuosity method will be used for calculations of the intrinsic kinetics. As well, the straight pore model of Ternan is not an adequate descriptor of catalyst behaviour, due to the straight pore assumption. Application of the tortuosity/porosity correction factors to the straight pore model yields effective diffusivities that are three to four times too low.

Chapter 4: EQUIPMENT and PROCEDURE

The samples for this study were narrow-boiling fractions of Syncrude Coker Gas Oil (SCGO), a wide-boiling gas oil produced by topping thermally-coked Athabasca bitumen. The first three samples (up to 400°C) were fractionated by Syncrude Canada Ltd. in a 50 L batch still at atmospheric pressure. The remaining residue was fractionated in a vacuum batch still by ESSO Petroleum Ltd. into the other three narrow-boiling fractions and a high-boiling residue. All oil samples were provided by Syncrude Canada Ltd.

The hydroprocessing apparatus used for this study was described by Man (1981) and Chung (1982), and consisted of three basic sections: a feed section, a reaction section, and a separation section. A schematic diagram of the apparatus is shown in Figure 4.1. The unit was equipped with automatic control units for control of hydrogen feed rate, reactor pressure, furnace temperature, high pressure separator pressure, low pressure separator pressure, and liquid level in the high pressure separator. The control loops were described in detail by Man (1981).

4.1: Feed Section

The hydrogen gas was supplied in 41.4 MPa cylinders from the Linde Division of Union Carbide. Hydrogen pressure was reduced to slightly above reactor pressure using a high pressure regulator. Hydrogen flow rate was controlled by measuring the laminar flow pressure drop, and using the pressure drop as input to the hydrogen flow rate control loop.

Two systems were used for delivering oil to the reactor. For light oil samples (CGOD1 to CGOD4), the oil was stored in a glass storage tank and fed to the reactor using a high-pressure positive displacement pump. A 100 mL burette connected to the feed line in parallel to the storage tank allowed accurate, direct measurement of the liquid feed rate. The two heavier feeds (CGOD5 and CGOD6)

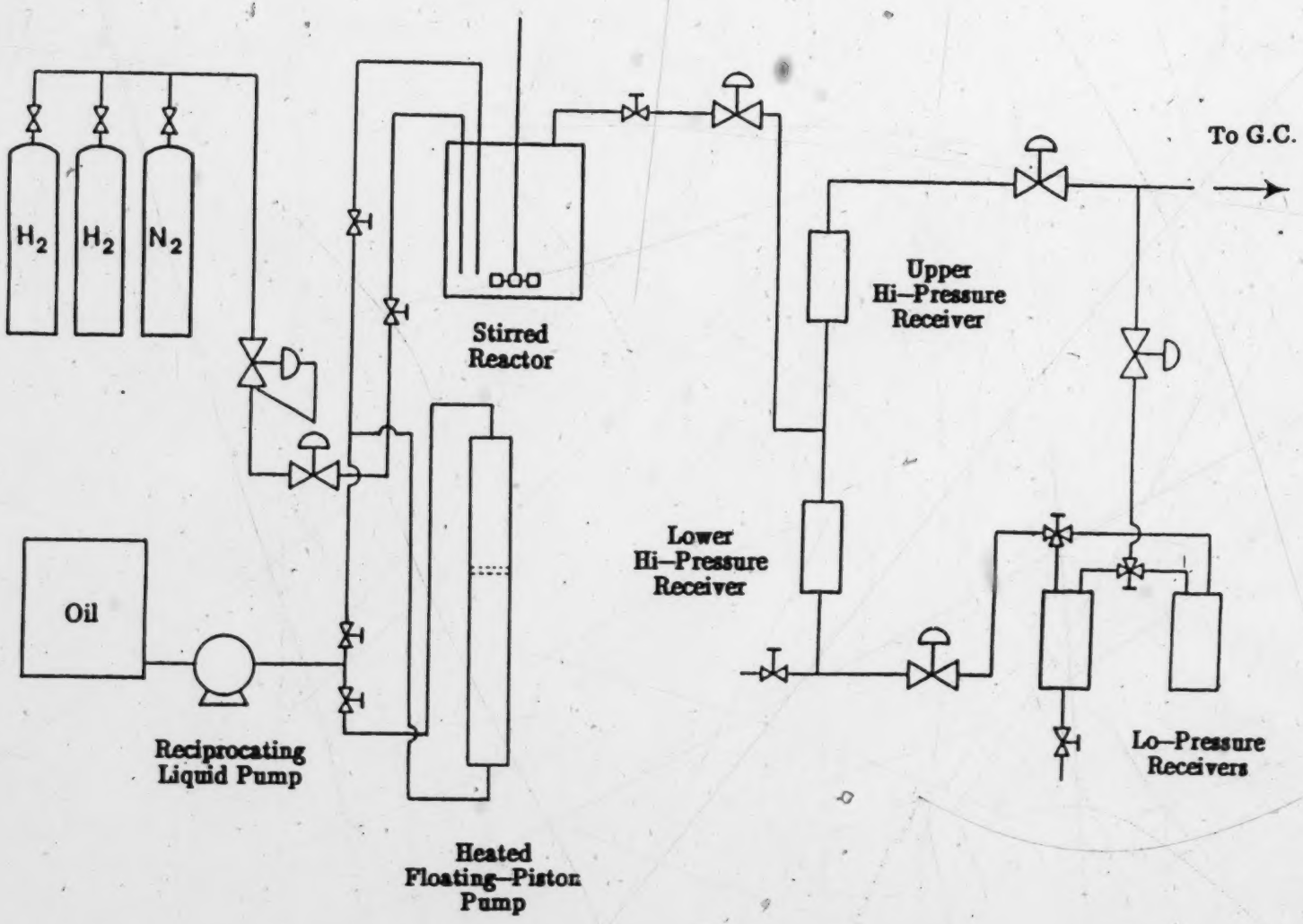

Figure 4.1: Schematic Diagram of Apparatus

were fed into the reactor in a slightly different fashion. The feed was placed on one side of a high pressure, floating-piston pump, which was then flushed with helium. The feed side of the floating-piston pump was connected to the reactor and the blank side to the reciprocating pump used previously. The whole floating-piston pump assembly was then placed inside a cabinet and heated to approximately 110°C. A light oil (SCGO) was pumped into the blank side of the floating-piston pump, thereby forcing the heavier feed into the reactor. The liquid flowrate could be monitored in the same fashion as before, using the burette on the light displacement oil.

4.2: Reaction Section

The reactor used for this study was a Magne Drive Packless Autoclave, manufactured by Autoclave Engineers Inc. The reactor volume was 150 mL, and agitation was provided by a Magne Drive Agitator which was belt-driven by an Impak V–S variable speed drive. Rotation speed was measured by a magnetic pick-up coil. Four cylindrical wire mesh catalyst baskets were suspended from the head of the autoclave on three implanted steel rods and the bomb-sample line. The autoclave was heated by a high-temperature furnace surrounding the base of the autoclave, and the furnace and head of the autoclave were insulated to provide better temperature control. The reactor pressure was controlled by a back-pressure-control loop.

The liquid and hydrogen were fed into the head of the autoclave, and the product froth was withdrawn through the head of the autoclave. A bomb sample line ran to the base of the reactor, and was used to withdraw samples. A safety head assembly with a rupture disc was attached to the head of the autoclave and to a blowdown tank.

4.3: Separation Section

The mixture of liquid and gaseous products leaving the reactor passed through a filter before entering the back-pressure valve. As the product line was not heated, the products were at ambient temperature when they entered the separation section. Gas and liquid were separated using a two-stage pressure-letdown system with high-pressure and low-pressure separators. The reactor products entered the separation system with the liquids draining into the lower high-pressure receiver and the gases entering the upper high-pressure receiver. This provided a two-stage gas/liquid disengaging system for complete gas/liquid separation. The lower high-pressure receiver was a low volume sight glass which provided minimal fluid retention and allowed a visual check of the liquid level (controlled by the liquid level control loop).

The liquid in the lower high-pressure receiver was continually transferred to the low-pressure receivers, where it was collected. A sample line was connected to the withdrawal line from the lower high-pressure receiver for liquid product sampling. The remainder of the product liquid was collected from the low-pressure receivers.

The exit gas flow rate from the upper high-pressure receiver was measured by a dry-gas-test meter and a laminar-flow pressure-drop meter, similar to that used for measurement of the flow rate of feed hydrogen. The exit gas composition was determined by means of gas chromatography, as outlined in Chapter 3.

4.4: Operating Procedure

Prior to the start of the hydroprocessing experiments, a quantity of the hydroprocessing catalyst (4.1% NiO, 17.4% MoO_3, S_a = 190 m^2/g, pore volume = 0.46 cm^3/g) was calcined by heating to 350°C in air for several hours. After calcination, the catalyst was weighed out into 8.00 g batches, capped, and stored in

a desiccator. Before the hydroprocessing experiment, the catalyst was placed into the four catalyst baskets, the catalyst baskets attached to the supports, and the reactor assembled. A polished metal gasket was placed between the body of the autoclave and the head to ensure retention of pressure. The feed and product lines were attached and the reactor was pressure tested for a period of at least ten hours.

At the start of a hydroprocessing experiment, the agitator speed was set at 800 rpm, fast enough to eliminate external mass transfer resistances and approximate CSTR behaviour (Rangwala *et al.*, 1986). The furnace and autoclave were heated to a temperature of 350°C over a time interval of 2.5 hours. At a temperature of 150°C, the hydrogen feed was initiated, and at 350°C the liquid feed was started. The reactor temperature was then slowly increased to the reaction temperature (generally 400°C). Minor adjustments to the pressure and temperature controllers were made to obtain the desired stable reaction conditions. Catalyst sulfiding was done *in-situ* by the feed oil.

While the system was running, the hydrogen feed rate, oil feed rate, and gas and liquid product rates were continuously measured, with the oil feed rate fine tuned manually to the desired rate. Liquid samples were withdrawn from the lower high-pressure separator every hour, and the remainder of the liquid product was collected every two hours. Portions of the hourly liquid samples were subjected to X-ray fluorescence using a Panalyzer 4000 with ^{55}Fe as the radioactive isotope, while the remainder of the sample was stored in a capped sample vial and refrigerated for subsequent analysis. The readings from the Panalyzer 4000 were proportional to the sulfur content (Chung, 1982), and this was used as a check on the steady-state of the sulfur conversion. Gas samples were analyzed periodically as a second check on steady-state conditions. When steady-state was reached, final liquid product samples were taken, and a final refinery gas analysis was performed. The bulk liquid was collected, and the system prepared for shut-down.

When the system was shut-down, the agitator was slowed to approximately 60 rpm and a bomb sample withdrawn into an evacuated container. This bomb sample was used for subsequent analysis of the reactor liquid concentrations, hydrogen solubility, and reactor gas analysis. Once the bomb sample was withdrawn, the furnace was turned off and the liquid feed was stopped. The furnace was lowered and insulation removed, and after the autoclave had cooled to 350°C the hydrogen feed was stopped. Before the start of the next run the liquid holdup was measured by withdrawing all reactor fluid through the bomb sample line. If necessary, the catalyst was changed; otherwise the next hydroprocessing experiment was prepared by changing the feed oil. For series of experiments where the same feed was used for three runs at varying temperatures, all three runs were completed in the same day by increasing the furnace temperature at the conclusion of a run without stopping the gas or liquid feed. The bomb sample was still taken for each run, but the liquid hold-up was only measured for the final run of the series. Because the perturbation involved in increasing the reaction temperature by 20°C was small, the times to steady state for the second and third runs of a series were substantially reduced (normal runs 4–6 hours, subsequent runs 2–3 hours). A list of all hydroprocessing experiments performed is shown in Table 4.1.

Table 4.1: List of Hydroprocessing Experiments

Experiment	Feed	Temperature (°C)
MG–32	CGOD1	400
MG–33	CGOD2	380
MG–34	CGOD2	400
MG–35	CGOD2	420
MG–36	CGOD3	400
MG–37	CGOD4	400
MG–38	CGOD5	395
MG–39	CGOD5	406
MG–40	CGOD5	425
MG–41	CGOD6	425

Chapter 5: RESULTS and DISCUSSION

5.1: Feedstock Properties

Boiling Ranges of Fractions

The feedstocks for this project were six narrow-boiling fractions and a high-boiling residue, all derived from a wide-boiling gas oil, Syncrude Coker Gas Oil (SCGO). The fractionation was described in Chapter 4. Table 5.1 shows, for each feed, the mean boiling point, the volume % of oil boiling within the nominal cutpoints, and the volume % of oil boiling within 50°C of the nominal cutpoints.

Table 5.1: Boiling Distributions of Feeds

Feed	Nominal Range (°C)	ABP (°C)	Vol % Boiling in Nominal Range	Vol % Boiling within 50°C
CGOD1	250–300	278	74.8	98.1
CGOD2	300–350	314	60.4	96.6
CGOD3	350–400	360	47.9	94.5
CGOD4	400–450	421	45.6	93.8
CGOD5	450–500	481	53.9	96.3
CGOD6	500–550	539	58.6	

For CGOD6, the volume % of oil boiling within 50°C of the cutpoints could not be estimated because the simulated-distillation analysis procedure is only effective up to approximately 575°C, and CGOD6 was a nominal 500°C to 550°C cut. From Table 5.1 it can be seen that the minimum amount of oil boiling within the cutpoints for these fractions was 46 volume % for CGOD4, and that the minimum amount of oil boiling within 50°C of the nominal cutpoints was 93.8 vol%, also for CGOD4. The fractions obtained were narrow boiling, especially when compared to the whole oil, which had a maximum of 23.6 vol% boiling within any 50°C fraction, and a standard deviation of approximately 75°C for the mean of 392°C. Examining Table 5.1 also indicates skew in the boiling distribution for each oil fraction.

Although the distributions for samples CGOD1 and CGOD4 had means very close to the nominal average (278°C and 421°C compared to 275°C and 425°C), this was not true of the other four feedstocks. The second and third feeds had mean boiling points significantly below the nominal average, while samples CGOD5 and CGOD6 had means significantly above the mean boiling point of the range. The first and fourth samples, therefore, were evenly weighted around the nominal range, while the other samples had a large proportion of the oil that was boiling outside the nominal range to either the high-boiling end or the low-boiling end, without an even weighting. The full boiling distributions are given in Table C5, Appendix C.

Chemical Composition and Physical Properties

An elemental analysis for the samples is shown in Table B3, Appendix B. The sulfur distribution is shown in Figure 5.1, as weight % of sulfur versus average molecular weight of the feedstock. This plot shows the monotonic increasing trend of sulfur with molecular weight, which is expected for any heteroatom. The largest increases in sulfur concentration were in the middle of the range of molecular weights, with very little change at high and low molecular weights. The same plot for oxygen and nitrogen is shown in Figure 5.2, along with the values for the atomic hydrogen/carbon ratio. This figure shows that the oxygen and nitrogen followed the same increasing trend seen for sulfur, while the atomic H/C ratio followed the opposite trend (decreasing with increasing average molecular weight). The decreasing trend for atomic H/C ratio was expected, as the heavier fractions should be more aromatic and more substituted than the light fractions.

The variation of specific gravity with average molecular weight is shown in Figure 5.3, and also showed the expected trend of increasing with increasing molecular weight. The specific gravities are reported at 15°C, and were calculated from the values at 23°C. The 15°C specific gravities are also given in Table C3,

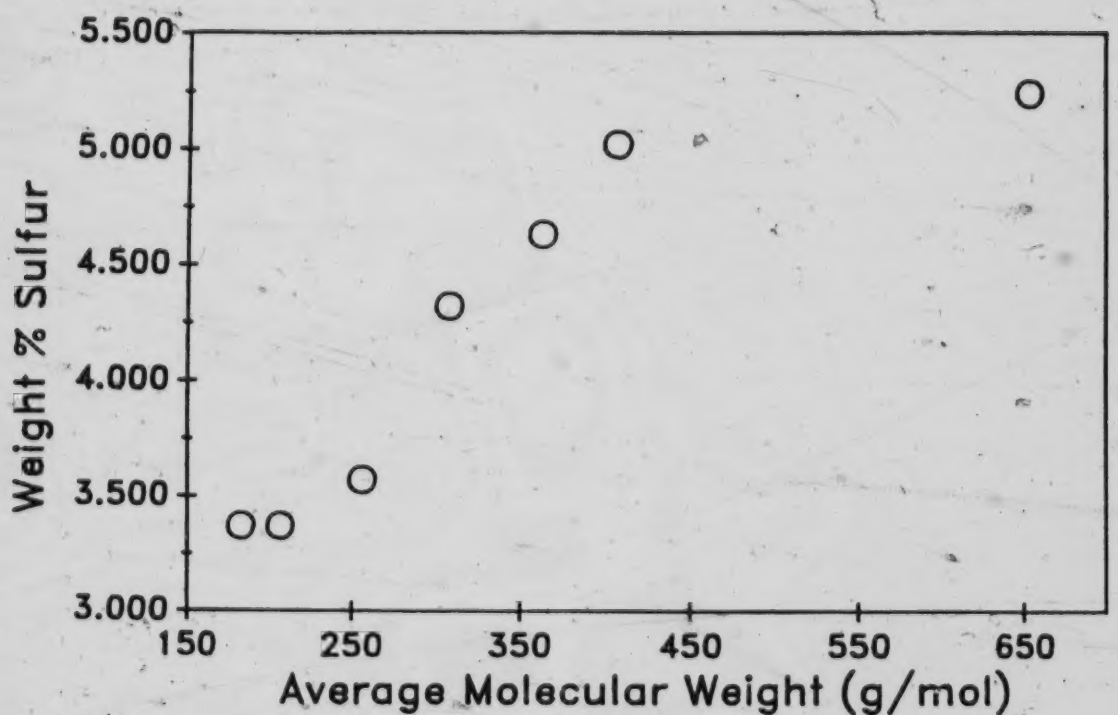

Figure 5.1: Distribution of Sulfur in SCGO

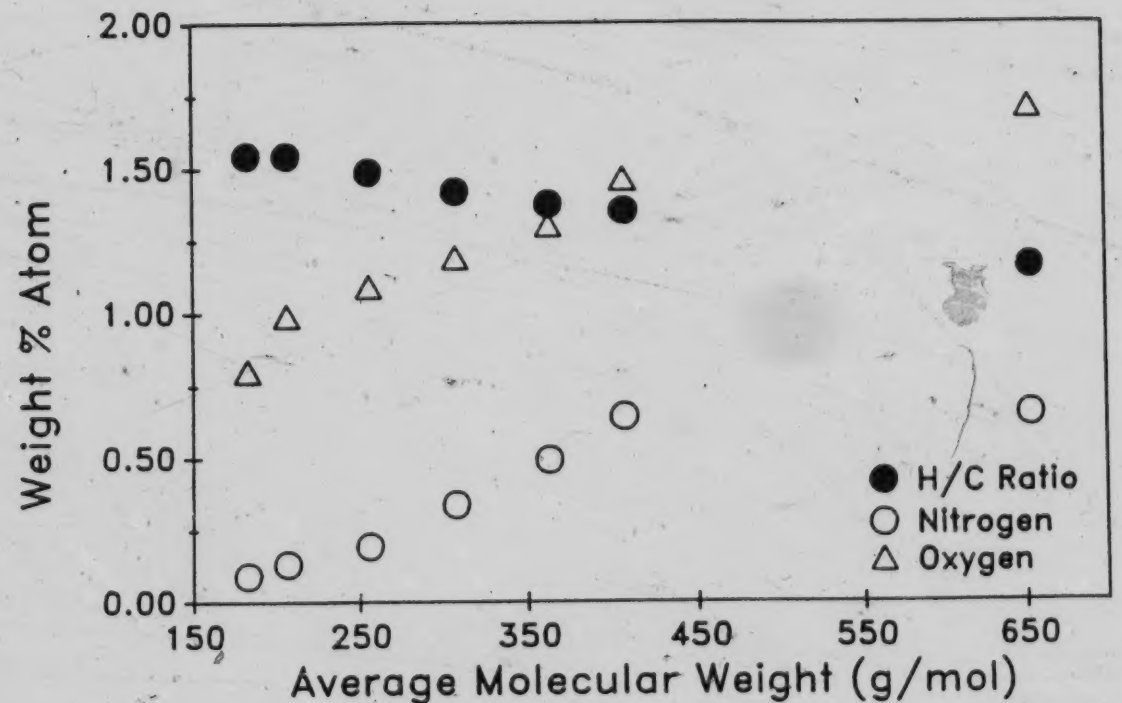

Figure 5.2: Distribution of Nitrogen, Oxygen, and Atomic H/C Ratio in SCGO

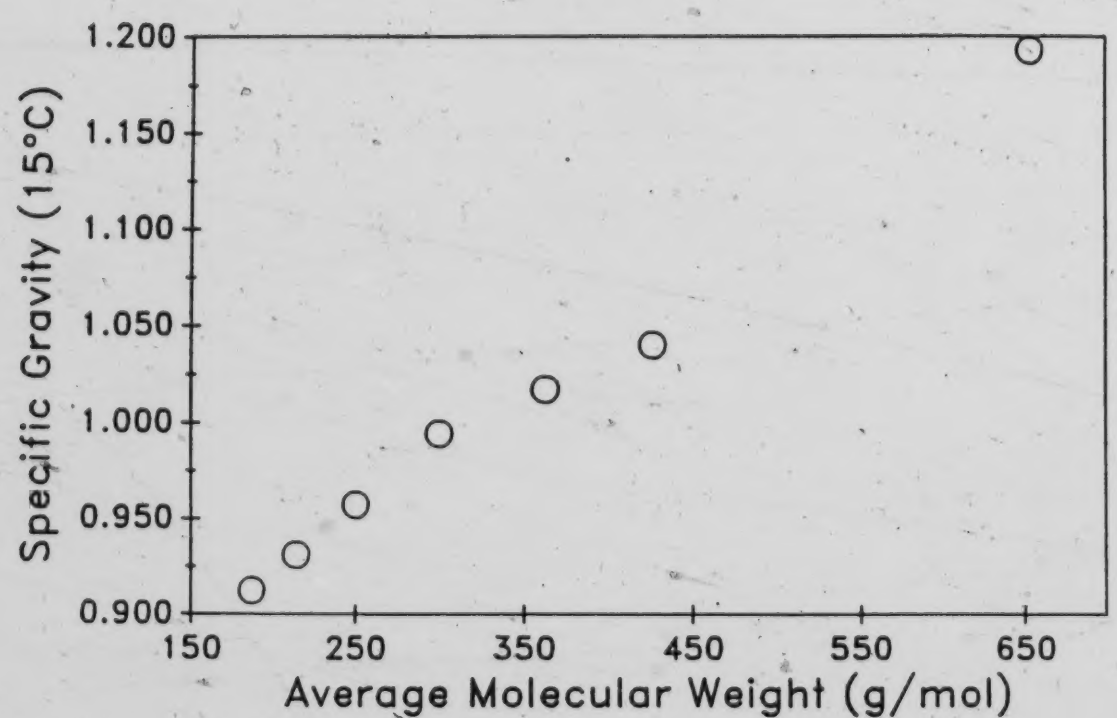

Figure 5.3: Distribution of Density in SCGO

Appendix C, and range from 0.912 for the lightest fraction to 1.040 for CGOD6 and 1.092 for the high-boiling residue, CGOD7. The specific gravity (15°C) for the whole oil was 0.987.

The average molecular weight of each sample was estimated as described in Chapter 3. The molecular weights were estimated by the re-correlated Winn equation for both feedstocks and products for consistency. Use of the original Winn equation would not yield different results for this study, as the values are internally consistent, and deviate systematically from the measured values. The average molecular weights for the feedstocks as calculated by the three methods are shown in Table C7, Appendix C. The differences between measured molecular weights and values from the revised correlation were within experimental error, with a maximum deviation of 6%. For the feedstocks, the average molecular weights ranged from 187 for the lightest sample to 425 for CGOD6 and 653 for CGOD7, the high-boiling residue. The value for the high-boiling residue was directly measured by vapor-pressure osmometry, as no mean boiling point could be estimated for this sample (due to limitations of the simulated-distillation analysis).

Structural Group Analysis

The data for the structural group analysis (^{13}C NMR, ^{1}H NMR, IR, basic nitrogen analysis) are given in Appendix B, as are the full structural group analyses for the feedstocks. The major types of carbon atom groups are presented in Figure 5.4. This plot shows very little change for the paraffinic carbon, with a slight decrease with molecular weight. This decrease, however, is on the order of the error in the method and is thus not significant. The aromatic carbon showed a moderate increasing trend over the range of average molecular weights, but the increase was not monotonic as it was for the heteroatoms and density. The first three samples had essentially the same concentration of aromatic carbon, with the increase

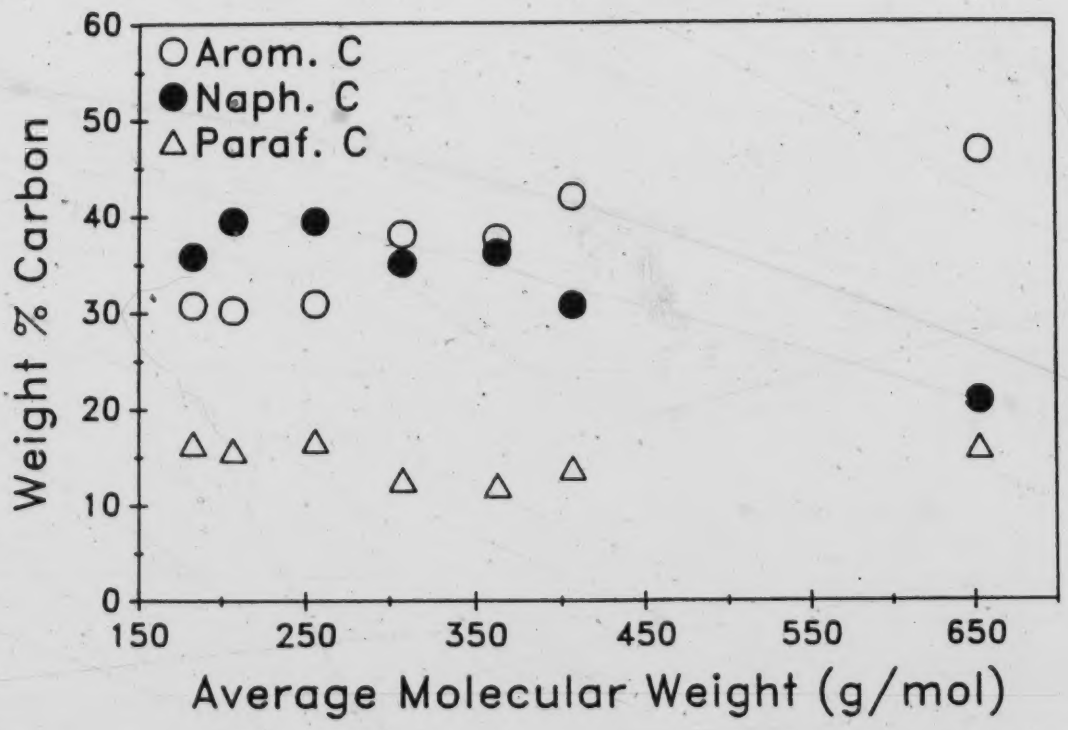

Figure 5.4: Distribution of Carbon Types in SCGO

starting at CGOD4 (AMW = 300). The fifth feedstock had a slightly lower aromatic carbon content than CGOD4 or CGOD6, but the increasing trend is still obvious when the entire data set is examined. Naphthenic carbon decreased with increasing molecular weight, but passed through a maximum between CGOD2 (AMW = 214) and CGOD3 (AMW = 250). This behaviour was not unreasonable, as very light fractions (*i.e.* CGOD1) would contain more substituted single ring compounds and non-aromatic compounds (and therefore have a lower naphthenic carbon content), while heavier fractions (*i.e.* CGOD6) would contain more condensed polyaromatic ring structures, leading to the decrease in naphthenic carbon content.

The estimated distribution of heteroatoms between aliphatic (*e.g.* sulfoxides) and aromatic (*e.g.* benzothiophenes) structures is shown in Figure 5.5. The distribution was calculated from the data from the structural group analysis, and although most of the heteroatoms were represented in aromatic structures, the "balance" groups for sulfur, nitrogen, and oxygen are aromatic. The only aliphatic groups were those seen in the infrared spectra, and therefore the values estimated for the heteroatom distribution are only rough estimates. The assumption of the balance groups being aromatic is in accord with the results of Payzant *et al.* (1988), which showed that the bulk of the sulfur present in the neutral oils fraction of heavy distillates from coal was in polycyclic aromatic structures such as benzothiophene or dibenzothiophene. The structural group analyses for the CGOD feedstocks showed a random distribution of the % of heteroatoms bound in aromatic structures, with a mean of approximately 87% aromatic (on a weight % basis).

The values of two molecular parameters, the mean side chain length and the average number of rings per aromatic structure, were calculated and are shown in Figure 5.6. A discussion of the calculation of these two parameters is given in Appendix B. The mean side chain length seemed to follow a pattern opposite to

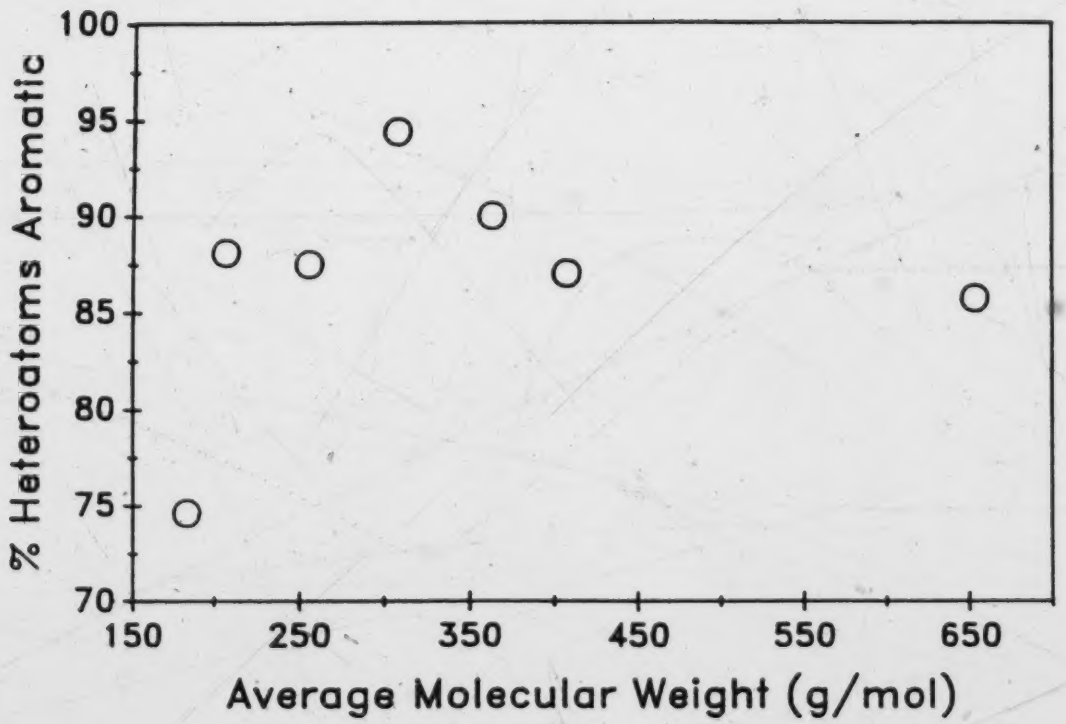

Figure 5.5: Distribution of Heteroatom Types in SCGO

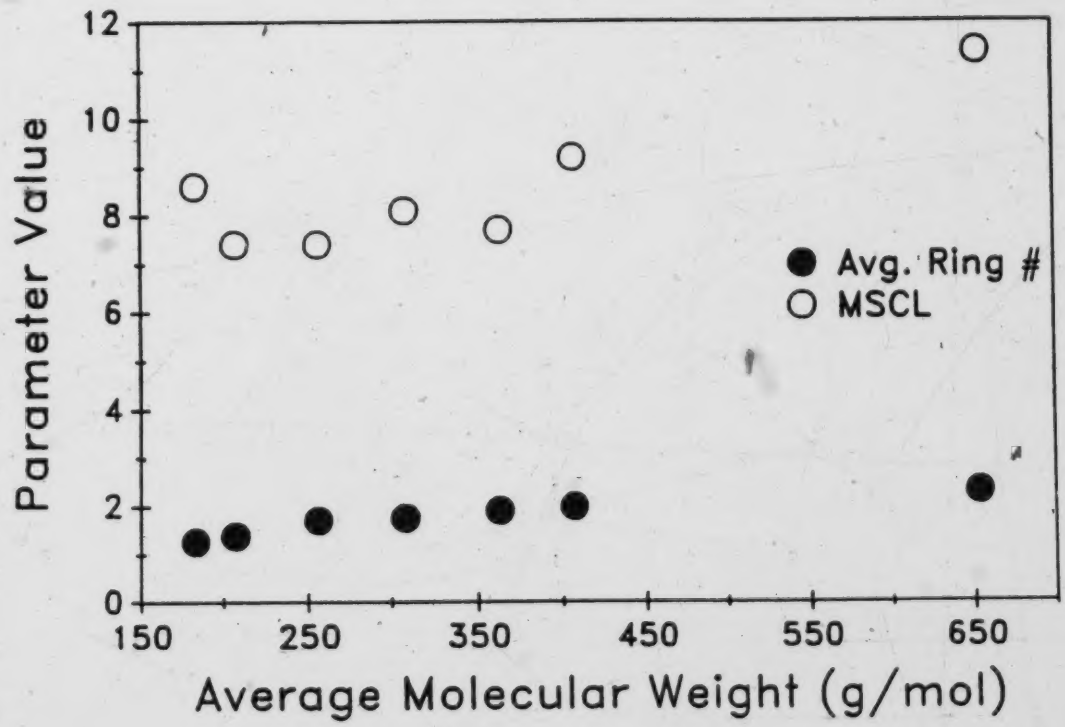

Figure 5.6: Distribution of Mean Side Chain Length and Average Ring Number in SCGO

that of naphthenic carbon, with a minimum between feeds CGOD2 and CGOD3, and then a gradual increase over the remainder of the molecular weight range studied. This may, however, represent a gradual increasing trend in the mean side chain length with increasing molecular weight. The average number of rings per aromatic structure, or mean ring number, followed an increasing trend with molecular weight, from 1.3 for the lightest samples to mean ring numbers of 2.0 and 2.3 for the heaviest samples. This result shows the increasing condensation of the ring structures with increasing molecular weight, and also indicates that large condensed aromatic structures are possible in the heavier fractions. These results for mean ring number coincide with those of atomic H/C ratio and aromatic carbon content, which both indicated increasing aromaticity and substitution.

5.2: Hydroprocessing Products

Heteroatom and Aromatic Carbon Conversion

The conversion of sulfur and nitrogen is shown in Figure 5.7 as a function of average molecular weight of the feed and reaction temperature. The conversions for the first four feedstocks were obtained at a reaction temperature of 400°C, while the conversions for CGOD5 and CGOD6 were obtained at 425°C. This plotting procedure illustrates the combined effects of increasing molecular weight and increasing temperature. The data of Figure 5.7 show a monotonic decrease in sulfur and nitrogen conversion with increasing average molecular weight of the feedstock, despite the differing reaction temperatures. An increase of 25°C in the reaction temperature should increase the rate of reaction, and thus the conversion. Since the conversion declines over the entire range of feedstock molecular weight, the effect due to increasing the feedstock molecular weight outweighs the effect due to increasing the reaction temperature. The estimated sulfur and nitrogen conversions at 400°C for CGOD5 are approximately 43.5% and 20%, respectively, and these

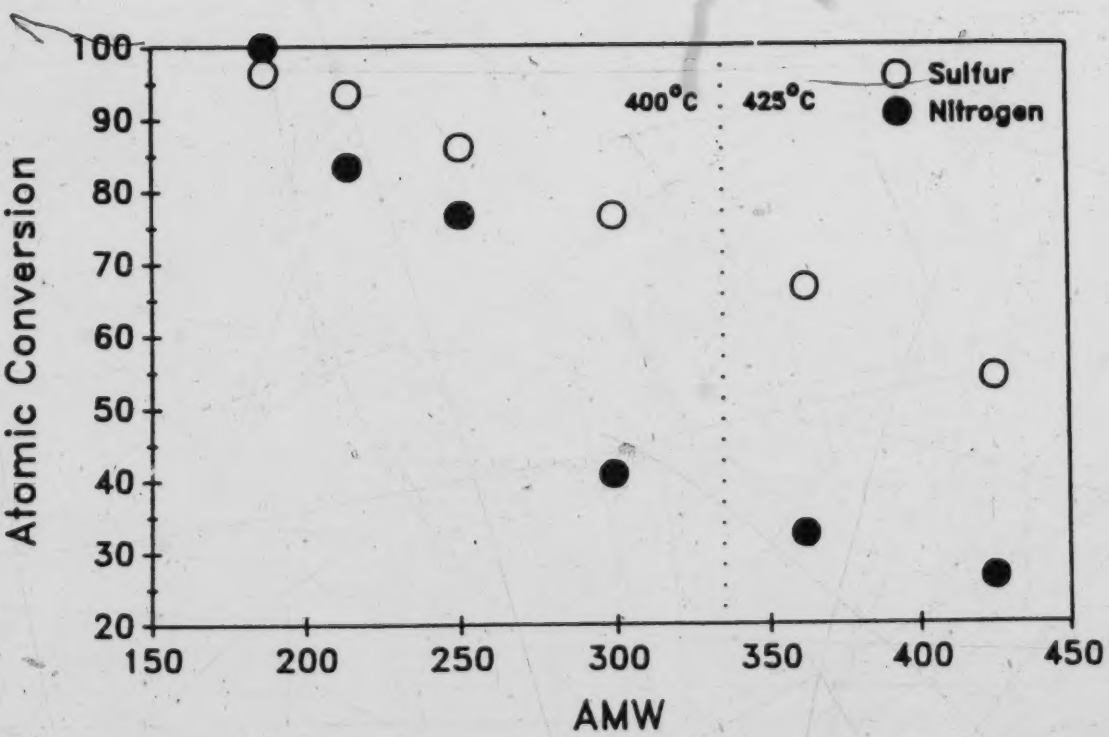

Figure 5.7: Sulfur and Nitrogen Conversion due to Hydroprocessing

values fall significantly lower on the plot than the 425°C values, illustrating the continued decline. Because heteroatom removal is primarily a catalytic process, this trend of decreasing conversion indicates that the rate of reaction is decreasing, due to increasing diffusion resistances, increasing steric hindrances, or decreasing intrinsic reactivity. Oxygen conversions are not plotted due to the inaccuracies in the method for measuring oxygen concentration in the samples. A better experimental determination of the oxygen content would allow tracking of the oxygen conversions as well. At present, estimates of the oxygen conversions are made based on the conversions of the nitrogen and sulfur and the experimental determinations of the oxygen content, a method which is only semi-quantitative.

The same type of plot is shown for the reduction in aromatic carbon in Figure 5.8. The percent reduction in aromatic carbon decreased with increasing feed average molecular weight, with the decrease continuing through the change in temperature. Reduction in aromatic carbon is also a catalytic process, and is due to both removal of heteroatoms and ring hydrogenation. As indicated by Furimsky (1978), Li *et al.* (1985), LaVopa and Satterfield (1987), and others, it is difficult to predict whether the ring hydrogenation reaction or the heteroatom removal before ring hydrogenation reaction (hydrogenolysis) is predominant (and whether each reaction goes to completion, with both heteroatom removal and aromatic carbon conversion). The selectivity of the catalyst may be examined indirectly, by examining the ratio of moles of aromatic carbon converted per mole of heteroatoms removed. This ratio may be calculated using equation 5.1.

$$RCH = \frac{Q_{in} \cdot \rho_{in} \cdot f_{ar,in} \cdot C_{in} - Q_o \cdot \rho_o \cdot f_{ar,o} \cdot C_o}{Q_{in} \cdot \rho_{in} \cdot SON_{in} - Q_o \cdot \rho_o \cdot SON_o} \qquad 5.1$$

Smaller molecules, such as thiophene, will yield 4 moles of aromatic carbon converted per mole of heteroatoms removed, while large sulfur-containing molecules

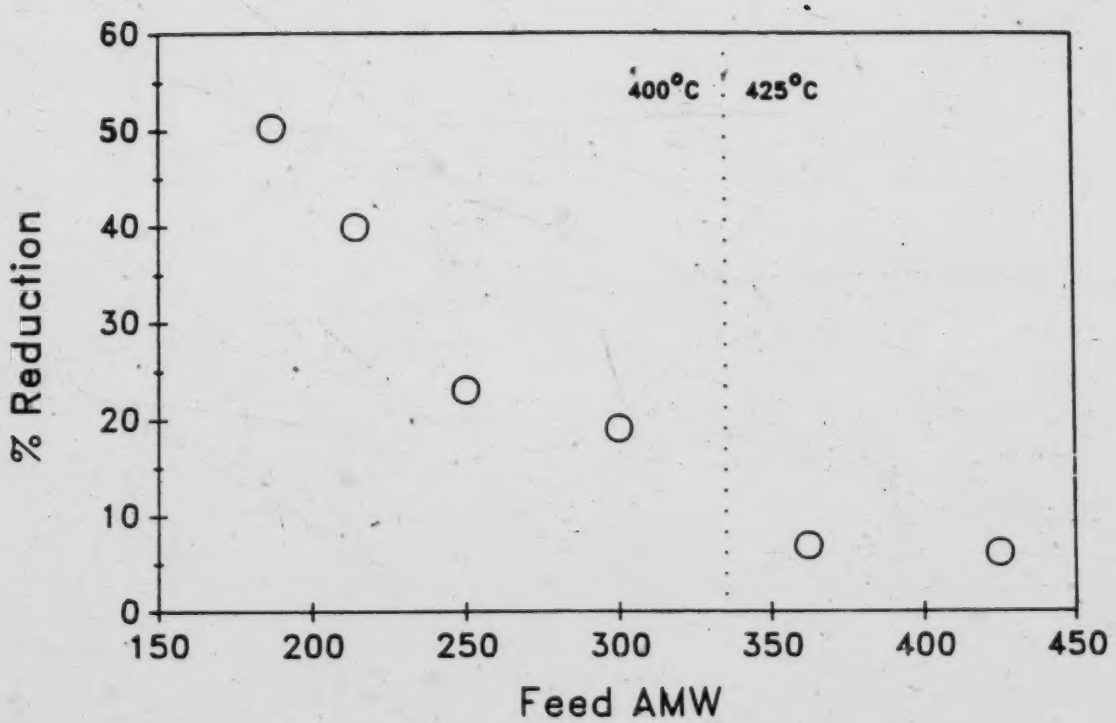

Figure 5.8: Reduction in Aromatic Carbon due to Hydroprocessing

such as dibenzothiophene will have 0 moles of aromatic carbon converted per mole of heteroatoms removed at optimal selectivity. If the ratio of moles of aromatic carbon converted per mole of heteroatoms removed is large for the heavy fractions, it indicates that the selectivity for removal of heteroatoms is poor (as there should be no thiophene compounds present, and therefore the ratio should be two or less). Performing this calculation on the whole oil gives a ratio of approximately 3, indicating that some hydrogenation of aromatic compounds proceeds in conjunction with heteroatom removal. For the SCGO fractions, the ratio decreases from 6.9 for the lightest fraction to 5.5, 3.8, and 3.1 for the next three fractions. For the two heaviest fractions, the ratios at 425°C are 0.4 and 2.3, indicating slight aromatic hydrogenation in conjunction with heteroatom removal.

Reduction in Density and Molecular Weight

The reduction in density (*i.e.* specific gravity at 23°C) is plotted in a similar fashion to the previous two figures in Figure 5.9. The effect of average molecular weight of the feedstock is similar to the previous figures, with the percent reduction decreasing with increasing molecular weight. The effect of temperature is much larger than in the two previous plots, however, and the increasing reduction due to increasing temperature dominates over the decreasing reduction in density expected from the increasing average molecular weight of the feedstock. The reduction in density was due to both catalytic and non-catalytic reactions, with heteroatom removal, hydrogenation, and thermal cracking all playing significant roles. The decreasing trend with molecular weight was most probably due to the decreasing rates of the catalytic reactions, while the large increase seen with the 25°C increase in temperature is likely due to the increasing rate of the thermal cracking reactions.

A different view on the thermal cracking reactions is provided by Figure 5.10, where the average molecular weight of the products is plotted against the

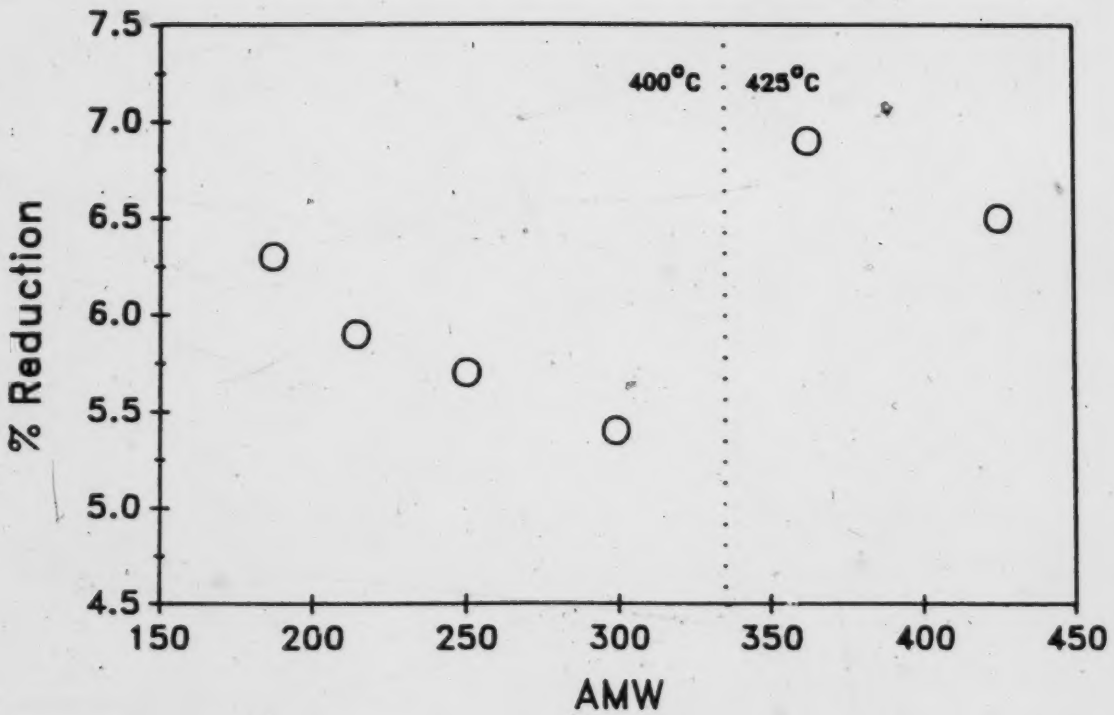

Figure 5.9: Reduction in Density due to Hydroprocessing

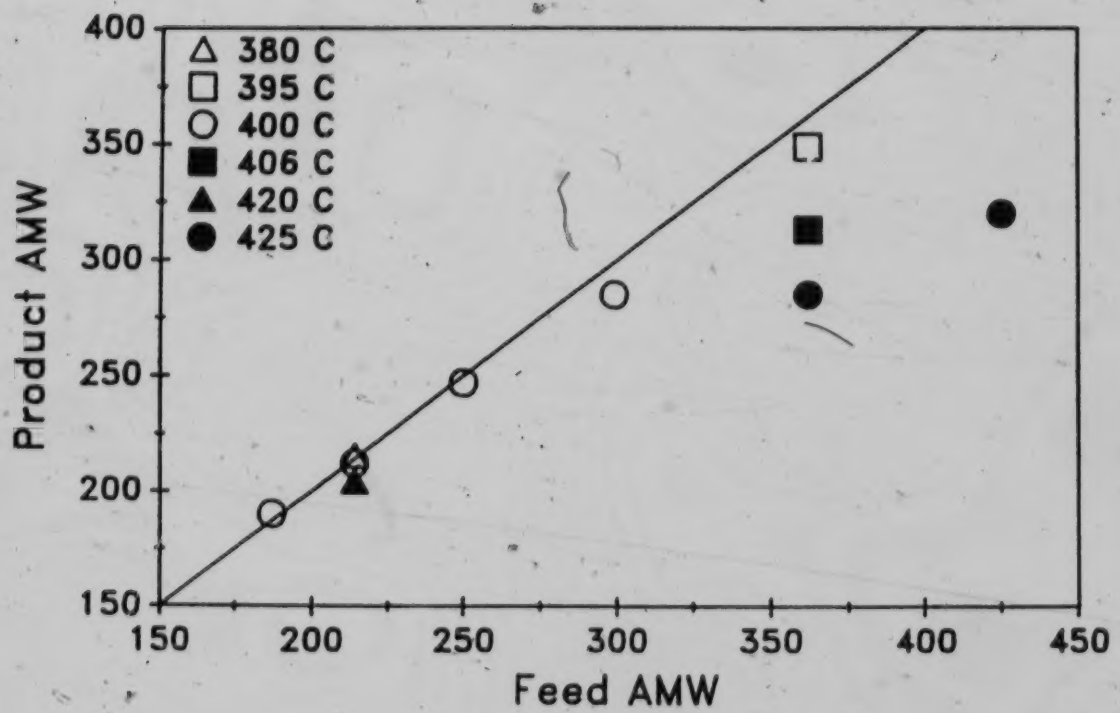

Figure 5.10: Reduction in Molecular Weight due to Hydroprocessing

average molecular weight of the feedstocks. The molecular weight of the products are plotted for each run, with different temperatures represented by different symbols on the plot. The diagonal line represents identical molecular weight in feeds and products. The first three feedstocks gave very little reduction in molecular weight (with the exception of CGOD2 at 420°C). As the molecular weight of the feedstocks was increased, however, greater reductions were observed in the molecular weights of the products. At 400°C, there was essentially no reduction in molecular weight with CGOD3, while a 5% reduction was observed for CGOD4. An estimated 9% decrease in molecular weight would be observed for CGOD5 at 400°C (based on interpolation). At 425°C, the reduction in molecular weight increased from 21% for CGOD5 to 25% for CGOD6. Since the reduction in molecular weight is primarily due to two reactions, removal of heteroatoms and thermal cracking of carbon-carbon bonds, and the rate of the heteroatom removal reactions decreased with increasing molecular weight, the rate of thermal cracking must be increasing with increasing average molecular weight of the feeds regardless of temperature effects. Hence, in reacting two similar feedstocks of differing molecular weights, thermal cracking will play a more important role in the hydroprocessing of the heavier feedstock.

A more direct method for studying cracking reactions is to estimate the moles of carbon-carbon bonds per mole of oil for feeds and products. The average molecular weight of the oil and the elemental analysis of the oil give the moles of carbon per mole of oil, and thus the total moles of carbon ligands per mole of oil. By subtracting the bonds used by hydrogen and heteroatoms, the total number of sites for carbon-carbon bonds can be estimated, as in Equation 5.2.

$$ABS = 4 \cdot n_c - n_h - 2 \cdot (n_s + n_o + n_n) \qquad 5.2$$

In Equation 5.2, the various ratios (n_c, n_h, n_o, n_n, n_s) are calculated by multiplying the weight percent of the element in the sample by the average molecular weight of the sample, and dividing by the molecular weight of the element. By multiplying the number of available sites (ABS) by the term $(\frac{1}{2} - \frac{1}{6} \cdot f_{ar})$, where f_{ar} is the fraction of carbon that is aromatic (from ^{13}C NMR), the number of actual carbon-carbon bonds was determined. The only uncertainty in this estimate for the total number of carbon-carbon bonds arises from the number of carbon-heteroatom bonds for each heteroatom (*e.g.* nitrogen may have 1, 2, or 3 C–N bonds corresponding to amides, indoles, and N–substituted indoles). Because the heteroatom content of the oils is relatively low, this uncertainty is negligible. A more detailed procedure for calculating the number of carbon-carbon bonds is given in Appendix C. Table 5.2 shows the average number of carbon-carbon bonds per molecule for the feeds and products, and also shows the percent carbon-carbon bond breakage.

Table 5.2: Carbon–Carbon Bond Estimates

Feed	T (°C)	Feed C–C	Prod C–C	% Breakage
CGOD1	400	14.0	14.1	0
CGOD2	380	16.1	16.1	0
CGOD2	400	16.1	15.9	0
CGOD2	420	16.1	16.2	0
CGOD3	400	19.3	19.3	0
CGOD4	400	22.9	23.0	0
CGOD5	395	27.8	27.9	0
CGOD5	406	27.8	24.6	12
CGOD5	425	27.8	22.8	18
CGOD6	425	32.3	25.6	21

For feedstocks CGOD1 through CGOD4, and for CGOD5 at 395°C, no breakage of carbon-carbon bonds was observed (within error limits). For feedstocks CGOD5 and CGOD6, however, bond breakage became significant, increasing from 0% to 18% for CGOD5 as the temperature was increased from 395°C to 425°C, and

increasing to 21% for CGOD6 at 425°C. This result showed a definite increase in breakage of carbon-carbon bonds, and therefore thermal cracking reactions, with increasing average molecular weight of the feedstocks.

The molar ratio of C_1 to C_2 is shown as a function of molecular weight in Figure 5.11. The ratio of methane to two-carbon gases in the effluent gas stream increased with increasing feed molecular weight, from 0.7 for the lightest feedstock to 2.0 for the fifth feedstock. There was a slight decrease in the molar ratio for CGOD6. Temperature had little effect on this ratio regardless of the oil fraction; there was essentially no change as the temperature was increased from 380°C to 420°C for CGOD2 (C_1/C_2 ratios of 1.107, 1.163, and 1.169) or with a temperature increase from 395°C to 425°C for CGOD5 (C_1/C_2 ratios of 2.006, 2.010, and 1.959). This tendency for a lower C_1 to C_2 ratio at lower molecular weight may indicate a greater proportion of side chains, especially side chains of three-carbon length. The lower C_1/C_2 ratio could be due to lower aromaticity and aromatic ring condensation for the lighter fractions.

Structural Group Analysis

The carbon distribution of the products is shown in Figure 5.12. The naphthenic carbon content of the products was very similar to that of the feedstocks; the distribution was similar both in shape and value. The aromatic carbon contents, as seen previously, were decreased for all fractions, with the largest decrease in the light fractions. The paraffinic carbon showed the opposite trend; the paraffinic carbon content increased for all fractions with the greatest increases in the lightest fractions. The large increases in paraffinic carbon and the large decreases in aromatic carbon for the light fractions may be due to the presence of substituted thiophenic compounds in the feedstocks (Payzant *et al.*, 1988). These compounds, upon desulfurization, would cause the loss of four aromatic carbon atoms and the

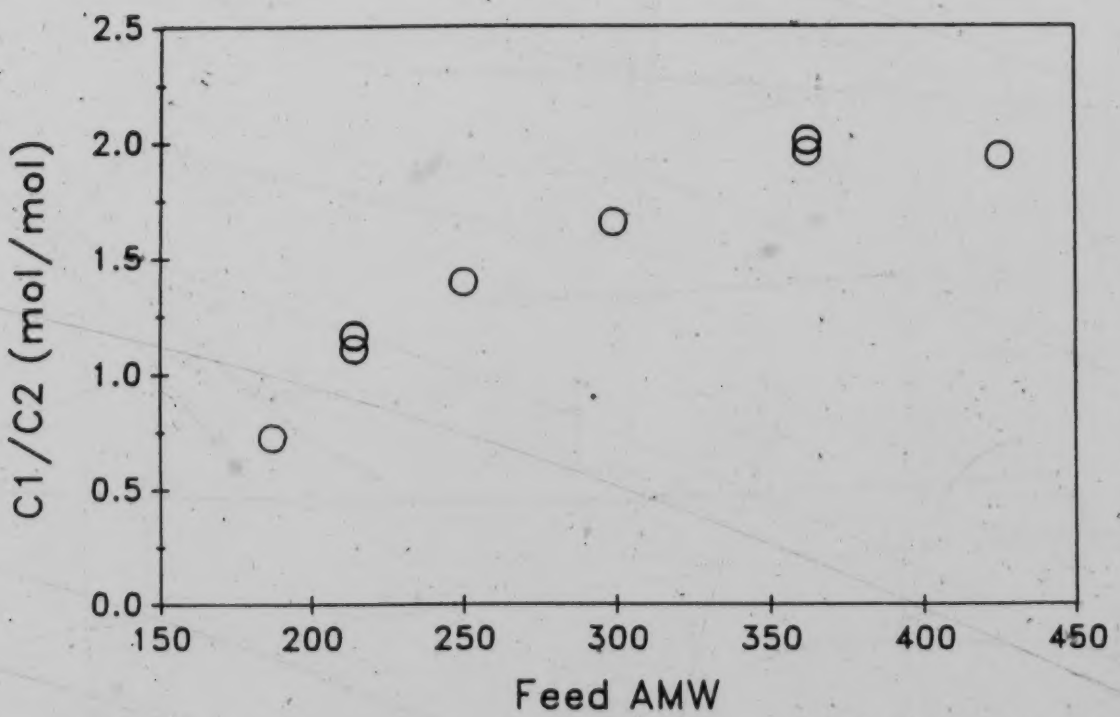

Figure 5.11: Molar C_1 to C_2 Ratio in the Effluent Gas

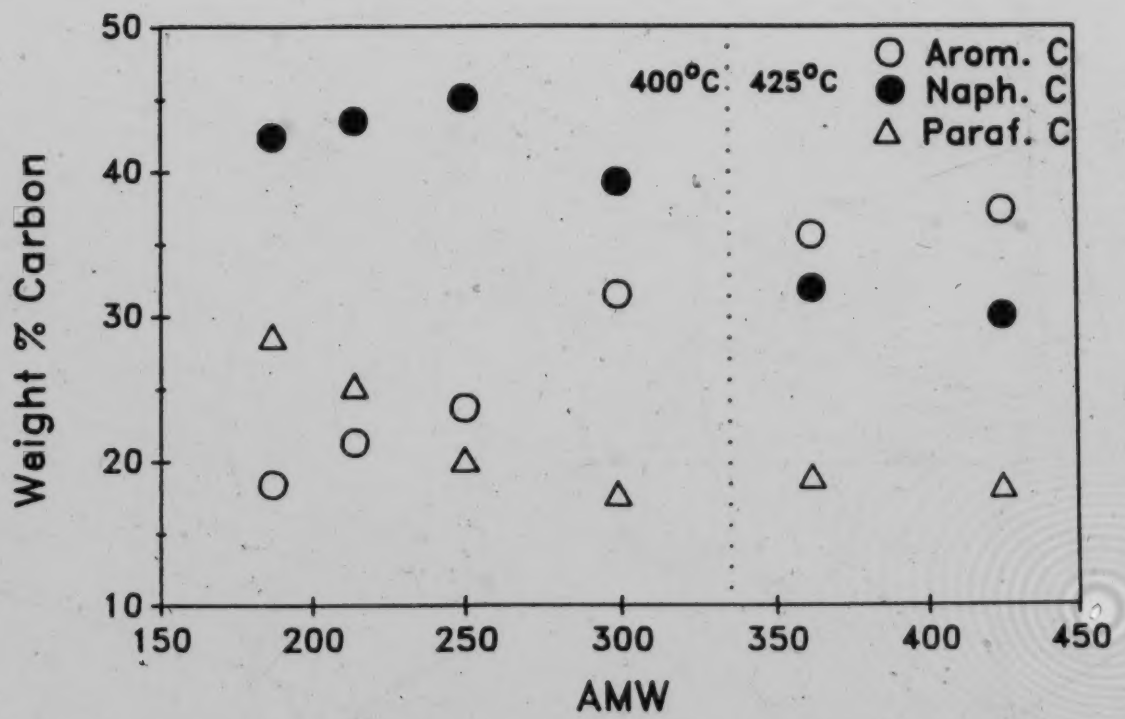

Figure 5.12: Distribution of Carbon Types in the Products

gain of at least four paraffinic carbons. There would also be a loss of some α–CH_2 groups associated with the original thiophene.

The molecular parameters that were calculated for the feedstock samples were also calculated for the products and are shown in Figure 5.13. The products did not exhibit a significant minimum in the mean side chain length, and there was little change in the mean side chain length with increasing feedstock average molecular weight or with increasing temperature. The mean ring number, or average number of rings per aromatic structure, was decreased for most fractions, with a slight increase for CGOD4 and CGOD5. This increase may indicate the loss of smaller, more reactive aromatic compounds and leaving behind of the larger, more refractory compounds.

5.3 Kinetics

The data and results from the kinetic analysis are given in Appendix D, beginning with the observed pseudo-first-order rate constants for HDS, HDN, pitch conversion, and gas formation. For this study, pitch was defined as material boiling over 343°C. The pseudo-first-order rate constants, conversions, and rates of reaction were calculated based on inlet and outlet concentrations, liquid-hourly-space velocity, and inlet and outlet densities, as shown in equations 5.3 to 5.5.

$$X = \frac{Q_{in} \cdot \rho_{in} \cdot S_{in} - Q_o \cdot \rho_o \cdot S_o}{Q_{in} \cdot \rho_{in} \cdot S_{in}} \qquad 5.3$$

$$k = X \cdot \frac{Q_{in} \cdot \rho_{in} \cdot S_{in}}{Q_o \cdot \rho_o \cdot S_o} \cdot \frac{LHSV}{3.6} \qquad 5.4$$

$$R_r = \frac{1000}{3.6} \cdot (\rho_{in} \cdot S_{in} - \rho_o \cdot S_o) \cdot LHSV \qquad 5.5$$

Rate constants for pitch conversion were not calculated for runs MG–32 to MG–35.

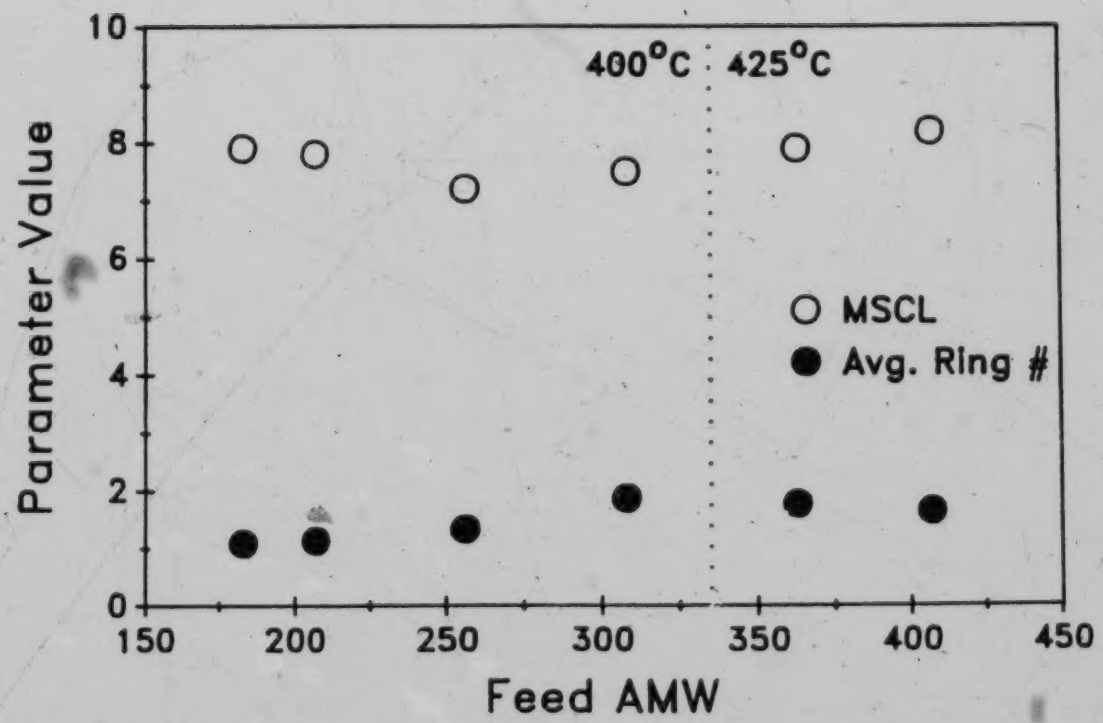

Figure 5.13: Distribution of Mean Side Chain Length and Average Ring Number in the Products

Apparent Activation Energies

Feedstocks CGOD2 and CGOD5 were each upgraded at three different temperatures to estimate apparent Arrhenius parameters. The Arrhenius plots [$\ln(k_1)$ vs. $1/T$] for HDS and HDN for the two feedstocks are shown in Figures 5.14 (HDS) and 5.15 (HDN). The summaries of the regressions are presented in Appendix D, Table D2. Table 5.3 shows the apparent activation energies for HDS and HDN for the two feedstocks.

Table 5.3: Summary of Activation Energies for Catalytic Reactions (kJ/mol)

Feed	Hydrodesulfurization		Hydrodenitrogenation	
	Apparent	Intrinsic	Apparent	Intrinsic
CGOD2	109 ± 21	165 ± 29	78 ± 23	103 ± 34
CGOD5	149 ± 5	205 ± 12	109 ± 14	121 ± 15

The apparent activation energy for HDS ($E_{a,app}$ ± standard deviation) increased approximately 37% from CGOD2 (AMW = 214) to CGOD5 (AMW = 362). The plot for HDN (Figure 5.15) shows similar behaviour, as the apparent activation energy increased from 78 kJ/mol to 109 kJ/mol over the same molecular weight range (an increase of approximately 40%). These increasing activation energies indicated that either the intrinsic activation energy was increasing, or that diffusion limitations were becoming less severe. The effect of diffusion limitations upon apparent activation energy was discussed by Massagutov *et al.* (1967), where a vacuum gas oil had increasing diffusion limitations at higher temperatures, causing a decrease in apparent activation energy. Since the feed samples in this study are of increasing molecular weight, and therefore decreasing diffusivity, the trends in the apparent activation energy suggest that diffusion limitations were not significant for the heavy fractions. Diffusion effects are considered in detail in a later section.

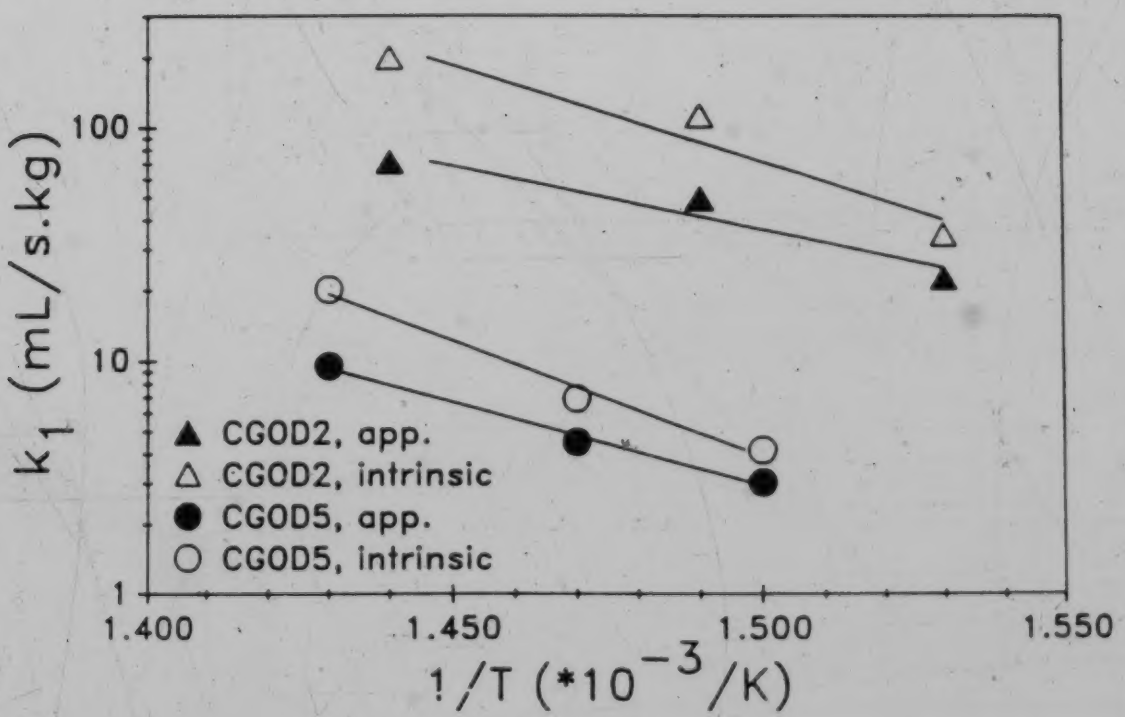

Figure 5.14: Arrhenius Plot for HDS

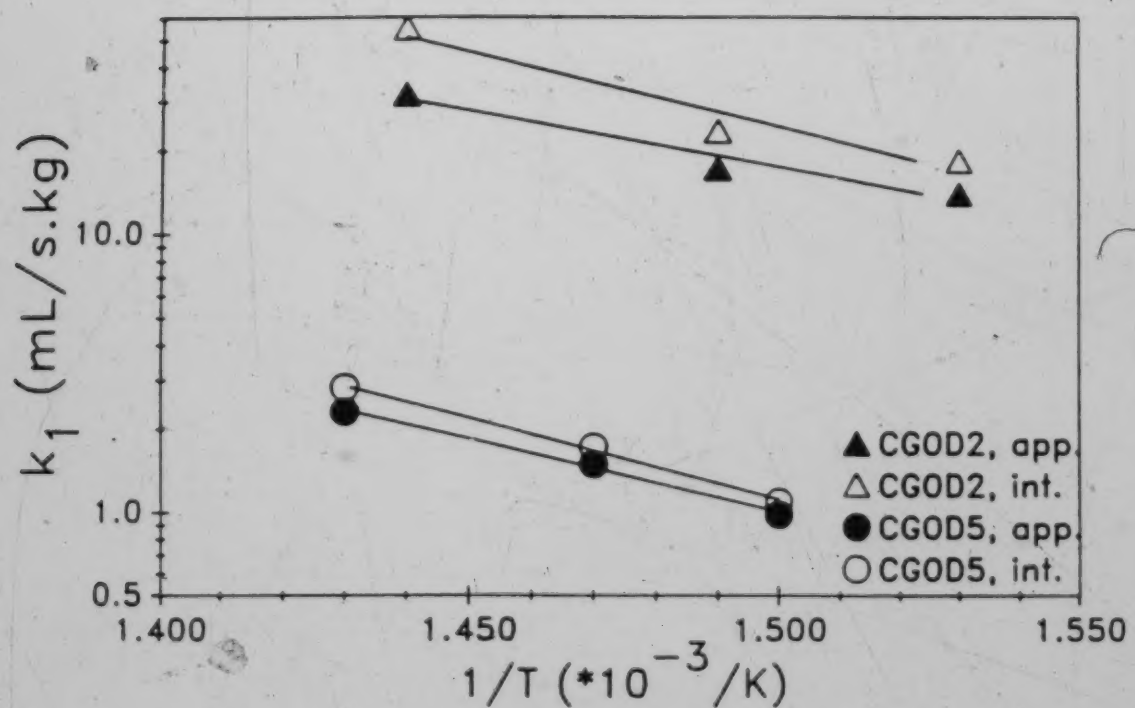

Figure 5.15: Arrhenius Plot for HDN

The apparent activation energy for gas formation remained approximately constant between the two samples (Figure 5.16). The apparent activation energy for CGOD5 was 153 ± 1 kJ/mol, while for CGOD2 the apparent activation energy was 145 ± 21 kJ/mol. Gas formation was primarily a thermal reaction, involving the thermal cracking of carbon-carbon bonds; therefore, molecular weight effects such as steric hindrances and diffusion limitations should not significantly affect the apparent activation energy observed for this non-catalytic reaction. No net effect of molecular weight on gas formation was observed in this study, although the rate of thermal cracking of C–C bonds did increase with molecular weight (indicating a decrease in the apparent activation energy for carbon-carbon bond breakage). Catalytic removal of heteroatoms from benzothiophene-type structures, with carbon chain substitution next to the heteroatom (the preferable location for chain substitution, as shown by Payzant *et al.* (1988)) would increase the average chain length, and thus decrease the apparent activation energy for gas formation. Since the heteroatom removal decreased with molecular weight, the catalytic effects must also have decreased with increasing molecular weight. If the net apparent activation energy is due to a combination of thermal and catalytic reactions, and the apparent activation energy for the thermal rupture of carbon-carbon bonds is decreasing while the apparent activation energy for catalytic heteroatom removal is increasing, the negligible net change seen in the apparent activation energy for gas formation must be due to these two effects cancelling out.

Figure 5.17 shows the Arrhenius plot for pitch conversion for CGOD5, which indicates an apparent activation energy of 239 ± 71 kJ/mol. The large standard error in the apparent activation energy was due to the large scatter in the data. Because of the large error, and the lack of an activation energy for pitch conversion for CGOD2, little can be said about this value. One item to note, however, is that if the low temperature (high 1/T) point is discarded, the apparent activation energy

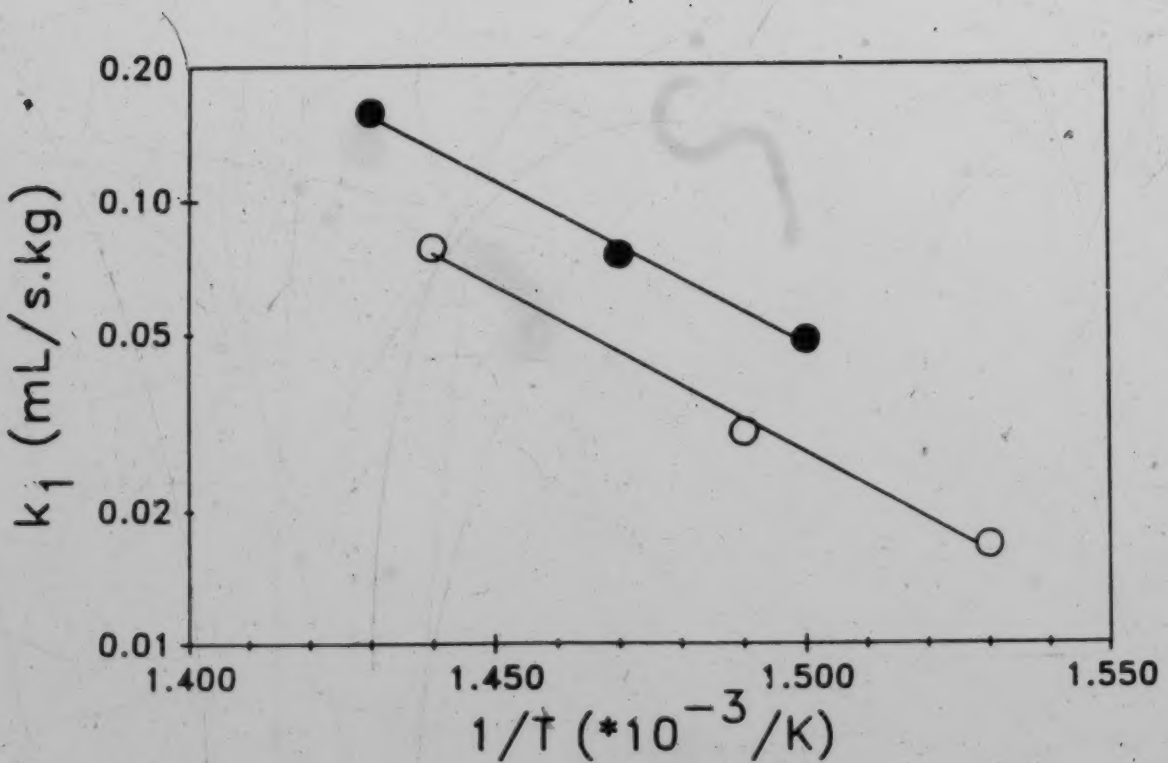

Figure 5.16: Arrhenius Plot for Gas Formation

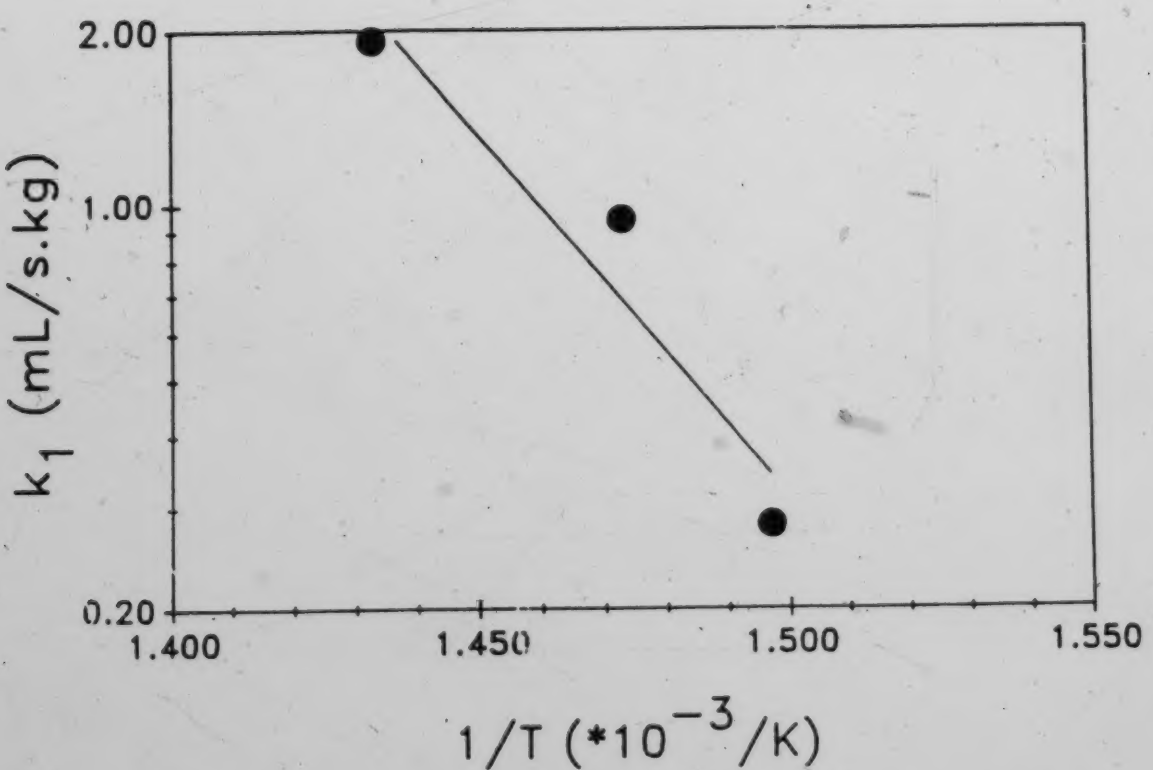

Figure 5.17: Arrhenius Plot for Pitch Conversion

for this reaction becomes 148 kJ/mol, essentially equal to that for gas formation. This result is encouraging, as the two reactions have similar mechanisms (primarily thermal cracking of carbon-carbon bonds, with a possible small contribution from catalytic effects), although the catalytic effects should be more noticeable with pitch conversion (due to hydrogenation and heteroatom removal also lowering the boiling point of a compound). Omitting the low temperature point is not entirely justified when only three points are available; however, the low temperature point is the one subject to the most error, with a pitch conversion of only 5.8% (compared to 15.9% and 28.7% for the two higher temperature cases).

Variation of Rate Constants with Molecular Weight of the Feedstocks

The rate constants for HDS and HDN, as shown in Figure 5.18, exhibit an obvious decreasing trend with molecular weight. A plot of the pseudo-first-order rate constants at 400°C for HDS and HDN versus average molecular weight of the feedstocks (Figure 5.18) shows a linear trend in log-log co-ordinates. The rate constant for CGOD5 at 400°C was interpolated using the three measured rate constants and the calculated apparent activation energy. The value for CGOD6 was estimated by extrapolating the known apparent activation energies to the higher molecular weight, and then estimating the rate constant at 400°C using the data at 425°C. Comparison to the rate constants for the whole oil indicates that the trend could be useful for interpolating estimates of the pseudo-first-order rate constants for any fraction of this oil, narrow- or wide-boiling. Given an estimate of the average boiling point and the specific gravity of the sample, the molecular weight may be estimated from the re-correlated Winn equation and used to estimate the rate constant. Given that this plot shows similar behaviour for sulfur and nitrogen, a question arises: why do HDS and HDN show apparent orders of 1.5 and 1.0, respectively, in industrial situations? The difference in behaviour arises from two

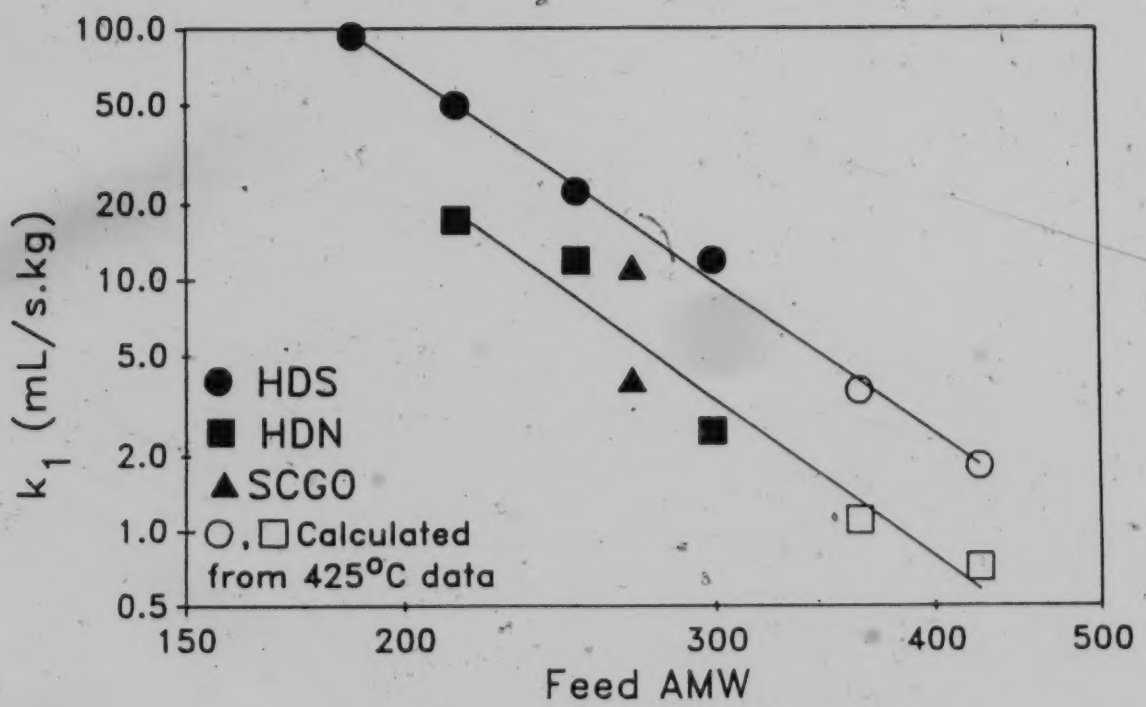

Figure 5.18: HDS and HDN Rate Constants versus Feed AMW

facts; nitrogen does not display as wide a range of reactivities as does sulfur, and HDN is generally at lower conversion levels than HDS. As both high conversion and wide ranges of reactivities are required for fractional order kinetics, the HDS and HDN need not have the same kinetic behaviour.

Given the conversions for the catalytic reactions for the fractions, an overall conversion for the whole oil may be estimated by summing over the fractions as in equation 5.6.

$$X_t = \frac{\Sigma f_i \cdot S_i \cdot X_i}{\Sigma f_i \cdot S_i} \qquad 5.6$$

Once this conversion has been calculated, an overall rate constant may be estimated by combining equations 5.3 and 5.4.

$$k_t = \frac{LHSV}{3.6} \cdot \frac{X_t}{1-X_t} \qquad 5.7$$

These two equations may be used to predict the conversions and rate constants for the whole oil from the data for the narrow-boiling fractions. Using these equations, the predicted sulfur and nitrogen conversions are 74% and 44%, giving rate constant predictions for sulfur and nitrogen of 10 and 2.7 mL/(s·kg catalyst), respectively. The actual results (Gray, 1989) show conversions of 76% and 53% for sulfur and nitrogen, with rate constants of 11.2 and 4.0 mL/(s·kg catalyst). Although the predicted and observed rate constants are substantially different, the predicted conversions are reasonably close to those observed in actual hydroprocessing experiments. The deviation may be due to solvent effects (a given fraction may behave differently in the whole oil than upon isolation) or differences between the oil used for the whole oil study and that used for this study.

The rate constants follow a power-law function of average molecular weight

only for catalytic reactions, and not for the thermal reaction of gas formation. The pseudo-first-order rate constants at 400°C for gas formation and pitch conversion are plotted in Figure 5.19. The gas-formation rate constants were not a linear function of molecular weight in log-log co-ordinates, as a definite curve is seen for the first four points. The jump in the gas formation rate constant for the fifth and sixth runs could be due to the pressure cycling that was observed for these runs (see Appendix A), or to inaccuracies in the calculation of the gas compositions due to normalizing on a basis of 100%, including the hydrogen concentration (on the order of 95%). A small error in the measurement of the hydrogen concentration can result in a large error for the yield of hydrocarbon gases. The three available data points for pitch conversion show possible power-law behaviour, although three points on a log-log scale are not conclusive. These data correspond to an apparent activation energy for pitch conversion for CGOD5 of 239 kJ/mol. This value was heavily weighted by the low temperature point, where the catalytic reactions (*i.e.* HDS) may be contributing more to the pitch conversion than the thermal reactions. Given that the data for pitch conversion for CGOD3 and CGOD4 were also at 400°C, the straight line for pitch conversion rate constants is expected as the thermal reactions should only play a minor role. If the rate constant for pitch conversion for CGOD5 is estimated based on only the two higher temperature points (apparent activation energy of 148 kJ/mol), as discussed previously, deviation from the linear behaviour is more pronounced. This estimated rate is shown by the triangle in Figure 5.19, where the open circles are the measured rate constants for pitch conversion.

Intrinsic Reaction Rates

The preceding kinetic analysis has all been based on observed rates of reaction. The intrinsic rates of reaction must be examined to show the amount of

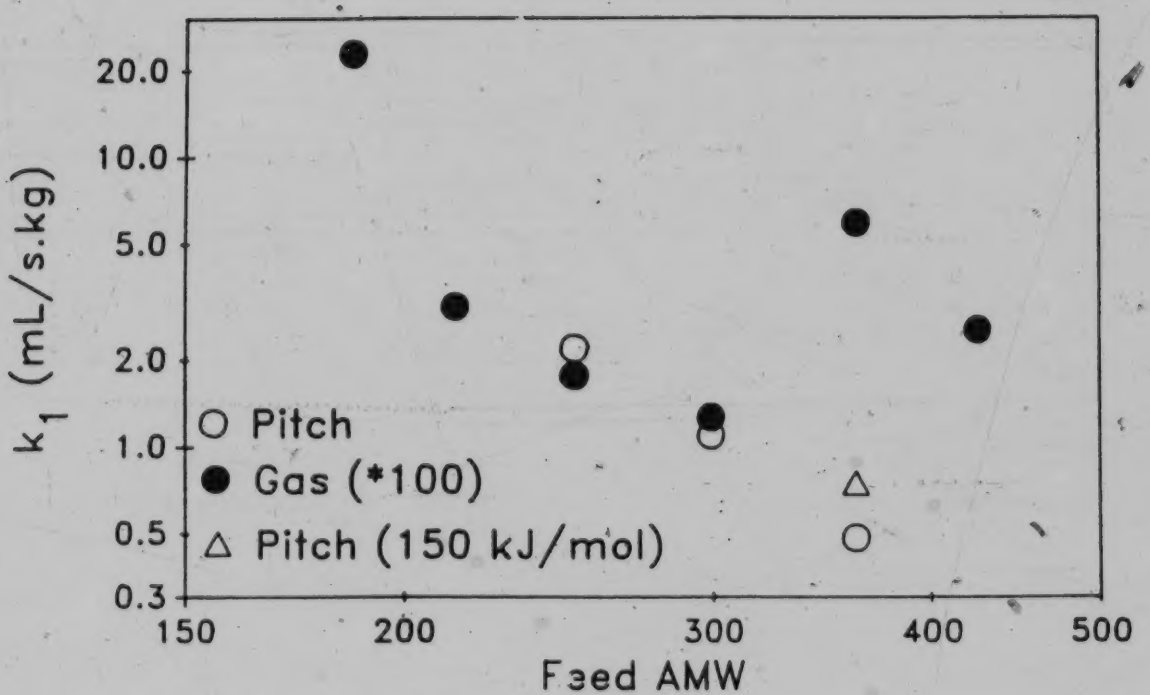

Figure 5.19: Gas Formation and Pitch Conversion Rate Constants vs. AMW

diffusion limitation in the reactions, and to examine the variation of intrinsic rates of reaction with molecular weight. Given the density, average boiling point, and average molecular weight of the sample, the density and viscosity of the oil at reactor conditions can be calculated, and hence the molecular diffusivity can also be calculated (see chapter 3). The effective diffusivity may be estimated from the molecular diffusivity via estimates of the catalyst porosity and tortuosity. With the effective diffusivity, catalyst density, catalyst specific surface area, and observed pseudo-first-order reaction rate constant, the intrinsic rate constant, effectiveness factor, and Thiele modulus may be calculated through solution of the non-linear algebraic equations shown below.

$$k_{obs} = \frac{3 \cdot \mathscr{D}_{eff}}{R^2 \cdot \rho \cdot S_a} \cdot \left[R \cdot I \cdot \coth(R \cdot I) - 1 \right] \qquad 5.8$$

$$I = \left[\frac{k_i \cdot \rho_c \cdot S_a}{\mathscr{D}_{eff}} \right] \qquad 5.9$$

This calculation used the feed properties to calculate the properties of the reactants at reactor conditions. The estimates for density and viscosity at reactor conditions are given in Table D3, Appendix D, as are the estimates for molecular diffusivity (based on the Wilke-Chang and Scheibel equations). The resulting intrinsic rate constants for HDS and HDN are given in Tables D4 and D5, and are summarized in Figure 5.20 as the logarithm of the intrinsic rate constants at 400°C versus the logarithm of the molecular weight. The plots are again linear on log-log co-ordinates, and show the reduction in intrinsic reactivity with increasing average molecular weight of the feedstocks. The apparent and intrinsic activation energies are summarized in Table 5.3. Although the apparent rate constants indicated an increase in apparent activation energy with increasing molecular weight, the data do not indicate a shift in the intrinsic activation energy with increasing molecular

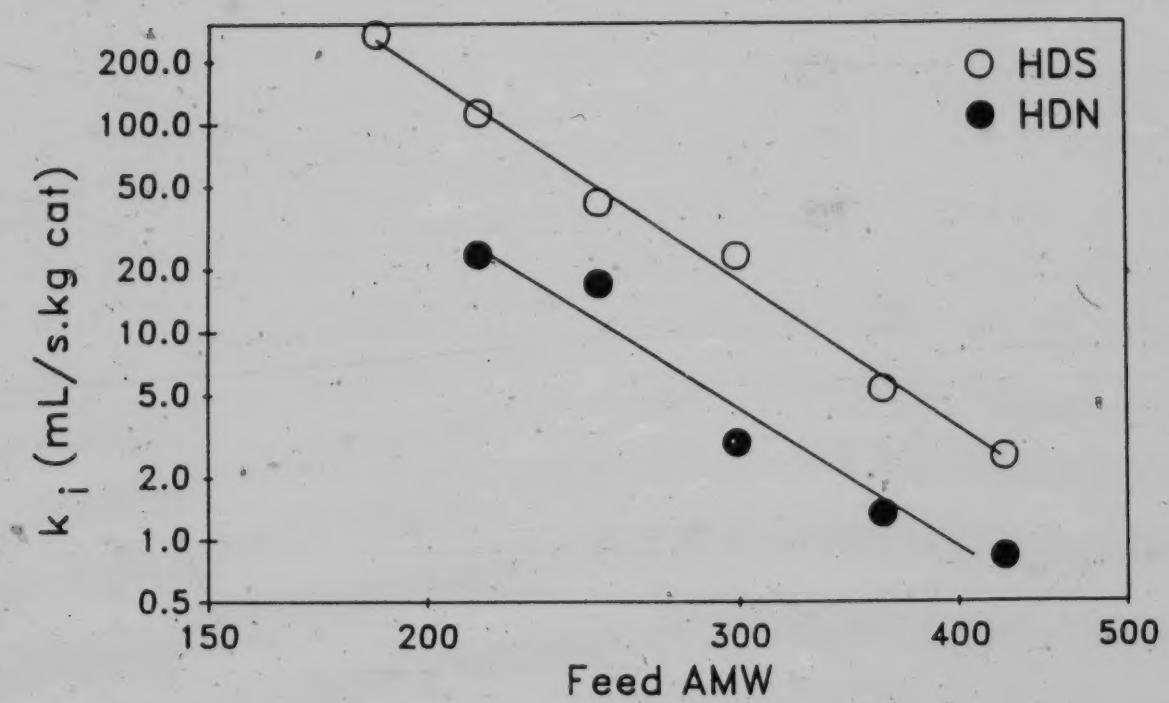

Figure 5.20: Intrinsic HDS and HDN Rate Constants versus Feed AMW

weight. The shift seen in the apparent activation energy may be due to decreasing diffusion limitations. Although the data do not support increasing intrinsic activation energies with increasing molecular weight, neither do they support decreasing pre-exponential factors as the basis for the decreasing rate constants.

The plot of effectiveness factor for HDS and HDN versus average molecular weight is shown in Figure 5.21. This figure shows the effectiveness factor at 400°C, with the value for CGOD5 interpolated from the 395°C and 406°C values, and the value for CGOD6 calculated on the assumption that the ratio of effectiveness factors for CGOD5 and CGOD6 at 425°C is the same as the ratio at 400°C. The effectiveness factor increased to a maximum for CGOD5, before starting to decrease at higher molecular weights. The maximum effectiveness factor was approximately 0.69 for HDS and 0.88 for HDN. This behaviour was mirrored in the plot of Thiele modulus versus feedstock average molecular weight (Figure 5.22). The values for the Thiele modulus declined to a minimum for CGOD5; approximately 2.86 for HDS and 1.44 for HDN. The Thiele modulus is defined as the intrinsic reaction rate divided by the rate of diffusion; thus for the first five feedstocks, the intrinsic reaction rate decreases faster than the diffusion rate, while for very heavy samples the diffusion rate decreases faster than the intrinsic reaction rate, causing the slight increase in the Thiele modulus. This analysis shows that the change in rate constants with molecular weight was not primarily due to diffusion limitations. The intrinsic rate of reaction for heteroatom removal decreases with increasing molecular weight of the feedstock, presumably due to increasing steric hindrances blocking the approach of the heteroatom to the catalyst surface.

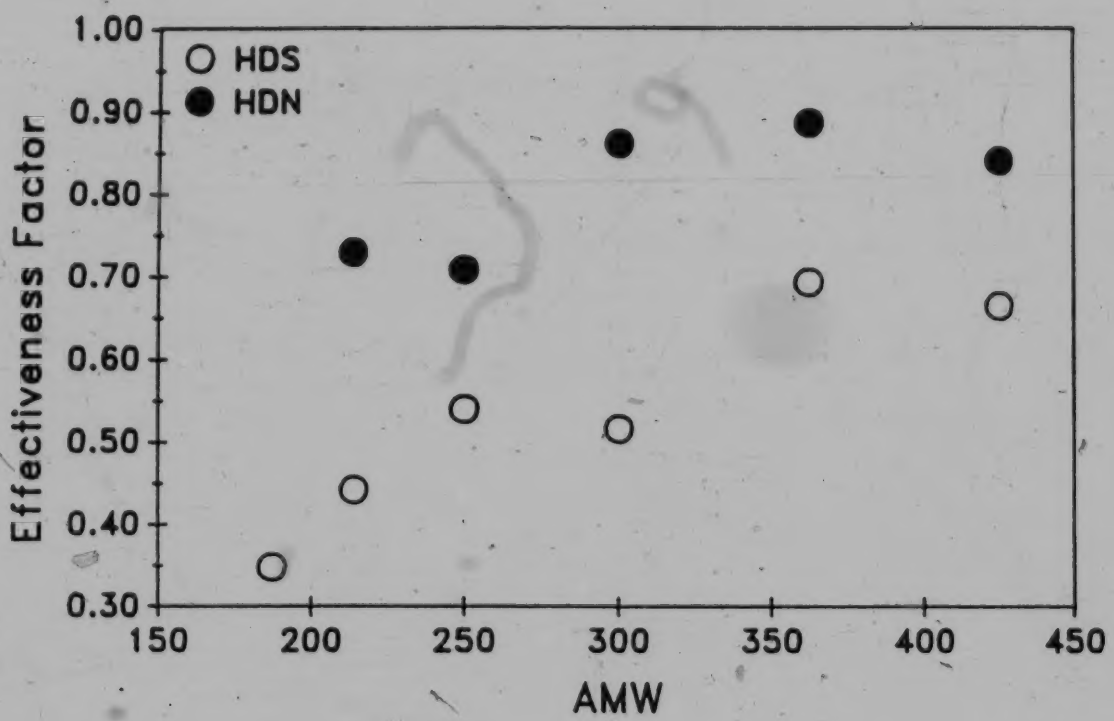

Figure 5.21: Effectiveness Factor versus Feed AMW for HDS and HDN

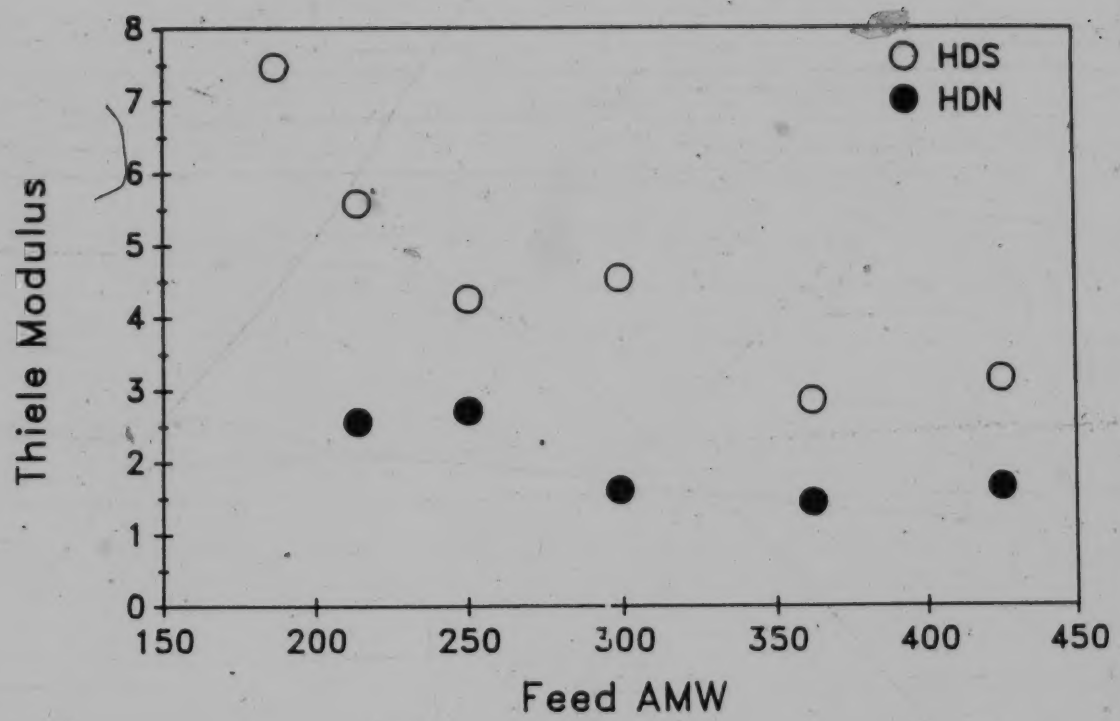

Figure 5.22: Thiele Modulus versus Feed AMW for HDS and HDN

Chapter 6: SUMMARY and CONCLUSIONS

The sulfur, nitrogen, and oxygen contents of the gas oil fractions all increased with increasing molecular weight. The atomic hydrogen to carbon ratio decreased with increasing molecular weight, indicating increasing aromaticity and carbon substitution. The specific gravity of the samples increased with increasing AMW. The aromatic carbon content increased over the range of molecular weights studied, while the naphthenic carbon content decreased after passing through a maximum at an average molecular weight of approximately 230. The mean number of aromatic rings per aromatic structure increased over the range of samples.

The Winn correlation was shown to be a useful model for predicting average molecular weights of oil samples, although systematic deviations were noted. With re-correlation, the deviations from the measured molecular weights were random, and on the order of 5%. Without re-correlation, the estimates were internally consistent, and would not yield different results for this study.

Thermal cracking of carbon-carbon bonds was examined by estimating the average number of carbon-carbon bonds per molecule. The rate of thermal cracking increased with increasing molecular weight. Negligible cracking activity was observed for the four lightest fractions, but increasing activity was noted for the heaviest two fractions. The apparent activation energy for gas formation did not change significantly with increasing molecular weight, but an Arrhenius plot for pitch conversion (the conversion of 343°C+ material) showed curvature corresponding to a possible changeover from dominance by catalytic reactions at low temperatures to dominance by thermal reactions at higher temperatures.

The rates of reaction for catalytic reactions (HDS, HDN, and aromatic carbon conversion) decreased with increasing average molecular weight of the feed for all samples. Although the rate of diffusion decreased for these samples, the decreasing reaction rates were not due to increasing diffusion limitations, but were

due to changes in the intrinsic reactivity of the fractions. Both the observed and intrinsic reaction rate constants followed a power-law relationship with molecular weight (linear on a log-log plot). The observed lack of diffusion limitations in reactions of heavy material was borne out both by increasing apparent activation energies for HDS and HDN and by a study of the Thiele moduli and effectiveness factors for these reactions. The diffusion limitations were significant only for the very light samples. The changes in intrinsic reactivities were likely due to increasing steric hindrances with increasing molecular weight, although other structural effects, such as aromatic carbon content, may have had an impact as well.

Chapter 7: RECOMMENDED FURTHER WORK

Follow-up studies are required to investigate the mechanism behind the decreasing reactivity for HDS and HDN and to investigate the thermal reactions in more details. A similar study with a more paraffinic oil would demonstrate the effects of aromaticity and provide information on whether the decreasing intrinsic reactivity was due to steric hindrances, aromaticity, or both.

A repeat of this study with approximately three or four fractions and thermal runs only would allow investigation of the behaviour of the thermal reactions with molecular weight, and would also allow investigation of the thermal reaction activation energies. Such a study would have to be carried out at temperatures in the 410°C to 440°C range to give precise estimates of rate constants.

One technique that needs to be further developed is the determination of the oxygen content of oil samples. The oxygen content of oil samples is notoriously difficult to determine precisely, and a better estimation method would allow tracking of the HDO reactions. Oxygen contents are not generally determined in industrial refineries, and oxygen conversions are generally assumed to follow the nitrogen conversions. A better method for determination of the oxygen contents would allow tracking of the HDS, HDN, and HDO reactions on an individual basis, and would provide for a better characterization of feedstocks.

Chapter 8: REFERENCES

Broderick, D.H. and Gates, B.C.; "Hydrogenolysis and Hydrogenation of Dibenzothiophene Catalyzed by Sulfided $CoO-MoO_3/\gamma-Al_2O_3$: The Reaction Kinetics"; *A.I.Ch.E.J.*; 27 (4); pp. 663–673; (1981).

Buell, B.E.; "Non–Aqueous, Differential Titration Applied to a Classification of Basic and Very Weak Basic Nitrogen Compounds in Petroleum"; *Anal. Chem.*; 39; pp. 756–761; (1967).

Chu, C.I., and Wang, I.; "Kinetic Study on Hydrotreating"; *Ind. Eng. Chem. Proc. Des. Dev.*; 21 (2); pp. 338–344; (1982).

Chung, S.Y.K.; Thermal Hydroprocessing of Heavy Gas Oils; M.Sc. Thesis, University of Alberta; 1982.

Dorbon, M., Ignatiadis, I., Schmitter, J–M., Arpino, P., Guiochon, G., Toulhoat, H., and Huc, A.; "Identification of Carbazoles and Benzocarbazoles in a Coker Gas Oil and Influence of Catalytic Hydrotreatment on their Distribution"; *Fuel*; 63 (4); pp. 565–570; (1984).

Fairbridge, C. and Kriz, J.F.; "Hydroprocessing of Coal–Derived Middle Distillate"; *Fuel Sci. Technol. Int.*; 4 (2); pp. 171–189; (1986).

Fairbridge, C. and Farnand, B.; "Hydrotreating Coal–Derived Naphtha"; *Fuel Sci. Technol. Int.*; 4 (3);pp. 225–248; (1986)

Fogler, H.S.; Elements of Chemical Reaction Engineering; Prentice–Hall; Englewood Cliffs, NJ; 1986.

Furimsky, E.; "Catalytic Deoxygenation of Heavy Gas Oil"; *Fuel*; 57 (4); pp. 494-496; (1978).

Furimsky, E., Ranganathan, R., and Parsons, B.I.; "Catalytic Hydrodenitrogenation of Basic and Non–Basic Nitrogen Compounds in Athabasca Bitumen Distillates"; *Fuel*; 57 (7); pp. 427–430; (1978).

Galiasso, R., Garcia, W., Ramirez de Aguidelo, M.M., and Andreu, P.; "Hydrotreatment of Cracked Light Gas Oil"; *Catal. Rev. – Sci. Eng.*; 26 (3 & 4); pp. 445–480; (1980).

Gray, M.R.; personal communication; (1989).

Ho, T.C. and Aris, R.; "On Apparent Second Order Kinetics"; *A.I.Ch.E.J.*; 33 (6); pp. 1050–1051; (1987).

Hoog, H.; "Catalytic Hydro–desulphurization of Gas Oil: Analysis of the Kinetics of the Reaction"; *Inst. Pet. J.*; 36; pp. 738–751; (1950).

Hughes, E.C., Stine, H.M., and Faris, R.B.; "Hydrodesulfurization of Heavy Petroleum Oils"; *Ind. Eng. Chem.*; 42 (9); pp. 1879–1882; (1950).

Jacobson, J.M. and Gray, M.R.; "Use of IR Spectroscopy and Nitrogen Titration Data in Structural Group Analysis of Bitumen"; *Fuel*; 66 (6); pp. 749–752; (1987).

Katti, S.S., Waterman, D.W.B., Gates, B.C., Youngless, T., and Petrakis, L.; "Catalytic Hydroprocessing of SRC–II Heavy Distillate Fractions. 3. Hydrodesulphurization of the Neutral Oils"; *Ind. Eng. Chem. Proc. Des. Dev.*; 23 (4); pp. 773–778; (1984).

Khorasheh, F.; "Structural Characterization of Alberta Gas Oils"; M.Sc. Thesis, University of Alberta; 1986.

Khorasheh, F., Gray, M.R., and Dalla Lana, I.G.; "Structural Analysis of Alberta Heavy Gas Oils"; *Fuel*; 66 (4); pp. 505–511; (1987).

Lapinas, A.T., Klein, M.T., Gates, B.C., Macris, A., and Lyons, J.E.; "Catalytic Hydrogenation and Hydrocracking of Fluoranthene: Reaction Pathways and Kinetics"; *Ind. Eng. Chem. Res.*; 26 (5); pp. 1026–1033; (1987).

Lavopa, V. and Satterfield, C.N.; "Catalytic Hydrodeoxygenation of Dibenzofuran"; *Energy and Fuels*; 1 (4); pp. 323–331; (1987).

Li, C–L., Xu, Z–R., and Gates, B.C.; "Catalytic Hydroprocessing of SRC–II Heavy Distillate Fractions. 4. Hydrodeoxygenation of Phenolic Compounds in the Acidic Fractions"; *Ind. Eng. Chem. Proc. Des. Dev.*; 24 (1); pp. 92–97; (1985).

Man, G.P.; Hydroprocessing of Heavy Gas Oil in a Continuous Stirred Tank Reactor; M.Sc. Thesis, University of Alberta; 1981.

Mann, R.S., Sambi, I.S., and Khulbe, K.C.; "Catalytic Hydrofining of Heavy Gas Oil"; *Ind. Eng. Chem. Res.*; 26 (3); pp. 410–414; (1987).

Massagutov, R.M., Berg, G.A., Kulinich, G.M., and Kirillov, T.S.; "Kinetics of High–Sulphur Distillate Hydrotreating"; *7th World Pet. Congr. Proc.*; 4; pp. 177–183; (1967).

Miki, Y., Yamadaya, S., Oba, M., and Sugimoto, Y.; "Role of Catalyst in Hydrocracking of Heavy Oil"; *J. Catal.*; 83; pp. 371–383; (1983).

Netzel, D.A., McKay, D.R., Heppner, R.A., Guffey, F.D., Cooke, S.D., Varie, D.L., Linn, D.E.; "^{1}H and ^{13}C–NMR Studies on Naphtha and Light Distillate Saturate Hydrocarbon Fractions Obtained from *in–situ* Shale Oil"; *Fuel*; 60; pp. 307–320; (1981).

Payzant, J.D., Montgomery, D.S., and Strauss, O.P.; "The Identification of Homologous Series of Benzo[b]thiophenes, Thiophenes, Thiolanes, and Thianes Possessing a Linear Carbon Framework in the Pyrolysis Oil of Athabasca Asphaltene"; *AOSTRA J. Research*; 4 (2); pp. 117–131; 1988.

Perry, R.H., Green, D.W., and Maloney, J.O., eds.; Perry's Chemical Engineer's Handbook, 6th ed.; McGraw–Hill; New York; 1984.

Rangwala, H.A., Dalla Lana, I.G., Otto, F.D., and Wanke, S.E.; "Hydroprocessing of Syncrude Coker Gas Oil"; Catalysis on the Energy Scene, ed. S. Kaliaguine; Elsevier Science Publishers, Amsterdam; pp. 537–544; (1984).

Rangwala, H.A., Wanke, S.E., Otto, F.D., and Dalla Lana, I.G.; "The Hydrotreating of Coker Gas Oil: Effects of Operating Conditions and Catalyst Properties"; preprint from *10th Can. Symp. on Catalysis*; Kingston, ON; June, 1986; pp. 20–29.

Sambi, I.S., Khulbe, K.C., and Mann, R.S.; "Catalytic Hydrotreatment of Heavy Gas Oil"; *Ind. Eng. Chem. Prod. Res. Dev.*; 21 (4); pp. 575–580; (1982).

Sapre, A.V. and Gates, B.C.; "Hydrogenation of Aromatic Hydrocarbons Catalyzed by Sulfided $CoO–MoO_3/\gamma–Al_2O_3$. Reactivities and Reaction Networks"; *Ind. Eng. Chem. Proc. Des. Dev.*; 20 (1); pp. 68–73; (1981).

Satterfield, C.N.; Heterogeneous Catalysis in Practice; McGraw–Hill; New York; 1980.

Satterfield, C.N., Modell, M., and Wilkens, J.A.; "Simultaneous Catalytic Hydrodenitrogenation of Pyridine and Hydrodesulfurization of Thiophene"; *Ind. Eng. Chem. Proc. Des. Dev.*; 19 (1); pp. 154–160; (1980).

Satterfield, C.N., Smith, C.M., and Ingalls, M.; "Catalytic Hydrodenitrogenation of Quinoline. Effect of Water and H_2S"; *Ind. Eng. Chem. Proc. Des. Dev.*; 24 (4); pp. 1000–1004; (1985).

Sim, W.J. and Daubert, T.E.; "Prediction of Vapor–Liquid Equilibria of Undefined Mixtures"; *Ind. Eng. Chem. Proc. Des. Dev.*; 19 (3); pp. 386–393; (1980).

Stangeland, B.E.; "A Kinetic Model for the Prediction of Hydrocracker Yields"; *Ind. Eng. Chem. Proc. Des. Dev.*; 13 (1); pp. 71–76; (1974).

Ternan, M.; "The Effective Diffusivity of Residuum Molecules in Hydrocracking Catalysts"; preprint from *10th Can. Symp. on Catalysis*; Kingston, ON; June, 1986; pp. 60–69.

Thiel, J. and Gray, M.R.; "NMR Spectroscopic Characteristics of Alberta Bitumens"; *AOSTRA Journal of Research*; 4 (1); pp. 63–73; (1988).

van Zjill Langhout, W.C., Stijntjes, G.J.F., and Waterman, W.I.; "Desulphurization of Gas Oils by Catalytic Hydrogenation"; *Inst. Pet. J.*; 41; pp. 263–272; (1955).

Voorhies, A. and Smith, W.M.; "Desulfurization–Hydrogenation of High Sulfur Catalytically Cracked Cycle Stock"; *Ind. Eng. Chem.*; 41 (12); pp. 2708–2710; (1949).

Wilson, M.F. and Kriz, J.F.; "Upgrading of Middle Distillate Fractions of a Syncrude from Athabasca Oil Sands"; *Fuel*; 63 (2); pp. 190–196; (1984).

Wilson, M.F., Fisher, I.P., and Kriz, J.F.; "Hydrogenation of Aromatic Compounds in Synthetic Crude Distillates Catalyzed by Sulfided $Ni–W/\gamma–Al_2O_3$"; *J. Catal.*; 95; pp. 155–166; (1985).

Yitzhaki, D. and Aharoni, C.; "Hydrodesulfurization of Gas Oil, Reaction Rates in Narrow Boiling Range Fractions"; *A.I.Ch.E.J.*; 23 (3); pp. 342–346; (1988).

Yui, S.M.; "Hydrotreating of Bitumen–Derived Coker Gas Oil: Kinetics of Hydrodesulfurization, Hydrodenitrogenation, and Mild Hydrocracking, and Correlations to Predict Product Yields and Properties"; *AOSTRA J. Research*; in press; May, 1989.

Appendix A: Reactor Hydroprocessing Data

Table A1: Hydroprocessing Conditions

Table A2: Estimation of Mean Reaction Temperature

Hydroprocessing Reactor Data Sheets

This appendix contains the data sheets from the 10 hydroprocessing experiments. The data sheets contain the liquid and gas flow rates, gas compositions, liquid density, organic sulfur and nitrogen concentrations in the liquid, liquid properties at reactor conditions, transient gas and liquid data, conversions, rates of reaction, and first order rate constants. Table A1 lists the hydroprocessing conditions for each run, along with the feed oil used.

For runs MG–38, MG–39, and MG–40, pressure fluctuations were observed due to plugging of the outlet filter and valve system. These fluctuations led to a continuously oscillating temperature. An average temperature must be estimated in order to conduct proper kinetic analyses on the data. The temperature was recorded every 1.6 minutes by an automated chart recorder, and the temperature versus time log for the last hour of each run is shown in Table A2. A regression was conducted on each set of data, for which the largest r^2 value was 0.035, indicating random scatter about the mean. An arithmetic mean temperature was calculated, along with a 99% confidence interval, and this mean was used as the run temperature for all kinetic analyses.

Table A1: Hydroprocessing Conditions

Run	Feed	T (°C)
MG–32	CGOD1	400
MG–33	CGOD2	380
MG–34	CGOD2	400
MG–35	CGOD2	420
MG–36	CGOD3	400
MG–37	CGOD4	400
MG–38	CGOD5	395
MG–39	CGOD5	406
MG–40	CGOD5	425
MG–41	CGOD6	425

Table A2: Mean Temperature Estimation

Time (min)	Temperature (°C) MG–38	MG–39	MG–40
0.000	403	392	408
1.667	392	407	428
3.333	378	418	428
5.000	408	375	423
6.667	398	393	437
8.333	385	415	418
10.000	412	422	432
11.667	403	397	407
13.333	392	408	425
15.000	372	423	427
16.667	407	388	420
18.333	397	405	433
20.000	383	418	417
21.667	409	373	430
23.333	398	403	428
25.000	387	415	427
26.667	408	420	423
28.333	400	398	422
30.000	387	412	433
31.667	408	423	413
33.333	400	392	428
35.000	388	408	425
36.667	397	420	422
38.333	397	385	432
40.000	378	403	412
41.667	403	415	428
43.333	392	423	427
45.000	383	393	420
46.667	395	410	433
48.333	390	422	415
50.000	375	385	430
51.667	402	403	430
53.333	390	417	425
55.000	403	417	438
56.667	400	397	420
58.333	388	412	433
60.000	408	423	422
Mean	395.0	406.2	424.8
99% C.I.	± 4.7	± 6.3	± 3.4
r^2	0.003	0.035	0.025

DATA SHEET FOR CATALYTIC HYDROPROCESSING (steady-state results)

RUN NUMBER: MG- 32 DATE OF RUN: July 5, 1988
FEED: CGOD1
CATALYST: D AMOUNT: 8.0g

PRESULFIDING: None
REACTOR PRESSURE = 13.9 MPa
REACTOR TEMPERATURE = 400°C

FLOW RATES (at steady state)

STREAM	LIQUID mL/min(*)	GAS L(STP)/min
Feed	1.6800	1.056
Product	1.6890	0.831

LIQUID ANALYSES

STREAM	DENSITY	COMPOSITION			AVERAGE M.W.(**)	
	g/mL	wt% S	wt% N	wt% distil	stream	dist(#)
Feed	0.90740	3.38	0.091	97.52	223.2	220.0
Product	0.84980	0.13	0.001	92.74	203.6	203.8
Bomb (@)	0.86071	0.47	0.005	92.08	208.5	207.7

GAS ANALYSES (##)

STREAM	COMPOSITION (mol %)							
	H2	H2S	C1	C2	C3	C4	C5	C6
Feed	100.0							
Product	91.322	3.220	0.657	0.907	0.643	1.804	0.877	0.305
Bomb (@)	95.282		2.153	1.245	0.860	0.335	0.105	0.020

LIQUID PROPERTIES AT REACTOR CONDITIONS (calculated)

Liquid Density = 0.5711 g/mL
Liquid Hold-up = 131 mL
Hydrogen Solubility = 2.812 mg H2/g oil

* Liquid flows and densities at 23°C
** Average molecular weight (simulated distillation)
\# Distillate is defined as the fraction of liquid with boiling point between 177-343°C
@ Bomb sample is a sample of liquid taken from reactor at reaction conditions (stirrer at low r.p.m)

CATALYTIC HYDROPROCESSING DATA
(Product Compositions as a Function of Time)

RUN NUMBER: MG- 32 DATE OF RUN: July 5, 1988

TIME	DENSITY	COMPOSITION			CONVERSION (%)		
h	g/mL	wt% S	wt% N	wt% distil	S	N	Distillate
2.0	0.84813	0.13	0.001	--	96.4	100.0	
3.0	0.85072	0.13	0.001	--	96.4	100.0	
4.0	0.84890	0.13	0.001	--	96.4	100.0	
5.0	0.84890	0.13	0.001	92.74	96.4	100.0	10.6

GAS PRODUCT ANALYSES

TIME	COMPOSITION (mol %)							
h	H2	H2S	C1	C2	C3	C4	C5	C6
1.0	91.82	3.220	0.668	0.854	0.633	1.570	0.736	0.239
3.0	91.29	3.220	0.667	0.940	0.672	1.810	0.871	0.282
4.0	90.86	3.220	0.715	0.997	0.724	1.974	0.944	0.303
5.0	91.32	3.220	0.657	0.907	0.643	1.804	0.877	0.305

University of Alberta

DATA SHEET FOR CATALYTIC HYDROPROCESSING (steady-state results)

RUN NUMBER: MG- 33 DATE OF RUN: July 6, 1988
FEED: CGOD2
CATALYST: D AMOUNT: 8.0g

PRESULFIDING: None
REACTOR PRESSURE = 13.9 MPa
REACTOR TEMPERATURE = 380°C

FLOW RATES (at steady state)

STREAM	LIQUID mL/min(*)	GAS L(STP)/min
Feed	1.6750	1.060
Product	1.6290	0.776

LIQUID ANALYSES

STREAM	DENSITY g/mL	COMPOSITION wt% S	wt% N	wt% distil	AVERAGE M.W.(**) stream	dist(#)
Feed	0.92622	3.39	0.132	95.27	256.1	250.3
Product	0.88107	0.47	0.028	95.18	238.4	234.3
Bomb (@)	0.88167	0.49	0.028	96.67	241.5	237.7

GAS ANALYSES (##)

STREAM	COMPOSITION (mol %) H2	H2S	C1	C2	C3	C4	C5	C6
Feed	100.0							
Product	97.113	1.887	0.196	0.177	0.165	0.087	0.028	0.004
Bomb (@)	99.280		0.231	0.218	0.174	0.074	0.022	0.002

LIQUID PROPERTIES AT REACTOR CONDITIONS (calculated)

Liquid Density = 0.6202 g/mL
Liquid Hold-up = 115 mL
Hydrogen Solubility = 2.686 mg H2/g oil

* Liquid flows and densities at 23°C
** Average molecular weight (simulated distillation)
\# Distillate is defined as the fraction of liquid with boiling point between 177-343°C
@ Bomb sample is a sample of liquid taken from reactor at reaction conditions (stirrer at low r.p.m)

CATALYTIC HYDROPROCESSING DATA
(Product Compositions as a Function of Time)

RUN NUMBER: MG- 33 DATE OF RUN: July 6, 1988

TIME	DENSITY	COMPOSITION			CONVERSION (%)		
h	g/mL	wt% S	wt% N	wt% distil	S	N	Distillate
1.0	0.87928	0.47	0.028	--	87.2	80.4	
2.0	0.87876	0.47	0.028	--	87.2	80.4	
3.0	0.87891	0.47	0.028	--	87.2	80.4	
4.0	0.88107	0.47	0.028	95.18	87.2	80.4	7.6

GAS PRODUCT ANALYSES

TIME	COMPOSITION (mol %)							
h	H2	H2S	C1	C2	C3	C4	C5	C6
1.0	96.94	1.887	0.248	0.228	0.205	0.105	0.039	0.007
3.0	96.63	1.887	0.291	0.282	0.266	0.168	0.117	0.016
4.0	97.11	1.887	0.196	0.177	0.165	0.087	0.028	0.004

DATA SHEET FOR CATALYTIC HYDROPROCESSING (steady-state results)

RUN NUMBER: MG- 34 DATE OF RUN: July 6, 1988
FEED: CGOD2
CATALYST: D AMOUNT: 8.0g

PRESULFIDING: None
REACTOR PRESSURE = 13.9 MPa
REACTOR TEMPERATURE = 400°C

FLOW RATES (at steady state)

STREAM	LIQUID mL/min(*)	GAS L(STP)/min
Feed	1.6960	1.053
Product	1.6490	0.583

LIQUID ANALYSES

STREAM	DENSITY g/mL	COMPOSITION wt% S	wt% N	wt% distil	AVERAGE M.W.(**) stream	dist(#)
Feed	0.92622	3.39	0.132	95.27	256.1	250.3
Product	0.87170	0.24	0.024	93.88	232.1	232.0
Bomb (@)	0.87590	0.31	0.024	95.39	238.6	235.2

GAS ANALYSES (##)

STREAM	COMPOSITION (mol %) H2	H2S	C1	C2	C3	C4	C5	C6
Feed	100.0							
Product	96.019	2.005	0.414	0.356	0.392	0.237	0.083	0.018
Bomb (@)	98.469		0:480	0.429	0.392	0.175	0.049	0.006

LIQUID PROPERTIES AT REACTOR CONDITIONS (calculated)

Liquid Density = 0.5937 g/mL
Liquid Hold-up = 118 mL
Hydrogen Solubility = 2.955 mg H2/g oil

* Liquid flows and densities at 23°C
** Average molecular weight (simulated distillation)
\# Distillate is defined as the fraction of liquid with boiling point between 177-343°C
@ Bomb sample is a sample of liquid taken from reactor at reaction conditions (stirrer at low r.p.m)

CATALYTIC HYDROPROCESSING DATA
(Product Compositions as a Function of Time)

RUN NUMBER: MG- 34 DATE OF RUN: July 6, 1988

TIME	DENSITY	COMPOSITION			CONVERSION (%)		
h	g/mL	wt% S	wt% N	wt% distil	S	N	Distillate
1.0	0.87249	0.26	0.024	--	93.0	83.3	
2.0	0.87114	0.23	0.024	--	93.8	83.4	
3.0	0.87170	0.24	0.024	93.88	93.5	83.4	9.8

GAS PRODUCT ANALYSES

TIME	COMPOSITION (mol %)							
h	H2	H2S	C1	C2	C3	C4	C5	C6
2.0	96.08	2.005	0.413	0.345	0.370	0.221	0.079	0.012
3.0	96.02	2.005	0.414	0.356	0.392	0.237	0.083	0.018

DATA SHEET FOR CATALYTIC HYDROPROCESSING (steady-state results)

RUN NUMBER: MG- 35 DATE OF RUN: July 6, 1988
FEED: CGOD2
CATALYST: D AMOUNT: 8.0g

PRESULFIDING: None
REACTOR PRESSURE = 13.9 MPa
REACTOR TEMPERATURE = 420°C

FLOW RATES (at steady state)

STREAM	LIQUID mL/min(*)	GAS L(STP)/min
Feed	1.6770	1.048
Product	1.6490	0.504

LIQUID ANALYSES

STREAM	DENSITY	COMPOSITION			AVERAGE M.W.(**)	
	g/mL	wt% S	wt% N	wt% distil	stream	dist(#)
Feed	0.92622	3.39	0.132	95.27	256.1	250.3
Product	0.86258	0.17	0.014	90.53	223.3	225.9
Bomb (@)	0.86997	0.15	0.014	92.86	234.5	232.2

GAS ANALYSES (##)

STREAM	COMPOSITION (mol %)							
	H2	H2S	C1	C2	C3	C4	C5	C6
Feed	100.0							
Product	93.092	1.994	1.164	0.996	1.123	0.723	0.263	0.037
Bomb (@)	81.538		0.092	0.105	8.842	3.345	0.872	5.205

LIQUID PROPERTIES AT REACTOR CONDITIONS (calculated)

Liquid Density = 0.5658 g/mL
Liquid Hold-up = 120 mL
Hydrogen Solubility = 3.046 mg H2/g oil

* Liquid flows and densities at 23°C
** Average molecular weight (simulated distillation)
\# Distillate is defined as the fraction of liquid with boiling point between 177-343°C
@ Bomb sample is a sample of liquid taken from reactor at reaction conditions (stirrer at low r.p.m)

CATALYTIC HYDROPROCESSING DATA
(Product Compositions as a Function of Time)

RUN NUMBER: MG- 35 DATE OF RUN: July 6, 1988

TIME	DENSITY	COMPOSITION			CONVERSION (%)		
h	g/mL	wt% S	wt% N	wt% distil	S	N	Distillate
1.0	0.86216	0.17	0.014	--	95.4	90.3	
2.0	0.86254	0.17	0.014	--	95.4	90.3	
3.0	0.86258	0.17	0.014	90.53	95.4	90.3	13.0

GAS PRODUCT ANALYSES

TIME	COMPOSITION (mol %)							
h	H2	H2S	C1	C2	C3	C4	C5	C6
1.0	93.68	1.994	1.049	0.866	0.956	0.603	0.212	0.029
2.0	93.09	1.994	1.164	0.996	1.123	0.723	0.263	0.037

DATA SHEET FOR CATALYTIC HYDROPROCESSING (steady-state results)

RUN NUMBER: MG- 36 DATE OF RUN: July 13, 1988
FEED: CGOD3
CATALYST: D AMOUNT: 8.0g

PRESULFIDING: None
REACTOR PRESSURE = 13.0 MPa
REACTOR TEMPERATURE = 400°C

FLOW RATES (at steady state)

STREAM	LIQUID mL/min(*)	GAS L(STP)/min
Feed	1.6720	1.055
Product	1.7500	0.907

LIQUID ANALYSES

STREAM	DENSITY	COMPOSITION			AVERAGE M.W.(**)	
	g/mL	wt% S	wt% N	wt% pitch	stream	pitch(#)
Feed	0.95208	3.59	0.194	64.16	304.7	325.4
Product	0.89759	0.51	0.046	40.71	276.2	326.5
Bomb (@)	0.90275	0.67	0.048	43.11	281.6	319.3

GAS ANALYSES (##)

STREAM	COMPOSITION (mol %)							
	H2	H2S	C1	C2	C3	C4	C5	C6
Feed	100.0							
Product	95.461	3.553	0.183	0.131	0.131	0.080	0.031	0.005
Bomb (@)	88.232		0.041	6.264	4.324	0.0	0.0	0.0

LIQUID PROPERTIES AT REACTOR CONDITIONS (calculated)

Liquid Density = 0.6327 g/mL
Liquid Hold-up = 145 mL
Hydrogen Solubility = 2.473 mg H2/g oil

* Liquid flows and densities at 23°C
** Average molecular weight (simulated distillation)
\# Pitch is defined as the fraction of liquid with boiling point above 343°C
@ Bomb sample is a sample of liquid taken from reactor at reaction conditions (stirrer at low r.p.m)

CATALYTIC HYDROPROCESSING DATA
(Product Compositions as a Function of Time)

RUN NUMBER: MG- 36 DATE OF RUN: July 13, 1988

TIME	DENSITY	COMPOSITION			CONVERSION (%)		
h	g/mL	wt% S	wt% N	wt% pitch	S	N	Pitch
1.0	0.90319	--	0.062	--		68.3	
2.0	0.89775	--	0.047	--		76.1	
3.0	0.89763	0.51	0.045	--	86.0	77.1	
4.0	0.89765	0.51	0.045	--	86.0	77.1	
5.0	0.89759	0.51	0.046	40.71	86.0	76.6	37.4

GAS PRODUCT ANALYSES

TIME	COMPOSITION (mol %)							
h	H2	H2S	C1	C2	C3	C4	C5	C6
1.0	94.63	3.553	0.501	0.335	0.315	0.174	0.062	0.007
3.0	95.46	3.553	0.184	0.131	0.130	0.079	0.031	0.004
4.0	95.39	3.553	0.206	0.147	0.148	0.089	0.035	0.005
5.0	95.46	3.553	0.183	0.131	0.131	0.080	0.031	0.005

DATA SHEET FOR CATALYTIC HYDROPROCESSING (steady-state results)

RUN NUMBER: MG- 37 DATE OF RUN: July 13, 1988
FEED: CGOD4
CATALYST: D AMOUNT: 8.0g

PRESULFIDING: None
REACTOR PRESSURE = 13.9 MPa
REACTOR TEMPERATURE = 400°C

FLOW RATES (at steady state)

STREAM	LIQUID mL/min(*)	GAS L(STP)/min
Feed	1.6720	1.055
Product	1.7500	0.907

LIQUID ANALYSES

STREAM	DENSITY g/mL	COMPOSITION wt% S	wt% N	wt% pitch	AVERAGE M.W.(**) stream	pitch(#)
Feed	0.98961	4.35	0.338	97.71	382.2	385.0
Product	0.93648	1.09	0.202	75.92	338.6	372.3
Bomb (@)	0.94145	1.19	0.187	81.88	349.0	370.7

GAS ANALYSES (##)

STREAM	COMPOSITION (mol %) H2	H2S	C1	C2	C3	C4	C5	C6
Feed	100.0							
Product	95.517	3.620	0.172	0.104	0.092	0.053	0.020	0.004
Bomb (@)	99.548		0.175	0.104	0.093	0.148	0.021	0.004

LIQUID PROPERTIES AT REACTOR CONDITIONS (calculated)

Liquid Density = 0.6868 g/mL
Liquid Hold-up = 145 mL
Hydrogen Solubility = 1.861 mg H2/g oil

* Liquid flows and densities at 23°C
** Average molecular weight (simulated distillation)
\# Pitch is defined as the fraction of liquid with boiling point above 343°C
@ Bomb sample is a sample of liquid taken from reactor at reaction conditions (stirrer at low r.p.m)

CATALYTIC HYDROPROCESSING DATA
(Product Compositions as a Function of Time)

RUN NUMBER: MG- 37 DATE OF RUN: July 13, 1988

TIME	DENSITY	COMPOSITION			CONVERSION (%)		
h	g/mL	wt% S	wt% N	wt% pitch	S	N	Pitch
1.0	0.93554	1.17	0.200	--	73.4	41.5	
3.0	0.93486	1.09	0.196	--	75.2	42.7	
4.0	0.93554	1.09	0.202	--	75.2	40.9	
5.0	0.93648	1.09	0.202	75.92	75.2	40.8	23.0

GAS PRODUCT ANALYSES

TIME	COMPOSITION (mol %)							
h	H2	H2S	C1	C2	C3	C4	C5	C6
1.0	95.38	3.620	0.214	0.135	0.122	0.070	0.028	0.004
3.0	95.04	3.620	0.357	0.212	0.193	0.111	0.044	0.007
4.0	95.52	3.620	0.172	0.104	0.092	0.053	0.020	0.004

DATA SHEET FOR CATALYTIC HYDROPROCESSING (steady-state results)

RUN NUMBER: MG- 38 DATE OF RUN: August 18, 1988
FEED: CGOD5
CATALYST: D AMOUNT: 8.0g

PRESULFIDING: Insitu 1
REACTOR PRESSURE = 13.9 MPa
REACTOR TEMPERATURE = 395°C

FLOW RATES (at steady state)

STREAM	LIQUID mL/min(*)	GAS L(STP)/min
Feed	2.1530	1.047
Product	2.2230	0.778

LIQUID ANALYSES

STREAM	DENSITY	COMPOSITION			AVERAGE M.W.(**)	
	g/mL	wt% S	wt% N	wt% pitch	stream	pitch(#)
Feed	1.01292	4.66	0.492	99.95	483.1	473.5
Product	0.98109	2.82	0.406	94.19	454.1	440.4
Bomb (@)						

GAS ANALYSES (##)

STREAM	COMPOSITION (mol %)							
	H2	H2S	C1	C2	C3	C4	C5	C6
Feed	100.0							
Product	92.603	4.774	1.059	0.528	0.385	0.204	0.077	0.012
Bomb (@)								

LIQUID PROPERTIES AT REACTOR CONDITIONS (calculated)

Liquid Density = ****** g/mL
Liquid Hold-up = *** mL
Hydrogen Solubility = ***** mg H2/g oil

* Liquid flows and densities at 23°C
** Average molecular weight (simulated distillation)
\# Pitch is defined as the fraction of liquid with boiling point above 343°C
@ Bomb sample is a sample of liquid taken from reactor at reaction conditions (stirrer at low r.p.m)
Product gas analysis on ammonia-free basis
Bomb gas analysis on ammonia- and hydrogen sulfide-free basis

CATALYTIC HYDROPROCESSING DATA
(Product Compositions as a Function of Time)

RUN NUMBER: MG- 38 DATE OF RUN: August 18, 1988

TIME	DENSITY	COMPOSITION			CONVERSION (%)		
h	g/mL	wt% S	wt% N	wt% pitch	S	N	Pitch
1.0	0.98192	2.86	0.405	--	38.6	17.6	
2.0	0.98008	2.83	0.406	--	39.3	17.6	
3.0	0.98156	2.83	0.406	--	39.2	17.4	
4.0	0.98109	2.82	0.406	94.19	39.5	17.5	5.8

GAS PRODUCT ANALYSES

TIME	COMPOSITION (mol %)							
h	H2	H2S	C1	C2	C3	C4	C5	C6
1.0	92.27	4.774	1.196	0.594	0.419	0.250	0.108	0.035
2.0	92.65	4.774	1.037	0.518	0.370	0.200	0.077	0.013
3.0	92.55	4.774	1.097	0.542	0.382	0.206	0.079	0.013
4.0	92.60	4.774	1.059	0.528	0.385	0.204	0.077	0.012

DATA SHEET FOR CATALYTIC HYDROPROCESSING (steady-state results)

RUN NUMBER: MG- 39 DATE OF RUN: August 18, 1988
FEED: CGOD5
CATALYST: D AMOUNT: 8.0g

PRESULFIDING: Insitu 1
REACTOR PRESSURE = 13.9 MPa
REACTOR TEMPERATURE = 406°C

FLOW RATES (at steady state)

STREAM	LIQUID mL/min(*)	GAS L(STP)/min
Feed	2.2980	1.060
Product	2.3930	0.793

LIQUID ANALYSES

STREAM	DENSITY g/mL	COMPOSITION wt% S	wt% N	wt% pitch	AVERAGE M.W.(**) stream	pitch(#)
Feed	1.01292	4.66	0.492	99.95	483.1	473.5
Product	0.97273	2.45	0.379	84.09	443.4	404.8
Bomb (@)						

GAS ANALYSES (##)

STREAM	COMPOSITION (mol %) H2	H2S	C1	C2	C3	C4	C5	C6
Feed	100.0							
Product	91.161	4.997	1.596	0.794	0.585	0.311	0.113	0.014
Bomb (@)								

LIQUID PROPERTIES AT REACTOR CONDITIONS (calculated)

Liquid Density = ****** g/mL
Liquid Hold-up = *** mL
Hydrogen Solubility = ***** mg H2/g oil

* Liquid flows and densities at 23°C
** Average molecular weight (simulated distillation)
\# Pitch is defined as the fraction of liquid with boiling point above 343°C
@ Bomb sample is a sample of liquid taken from reactor at reaction conditions (stirrer at low r.p.m)
Product gas analysis on ammonia-free basis
Bomb gas analysis on ammonia- and hydrogen sulfide-free basis

CATALYTIC HYDROPROCESSING DATA
(Product Compositions as a Function of Time)

RUN NUMBER: MG- 39 DATE OF RUN: August 18, 1988

TIME	DENSITY	COMPOSITION			CONVERSION (%)		
h	g/mL	wt% S	wt% N	wt% pitch	S	N	Pitch
1.0	0.97273	2.48	0.381	--	46.8	22.6	
2.0	0.97123	2.45	0.380	--	47.5	22.9	
3.0	0.97273	2.45	0.379	84.09	47.4	23.0	15.9

GAS PRODUCT ANALYSES

TIME	COMPOSITION (mol %)							
h	H2	H2S	C1	C2	C3	C4	C5	C6
2.0	90.66	4.997	1.875	0.909	0.655	0.341	0.120	0.018
3.0	91.16	4.997	1.596	0.794	0.585	0.311	0.113	0.014

DATA SHEET FOR CATALYTIC HYDROPROCESSING (steady-state results)

RUN NUMBER: MG- 40 DATE OF RUN: August 18, 1988
FEED: CGOD5
CATALYST: D AMOUNT: 8.0g

PRESULFIDING: Insitu 1
REACTOR PRESSURE = 13.9 MPa
REACTOR TEMPERATURE = 425°C

FLOW RATES (at steady state)

STREAM	LIQUID mL/min(*)	GAS L(STP)/min
Feed	2.1430	1.059
Product	2.3000	0.865

LIQUID ANALYSES

STREAM	DENSITY g/mL	COMPOSITION wt% S	wt% N	wt% pitch	AVERAGE M.W.(**) stream	pitch(#)
Feed	1.01292	4.66	0.492	99.95	483.1	473.5
Product	0.94355	1.56	0.332	71.33	426.2	360.5
Bomb (@)						

GAS ANALYSES (##)

STREAM	COMPOSITION (mol %) H2	H2S	C1	C2	C3	C4	C5	C6
Feed	100.0							
Product	88.484	4.864	2.725	1.391	1.107	0.614	0.222	0.032
Bomb (@)								

LIQUID PROPERTIES AT REACTOR CONDITIONS (calculated)

Liquid Density = ****** g/mL
Liquid Hold-up = *** mL
Hydrogen Solubility = ***** mg H2/g oil

* Liquid flows and densities at 23°C
** Average molecular weight (simulated distillation)
\# Pitch is defined as the fraction of liquid with boiling point above 343°C
@ Bomb sample is a sample of liquid taken from reactor at reaction conditions (stirrer at low r.p.m)
Product gas analysis on ammonia-free basis
Bomb gas analysis on ammonia- and hydrogen sulfide-free basis

CATALYTIC HYDROPROCESSING DATA
(Product Compositions as a Function of Time)

RUN NUMBER: MG- 40 DATE OF RUN: August 18, 1988

TIME	DENSITY	COMPOSITION			CONVERSION (%)		
h	g/mL	wt% S	wt% N	wt% pitch	S	N	Pitch
1.0	0.95134	1.60	0.351	---	65.4	28.1	
2.0	0.94618	1.71	0.335	---	63.2	31.7	
3.0	0.94[illegible]5	1.56	0.332	71.33	66.5	32.5	28.7

GAS PRODUCT ANALYSES

TIME	COMPOSITION (mol %)							
h	H2	H2S	C1	C2	C3	C4	C5	C6
1.0	89.06	4.864	2.551	1.265	0.968	0.520	0.184	0.023
2.0	87.007	47.000	4.864	3.195	1.541	1.184	0.642	0.232
3.0	88.48	4.864	2.725	1.391	1.107	0.614	0.222	0.032

DATA SHEET FOR CATALYTIC HYDROPROCESSING (steady-state results)

RUN NUMBER: MG- 41 DATE OF RUN: November 28, 1988
FEED: SCGO
CATALYST: D AMOUNT: 8.0g

PRESULFIDING: Insitu 1
REACTOR PRESSURE = 13.9 MPa
REACTOR TEMPERATURE = 425°C

FLOW RATES (at steady state)

STREAM	LIQUID mL/min(*)	GAS L(STP)/min
Feed	1.6640	1.082
Product	1.8986	0.730

LIQUID ANALYSES

STREAM	DENSITY	COMPOSITION			AVERAGE M.W.(**)	
	g/mL	wt% S	wt% N	wt% resid	stream	resid(#)
Feed	1.03570	5.16	0.642	55.05	0.0	0.0
Product	0.96865	2.16	0.442	18.16	0.0	0.0
Bomb (@)	0.97947	2.28	0.434	0.0	0.0	0.0

GAS ANALYSES (##)

STREAM	COMPOSITION (mol %)							
	H2	H2S	C1	C2	C3	C4	C5	C6
Feed	100.0							
Product	89.564	6.933	1.274	0.656	0.552	0.290	0.106	0.016
Bomb (@)	92.707		3.320	1.946	1.318	0.559	0.134	0.016

LIQUID PROPERTIES AT REACTOR CONDITIONS (calculated)

Liquid Density = 0.7191 g/mL
Liquid Hold-up = 117 mL
Hydrogen Solubility = 0.0 mg H2/g oil

* Liquid flows and densities at 23°C
** Average molecular weight (simulated distillation)
\# Resid is defined as the fraction of liquid with boiling point above 524°C
@ Bomb sample is a sample of liquid taken from reactor at reaction conditions (stirrer at low r.p.m)
Product gas analysis on ammonia-free basis
Bomb gas analysis on ammonia- and hydrogen sulfide-free basis

CATALYTIC HYDROPROCESSING DATA
(Product Compositions as a Function of Time)

RUN NUMBER: MG- 41 DATE OF RUN: November 28, 1988

TIME	DENSITY	COMPOSITION			CONVERSION (%)		
h	g/mL	wt% S	wt% N	wt% resid	S	N	Resid
3.0	0.96838	2.48	0.449	--	48.7	25.4	
4.0	0.97084	2.44	0.449	--	49.4	25.2	
5.0	0.96778	2.24	0.444	--	53.7	26.3	
6.0	0.96865	2.16	0.442	18.16	55.3	26.5	64.8

GAS PRODUCT ANALYSES

TIME	COMPOSITION (mol %)							
h	H2	H2S	C1	C2	C3	C4	C5	C6
2.0	87.572	6.933	2.233	1.169	0.860	0.438	0.162	0.026
3.0	88.423	6.933	1.774	0.951	0.750	0.391	0.145	0.022
5.0	88.863	6.933	1.618	0.812	0.669	0.350	0.129	0.018
6.0	89.564	6.933	1.274	0.656	0.552	0.290	0.106	0.016

University of Alberta

CATALYTIC HYDROPROCESSING RESULTS
(Steady-state results from stirred reactor)

	RUN NUMBER			
	MG-32	MG-33	MG-34	MG-35
CONDITIONS				
Pressure, MPa	13.9	13.9	13.9	13.9
Temperature, °C	400	380	400	420
LHSV, mL/(h.g cat.)	12.6	12.6	12.7	12.6
Reactor volume, ml	150.0	150.0	150.0	150.0
PROPERTIES OF FEED				
Density, g/mL	0.9074	0.9262	0.9262	0.9262
Sulfur content, wt%	3.38	3.39	3.39	3.39
Nitrogen content, wt%	0.091	0.132	0.132	0.132
Distil. content, wt%	97.52	95.27	95.27	95.27
PROPERTIES OF PRODUCT				
Density, g/mL	0.8498	0.8811	0.8717	0.8626
Sulfur content, wt%	0.13	0.47	0.24	0.17
Nitrogen content, wt%	0.001	0.028	0.024	0.014
Distil. content, wt%	92.74	95.18	93.88	90.53
CONVERSIONS				
Sulfur, %	96.4	86.9	93.5	95.4
Nitrogen, %	99.0	80.4	83.4	90.3
Pitch, %	10.5	7.6	9.8	13.0
C1 TO C6 PRODUCTION (*)				
Methane	0.2557	0.0700	0.1097	0.2696
Ethane	0.6618	0.1185	0.1768	0.4326
Propane	0.6881	0.1620	0.2856	0.7153
Butanes	2.5447	0.1126	0.2276	0.6071
Pentanes	1.5357	0.0450	0.0990	0.2741
C6 s	0.6083	0.0073	0.0244	0.0439
PER CENT OF CARBON IN FEED CONVERTED TO GAS	6.08	0.49	0.88	2.22
HYDROGEN CONSUMPTION				
Total (#)	8.75	8.89	14.08	16.71
Gaseous products (@)	3.30	0.78	0.88	1.50
OVERALL MASS BALANCE, % (mass out/mass in)*100	101.4	93.2	91.4	92.2

* % mass of liquid feed converted to various gaseous products
\# mol hydrogen per kg of liquid feed
@ mol hydrogen per kg of liquid feed consumed for production of gaseous products (C1 to C6, ammonia and hydrogen sulfide)

CATALYTIC HYDROPROCESSING RESULTS
(Steady-state results from stirred reactor)

	RUN NUMBER			
	MG-36	MG-37	MG-38	MG-39
CONDITIONS				
Pressure, MPa	13.9	13.9	13.9	13.9
Temperature, °C	400	400	395	406
LHSV, mL/(h.g cat.)	12.5	12.5	16.1	17.2
Reactor volume, ml	150.0	150.0	150.0	150.0
PROPERTIES OF FEED				
Density, g/mL	0.9521	0.9896	1.0129	1.0129
Sulfur content, wt%	3.59	4.35	4.66	4.66
Nitrogen content, wt%	0.194	0.338	0.492	0.492
Pitch content, wt%	64.16	97.71	99.95	99.95
PROPERTIES OF PRODUCT				
Density, g/mL	0.8976	0.9365	0.9811	0.9727
Sulfur content, wt%	0.51	1.09	2.82	2.45
Nitrogen content, wt%	0.046	0.202	0.406	0.379
Pitch content, wt%	40.71	75.92	94.19	84.09
CONVERSIONS				
Sulfur, %	86.0	76.5	39.5	47.4
Nitrogen, %	76.6	40.8	17.5	23.0
Pitch, %	37.4	23.0	5.8	15.9
C1 TO C6 PRODUCTION (*)				
Methane	0.0744	0.0673	0.2697	0.3881
Ethane	0.0999	0.0763	0.2521	0.3621
Propane	0.1465	0.0990	0.2696	0.3912
Butanes	0.1180	0.0752	0.1883	0.2742
Pentanes	0.0567	0.0352	0.0882	0.1237
C6 s	0.0104	0.0080	0.0157	0.0174
PER CENT OF CARBON IN FEED CONVERTED TO GAS	0.48	0.34	1.03	1.48
HYDROGEN CONSUMPTION				
Total (#)	5.40	5.18	6.74	6.53
Gaseous products (@)	1.30	1.21	1.43	1.71
OVERALL MASS BALANCE, % (mass out/mass in)*100	101.3	101.5	102.3	102.9

* % mass of liquid feed converted to various gaseous products
\# mol hydrogen per kg of liquid feed
@ mol hydrogen per kg of liquid feed consumed for production of gaseous products (C1 to C6, ammonia and hydrogen sulfide)

CATALYTIC HYDROPROCESSING RESULTS
(Steady-state results from stirred reactor)

	RUN NUMBER MG-40	MG-41
CONDITIONS		
Pressure, MPa	13.9	13.9
Temperature, °C	425	425
LHSV, mL/(h.g cat.)	16.1	12.5
Reactor volume, ml	150.0	150.0
PROPERTIES OF FEED		
Density, g/mL	1.0129	1.0357
Sulfur content, wt%	4.66	5.16
Nitrogen content, wt%	0.492	0.642
Pitch content, wt%	99.95	55.05
PROPERTIES OF PRODUCT		
Density, g/mL	0.9435	0.9686
Sulfur content, wt%	1.56	2.16
Nitrogen content, wt%	0.332	0.442
Pitch content, wt%	71.33	18.16
CONVERSIONS		
Sulfur, %	66.5	54.1
Nitrogen, %	32.5	26.5
Pitch, %	28.7	64.8
C1 TO C6 PRODUCTION (*)		
Methane	0.7752	0.3852
Ethane	0.7419	0.3719
Propane	0.8660	0.4590
Butanes	0.6331	0.3179
Pentanes	0.2842	0.1442
C6 s	0.0467	0.0248
PER CENT OF CARBON IN FEED CONVERTED TO GAS	3.19	1.64
HYDROGEN CONSUMPTION		
Total (#)	6.14	11.19
Gaseous products (@)	2.78	2.38
OVERALL MASS BALANCE, % (mass out/mass in)*100	105.0	110.3

* % mass of liquid feed converted to various gaseous products
\# mol hydrogen per kg of liquid feed
@ mol hydrogen per kg of liquid feed consumed for production of gaseous products (C1 to C6, ammonia and hydrogen sulfide)

RATE DATA FOR CATALYTIC HYDROPROCESSING(1)

	RUN NUMBER			
	MG-32	MG-33	MG-34	MG-35
CONDITIONS				
Pressure, MPa	13.9	13.9	13.9	13.9
Temperature, °C	400	380	400	420
LHSV, mL/(h.g cat.)	12.6	12.6	12.7	12.6
Reactor volume, mL	150.0	150.0	150.0	150.0
RATES OF REACTION FOR: mg/(s.kg catalyst)				
Sulfur Conversion, HDS	103.46	95.22	103.76	104.66
Nitrogen Conversion, HDN	2.86	3.43	3.60	3.86
Pitch Conversion	324.0	233.2	306.5	400.2
Methane Formation	8.12	2.26	3.59	8.72
Ethane Formation	21.02	3.33	5.79	14.00
Propane Formation	21.85	5.24	9.35	23.15
Butanes Formation	80.82	3.64	7.45	19.64
Pentanes Formation	48.77	1.45	3.24	8.87
C6s Formation (gas)	19.32	0.24	0.80	1.42
CONCENTRATION IN REACTOR LIQUID, mol/cu.m (*)				
Hydrogen	803.	833.	877.	862.
Organic Sulfur	23.2	93.0	44.5	30.1
Organic Nitrogen	0.4	12.4	10.2	5.7
Hydrogen Sulfide	89.6	44.2	47.4	50.3
FIRST ORDER RATE CONSTANTS mL/(s.kg catalyst) (*)				
Sulfur Conversion, HDS	93.65	22.51	49.59	71.37
Nitrogen Conversion, HDN	336.56	13.90	17.21	31.94
Pitch Conversion	0.41	0.28	0.37	0.51
To Gas Conversion	0.22761	0.01661	0.03035	0.07810
H2 Consumption	39.14	38.30	57.65	69.60
BASED ON SINGLE PORE MODEL				
Thiele Parameter,				
Organic Nitrogen	50.44	2.55	3.12	5.72
Organic Sulfur	15.07	4.27	9.57	12.30
Effectiveness Factor				
Organic Nitrogen	0.02	0.39	0.32	0.17
Organic Sulfur	0.07	0.23	0.10	0.08
BASED ON CATALYST PELLET				
Thiele Parameter,				
Organic Nitrogen	34.42	1.97	2.38	4.30
Organic Sulfur	10.64	3.06	6.57	9.29
Effectiveness Factor				
Organic Nitrogen	0.03	0.44	0.37	0.22
Organic Sulfur	0.09	0.30	0.15	0.10

(1) Based on product sample analyses

RATE DATA FOR CATALYTIC HYDROPROCESSING(1)

	RUN NUMBER			
	MG-36	MG-37	MG-38	MG-39
CONDITIONS				
Pressure, MPa	13.9	13.9	13.9	13.9
Temperature, °C	400	400	395	406
LHSV, mL/(h.g cat.)	12.5	12.5	16.1	17.2
Reactor volume, mL	150.0	150.0	150.0	150.0
RATES OF REACTION FOR: mg/(s.kg catalyst)				
Sulfur Conversion, HDS	102.37	114.78	83.59	107.17
Nitrogen Conversion, HDN	4.93	4.75	3.91	5.48
Pitch Conversion	795.6	776.1	261.4	769.0
Methane Formation	2.47	2.32	12.25	18.82
Ethane Formation	3.31	2.63	11.45	17.56
Propane Formation	4.86	3.41	12.25	18.97
Butanes Formation	3.91	2.59	8.56	13.30
Pentanes Formation	1.88	1.21	4.01	6.00
C6s Formation (gas)	0.35	0.28	0.71	0.85
CONCENTRATION IN REACTOR LIQUID, mol/cu.m (*)				
Hydrogen	782.	639.	350.	350.
Organic Sulfur	100.8	221.1	616.9	535.9
Organic Nitrogen	20.8	99.1	203.0	189.5
Hydrogen Sulfide	76.1	67.8	70.0	70.0
FIRST ORDER RATE CONSTANTS mL/(s.Kg catalyst) (*)				
Sulfur Conversion, HDS	22.36	11.90	3.02	4.50
Nitrogen Conversion, HDN	11.94	2.51	0.98	1.49
Pitch Conversion	2.18	1.09	0.28	0.94
To Gas Conversion	0.01758	0.01259	0.04825	0.07494
H2 Consumption	24.80	29.11	69.12	67.04
BASED ON SINGLE PORE MODEL				
Thiele Parameter,				
Organic Nitrogen	2.21	0.74	0.44	0.55
Organic Sulfur	4.24	2.28	0.83	1.07
Effectiveness Factor				
Organic Nitrogen	0.44	0.85	0.94	0.91
Organic Sulfur	0.24	0.43	0.82	0.74
BASED ON CATALYST PELLET				
Thiele Parameter,				
Organic Nitrogen	1.74	0.60	0.36	0.44
Organic Sulfur	3.04	1.73	0.66	0.85
Effectiveness Factor				
Organic Nitrogen	0.48	0.86	0.94	0.91
Organic Sulfur	0.30	0.48	0.83	0.75

(1) Based on product sample analyses

RATE DATA FOR CATALYTIC HYDROPROCESSING(1)

	RUN NUMBER MG-40	MG-41
CONDITIONS		
Pressure, MPa	13.9	13.9
Temperature, °C	425	425
LHSV, mL/(h.g cat.)	16.1	12.5
Reactor volume, mL	150.0	150.0
RATES OF REACTION FOR: mg/(s.Kg catalyst)		
Sulfur Conversion, HDS	140.21	100.21
Nitrogen Conversion, HDN	7.24	6.12
Pitch Conversion	1295.0	1280.7
Methane Formation	35.05	13.83
Ethane Formation	33.55	13.35
Propane Formation	39.16	16.48
Butanes Formation	28.63	11.41
Pentanes Formation	12.85	5.18
C6s Formation (gas)	2.11	0.89
CONCENTRATION IN REACTOR LIQUID, mol/cu.m (*)		
Hydrogen	350.	360.
Organic Sulfur	341.3	498.9
Organic Nitrogen	166.0	227.0
Hydrogen Sulfide	70.0	71.9
FIRST ORDER RATE CONSTANTS mL/(s.Kg catalyst) (*)		
Sulfur Conversion, HDS	9.53	4.66
Nitrogen Conversion, HDN	2.31	1.43
Pitch Conversion	1.92	7.28
To Gas Conversion	0.15794	0.06578
H2 Consumption	62.95	111.78
BASED ON SINGLE PORE MODEL		
Thiele Parameter,		
Organic Nitrogen	0.70	0.54
Organic Sulfur	1.87	1.09
Effectiveness Factor		
Organic Nitrogen	0.86	0.91
Organic Sulfur	0.51	0.73
BASED ON CATALYST PELLET		
Thiele Parameter,		
Organic Nitrogen	0.57	0.44
Organic Sulfur	1.45	0.87
Effectiveness Factor		
Organic Nitrogen	0.87	0.92
Organic Sulfur	0.55	0.75

(1) Based on product sample analyses

Appendix B: Data for Structural Group Analysis

Table B1: Original Elemental Analyses — Feedstocks

Table B2: Original Elemental Analyses — Products

Table B3: Normalized Elemental Analyses — Feedstocks

Table B4: Normalized Elemental Analyses — Products

Table B5: Elemental Conversions

Table B6: ^{13}C NMR Analyses of Feedstocks

Table B7: ^{13}C NMR Analyses of Products

Table B8: ^{1}H NMR Analyses of Feedstocks

Table B9: ^{1}H NMR Analyses of Products

Table B10: IR Analyses of Feedstocks

Table B11: IR Analyses of Products

Table B12: Nitrogen Titration Analyses of Feedstocks

Table B13: Nitrogen Titration Analyses of Products

Table B14: Profile of Structural Groups

Table B15: Structural Group Analysis of Feedstocks

Table B16: Structural Group Analysis of Products

Table B17: Molecular Parameters for Feedstocks

Table B18: Molecular Parameters for Products

This appendix tabulates the data from elemental analysis, ^{1}H NMR spectroscopy, ^{13}C NMR spectroscopy, infrared spectroscopy, and nitrogen titration analysis. The elemental analysis data are given in both raw and normalized form (Tables B1 to B4), while the ^{13}C and ^{1}H NMR data are shown in weight % of the appropriate atom in each band of interest (Tables B6 to B9). The band assignments are detailed in Chapter 3. The weight percent is calculated by integrating the area under each band and calculating the percent of the total atom in each band by dividing the band area into the total integrated area. The infrared data (Tables B10 and B11) consist of the average area measured by planimetry and the concentration of each heteroatom group of interest (calculated as described in the Analytical Methods section). The concentrations are given in units of mol/100 g. Nitrogen titration, used to estimate the concentrations of basic and very weak basic nitrogen, involves titrating the sample with titrant of a known normality. The nitrogen titration data in Tables B12 and B13 include the volume of titrant at the neutralization point and the concentration of basic nitrogen in units of mol/100 g. Based on results from Buell and previous SGA work, all basic nitrogen is assigned to quinoline for these samples. The structural group analysis results for the feedstocks and products are shown in Tables B15 and B16. Table B14 shows the structural groups and their names. The values of two molecular parameters, mean side chain length and average number of rings per aromatic structure are shown in Tables B17 and B18.

For the elemental analysis data for the feedstocks, the values for Oxygen,1 are the first set of results from the Microanalytical Laboratory. A second set of results was obtained for CGOD1, CGOD4, and CGOD7. The first set was essentially linear with molecular weight while the second set showed a large increase with molecular weight. As a moderate increase with increasing AMW is expected from the results for sulfur and nitrogen, the following method was used to estimate

the oxygen concentration:

1) Interpolate data for CGOD2, 3, 5, and 6 from the second set of results.

2) Average the first and second sets of results to obtain a final concentration.

This procedure gave the moderate, monotonically increasing trend expected. The data were then normalized. The results are shown in Tables B1 to B4. For the products, a similar procedure was used. Oxygen analyses were obtained for all runs, and the oxygen conversion was calculated. Examining the conversions, there appeared to be a trend similar to that seen in sulfur and nitrogen, although this trend was masked by large random fluctuations. The oxygen conversions for runs MG–32, MG–33, MG–39, MG–40, and MG–41 all followed a consistent trend and had reasonable values. The oxygen concentrations for the products of the middle runs (MG–34 to MG–38) were then estimated based on the analytical results and expected conversion levels, as shown in Tables B1 to B4, which list the original and normalized data showing the original and estimated oxygen concentrations. The adjustments to the oxygen analysis were only significant for two (MG–36 and MG–38) out of the ten products. Table B5 lists the conversions for sulfur, nitrogen, and oxygen. The resulting data for oxygen conversion are not reliable, and should only be considered in ranking the extent of oxygen removed relative to sulfur and nitrogen. A reasonable estimate of oxygen content was required for the SGA analysis of the product samples, necessitating this estimation/correction procedure.

The groups used in structural group analysis are shown in Table B14, divided into aromatic, aliphatic, and heteroatomic group types. Tables B15 and B16 give the SGA of the feedstocks and products, using the groups shown in Table B14. Few heteroatomic groups were seen in the IR spectra for the products, and this is reflected in the structural group analysis results.

The values of two molecular parameters, the mean side chain length and the average number of rings per aromatic structure, have been calculated and are given in Tables B17 and B18. The equation for estimating the value of the mean side chain length is from Netzel *et al.* (1981), and is shown in equation B.1.

$$MSCL = 5 + 2 \cdot \frac{[\text{chain methylene}]}{[\gamma\text{-methyl}]} \qquad \text{B.1}$$

This equation is derived from a calibration of the ratio of chain methylene to γ–methyl groups against actual chain length for synthetic fuel samples from oil shales.

In determining the average number of rings per aromatic compound, the amount of 'bridgehead' carbon, or carbon bound solely to aromatic carbon, must be determined. The amount of bridgehead carbon can be found by subtracting the aromatic hydrogen and α–carbon from the total aromatic carbon. The bridgehead carbon, C_{ar}–$(C_{ar})_3$, can be in two types of structures: open structures such as biphenyl, or condensed structures such as naphthalene. Because NMR does not distinguish between the two, the average number of rings per aromatic group can be calculated two ways: by assuming all $C_{ar} - C_{ar}$ bonds are biphenyl bonds or by assuming all $C_{ar} - C_{ar}$ bonds are in condensed structures such as naphthalene. The estimate of the mean ring number obtained by assuming that all biphenyl structures represent actual ring linkages can be calculated as in equation B.2.

$$\text{Mean Ring Number} = \frac{\Sigma x_i \cdot N_i}{\Sigma x_i} \qquad \text{B.2}$$

In equation B.2, x_i is the concentration of any aromatic structural group, and N_i is the number of rings in that group. The second estimate of the average ring number is calculated by assuming that all biphenyl structures are actually condensed ring aromatics. Regression of the ratio of bridgehead carbon to non–bridgehead aromatic carbon for various representative condensed aromatic compounds gives

equation B.3.

$$\text{Mean Ring Number} = \exp\left[\frac{\text{Brdghd/Non-Brdghd} + 0.001}{0.407}\right] \qquad \text{B.3}$$

For these purposes the bridgehead carbon is defined as the sum of the bridgehead carbon in various structures (phenanthrene, benzofuran, *etc.*), while the non–bridgehead carbon may be simply calculated by subtracting the bridgehead carbon from the total aromatic carbon. The average number of rings per aromatic structure will be represented as the average of these two estimates. Both estimates are shown, along with the average, in Tables B17 and B18.

Table B1: Original Elemental Analyses — Feedstocks

Element	CGOD1	CGOD2	CGOD3	CGOD4
Carbon	85.15%	85.27%	85.29%	85.04%
Hydrogen	11.03%	11.04%	10.64%	10.12%
Sulfur	3.38%	3.39%	3.59%	4.35%
Nitrogen	0.09%	0.13%	0.19%	0.34%
Oxygen 1	0.74%	0.90%	0.89%	0.87%
Oxygen 2	0.87%	1.09%	1.32%	1.54%
Oxygen avg	0.81%	1.00%	1.10%	1.21%
Total	100.46%	100.83%	100.82%	101.05%

Element	CGOD5	CGOD6	CGOD7
Carbon	84.89%	84.58%	85.21%
Hydrogen	9.79%	9.59%	8.30%
Sulfur	4.66%	5.05%	5.27%
Nitrogen	0.49%	0.64%	0.65%
Oxygen 1	0.82%	0.88%	1.11%
Oxygen 2	1.81%	2.07%	2.34%
Oxygen avg	1.31%	1.48%	1.73%
Total	101.14%	101.34%	101.16%

Table B2: Original Elemental Analyses — Products

Element	MG–32	MG–33	MG–34	MG–35	MG–36
Carbon	86.05%	87.44%	87.37%	87.73%	87.30%
Hydrogen	13.01%	12.58%	12.80%	12.08%	11.92%
Sulfur	0.13%	0.48%	0.24%	0.17%	0.51%
Nitrogen	0.00%	0.03%	0.02%	0.01%	0.05%
Oxygen 1	0.32%	0.58%	0.42%	0.47%	0.36%
Oxygen 2			0.78%		
Oxygen Est.	0.32%	0.58%	0.50%	0.40%	0.65%
Total	99.51%	101.11%	100.93%	100.39%	100.43%

Element	MG–37	MG–38	MG–39	MG–40	MG–41
Carbon	87.69%	86.07%	85.96%	87.69%	87.52%
Hydrogen	11.10%	10.14%	10.43%	10.96%	10.48%
Sulfur	1.03%	2.82%	2.45%	1.56%	2.22%
Nitrogen	0.20%	0.41%	0.38%	0.33%	0.44%
Oxygen 1	1.03%	1.80%	0.60%	0.24%	0.38%
Oxygen 2	0.64%				
Oxygen Est.	0.83%	0.85%	0.60%	0.24%	0.38%
Total	100.85%	100.29%	99.82%	100.78%	101.04%

Table B3: Normalized Elemental Analyses — Feedstocks

Element	CGOD1	CGOD2	CGOD3	CGOD4
Carbon	84.76%	84.57%	84.60%	84.15%
Hydrogen	10.98%	10.95%	10.55%	10.01%
Sulfur	3.36%	3.36%	3.56%	4.30%
Nitrogen	0.09%	0.13%	0.19%	0.33%
Oxygen	0.80%	0.99%	1.09%	1.19%

Element	CGOD5	CGOD6	CGOD7
Carbon	83.93%	83.46%	84.24%
Hydrogen	9.68%	9.46%	8.21%
Sulfur	4.61%	4.99%	5.21%
Nitrogen	0.49%	0.63%	0.64%
Oxygen	1.30%	1.46%	1.71%

Table B4: Normalized Elemental Analyses — Products

Element	MG–32	MG–33	MG–34	MG–35	MG–36
Carbon	86.47%	86.48%	86.56%	87.39%	86.93%
Hydrogen	13.07%	12.44%	12.68%	12.03%	11.87%
Sulfur	0.13%	0.47%	0.24%	0.17%	0.51%
Nitrogen	0.00%	0.03%	0.02%	0.01%	0.05%
Oxygen	0.32%	0.57%	0.50%	0.40%	0.65%

Element	MG–37	MG–38	MG–39	MG–40	MG–41
Carbon	86.95%	85.82%	86.12%	87.01%	86.62%
Hydrogen	11.01%	10.11%	10.45%	10.87%	10.37%
Sulfur	1.02%	2.81%	2.45%	1.55%	2.19%
Nitrogen	0.20%	0.40%	0.38%	0.33%	0.44%
Oxygen	0.82%	0.85%	0.60%	0.24%	0.38%

Table B5: Elemental Conversions

Element	MG–32	MG–33	MG–34	MG–35	MG–36
Sulfur	96.1%	85.9%	92.9%	95.0%	85.7%
Nitrogen	100.0%	78.8%	81.8%	89.3%	76.2%
Oxygen	59.9%	42.0%	49.9%	59.7%	40.9%
Element	**MG–37**	**MG–38**	**MG–39**	**MG–40**	**MG–41**
Sulfur	76.3%	38.9%	46.7%	66.4%	56.0%
Nitrogen	40.1%	16.8%	21.9%	32.3%	30.9%
Oxygen	31.0%	34.7%	53.7%	81.7%	74.2%

Table B6: ^{13}C NMR Analyses of Feedstocks
(Weight % of Carbon)

Band	CGOD1	CGOD2	CGOD3	CGOD4
Aromatic	35.9%	34.0%	32.3%	39.2%
Aliphatic	64.1%	66.0%	67.7%	60.8%
Band 1	5.2%	6.5%	5.1%	3.9%
Band 2	2.9%	2.4%	2.1%	1.6%
Bands 3&4	8.6%	8.4%	9.1%	8.0%
Bands 5&6	30.8%	31.8%	33.0%	28.3%
Band 7	16.5%	16.8%	18.3%	19.0%
Band 9	16.3%	16.0%	15.5%	18.4%
Band 10	13.2%	12.5%	11.0%	15.6%
Band 11	6.4%	5.6%	5.8%	5.1%
Band 6.1	2.5%	1.9%	2.1%	1.9%
Band 6.2	5.1%	4.1%	3.7%	3.7%
Band 6.3	1.9%	1.8%	1.9%	1.3%
Band 7.1	0.6%	0.6%	0.5%	0.6%
Band 7.2	0.3%	0.3%	0.7%	0.7%
Band 7.3	0.8%	0.6%	1.3%	0.0%

Band	CGOD5	CGOD6	CGOD7
Aromatic	41.2%	44.4%	47.9%
Aliphatic	58.8%	55.6%	52.1%
Band 1	4.6%	3.7%	2.8%
Band 2	2.1%	1.8%	2.0%
Bands 3&4	8.6%	7.3%	6.0%
Bands 5&6	28.6%	27.3%	26.8%
Band 7	14.8%	15.5%	14.5%
Band 9	18.5%	21.7%	23.5%
Band 10	15.8%	17.0%	19.0%
Band 11	6.9%	5.6%	5.4%
Band 6.1	1.2%	2.0%	2.2%
Band 6.2	3.6%	4.6%	4.8%
Band 6.3	1.3%	1.4%	1.7%
Band 7.1	0.5%	0.4%	1.4%
Band 7.2	0.2%	1.3%	1.6%
Band 7.3	0.1%	0.0%	1.4%

Table B7: ^{13}C NMR Analyses of Products (Weight % of Carbon)

Band	MG–32	MG–33	MG–34	MG–35	MG–36
Aromatic	18.6%	24.6%	21.8%	21.4%	24.5%
Aliphatic	81.4%	75.4%	78.2%	78.6%	75.5%
Band 1	7.2%	7.2%	6.5%	8.6%	6.5%
Band 2	1.4%	1.9%	1.5%	1.8%	1.8%
Bands 3&4	9.6%	9.4%	9.7%	10.7%	9.3%
Bands 5&6	45.2%	39.4%	42.3%	40.0%	38.3%
Band 7	18.0%	17.4%	18.2%	17.5%	19.6%
Band 9	7.8%	9.9%	9.3%	8.1%	11.5%
Band 10	6.3%	9.4%	7.7%	8.3%	9.0%
Band 11	4.5%	5.3%	4.7%	5.0%	4.1%
Band 6.1	4.0%	2.5%	3.2%	3.3%	2.7%
Band 6.2	6.3%	4.6%	5.8%	6.1%	3.6%
Band 6.3	4.2%	3.0%	3.5%	3.0%	2.8%
Band 7.1	1.3%	1.0%	1.2%	1.3%	0.8%
Band 7.2	1.6%	0.6%	0.9%	1.3%	0.9%
Band 7.3	1.3%	0.5%	1.6%	1.1%	1.0%

Band	MG–37	MG–38	MG–39	MG–40	MG–41
Aromatic	31.0%	37.3%	37.6%	35.6%	40.4%
Aliphatic	69.0%	62.7%	62.4%	64.4%	59.6%
Band 1	5.2%	6.9%	9.2%	8.7%	7.0%
Band 2	1.9%	1.9%	2.0%	1.7%	1.7%
Bands 3&4	8.7%	9.7%	10.5%	11.3%	9.2%
Bands 5&6	36.1%	32.7%	34.0%	33.7%	30.0%
Band 7	17.1%	11.5%	6.7%	9.0%	11.6%
Band 9	14.4%	21.1%	19.3%	20.2%	20.5%
Band 10	12.0%	12.4%	13.3%	12.5%	13.6%
Band 11	4.6%	3.8%	5.0%	3.0%	6.3%
Band 6.1	2.3%	2.1%	3.4%	3.1%	2.1%
Band 6.2	3.7%	4.7%	5.9%	5.0%	6.0%
Band 6.3	2.5%	2.3%	5.1%	2.2%	2.0%
Band 7.1	0.4%	0.4%	0.3%	0.3%	0.5%
Band 7.2	0.9%	0.6%	0.6%	0.3%	0.5%
Band 7.3	1.1%	1.0%	0.9%	0.9%	0.7%

Table B8: ^{1}H NMR Analyses of Feedstocks (Weight % of Hydrogen)

Band	CGOD1	CGOD2	CGOD3	CGOD4
Aromatic	8.3%	8.4%	7.6%	11.7%
Aliphatic	86.5%	91.6%	92.4%	88.3%
Band 1	21.8%	28.4%	23.3%	22.8%
Band 2	46.5%	44.9%	48.8%	44.8%
Band 3	20.2%	15.9%	20.3%	20.7%
Band 4	3.2%	2.3%	0.0%	0.0%
Band 5	8.3%	8.4%	7.6%	10.8%
Band 6	0.0%	0.0%	0.0%	0.9%

Band	CGOD5	CGOD6	CGOD7
Aromatic	10.5%	13.5%	12.6%
Aliphatic	89.5%	86.5%	87.4%
Band 1	21.9%	22.1%	13.9%
Band 2	47.8%	49.0%	45.2%
Band 3	19 9%	21.6%	28.3%
Band 4	0.0%	0.0%	0.0%
Band 5	9.8%	6.5%	11.2%
Band 6	0.7%	0.7%	1.4%

Table B9: ^{1}H NMR Analyses of Products (Weight % of Hydrogen)

Band	MG–32	MG–33	MG–34	MG–35	MG–36
Aromatic	4.8%	6.5%	6.6%	6.3%	6.5%
Aliphatic	95.2%	93.5%	93.4%	93.7%	93.5%
Band 1	28.2%	25.9%	29.7%	26.7%	26.1%
Band 2	51.4%	50.4%	50.1%	51.2%	51.6%
Band 3	14.4%	17.2%	13.6%	15.7%	15.9%
Band 4	1.2%	0.0%	0.0%	0.0%	0.0%
Band 5	4.8%	6.5%	6.6%	6.3%	6.5%
Band 6	0.0%	0.0%	0.0%	0.0%	0.0%

Band	MG–37	MG–38	MG–39	MG–40	MG–41
Aromatic	8.3%	9.5%	10.3%	9.1%	10.5%
Aliphatic	91.7%	90.5%	89.7%	90.9%	89.5%
Band 1	24.3%	22.4%	24.1%	24.0%	22.9%
Band 2	49.8%	48.1%	48.4%	48.1%	45.8%
Band 3	17.6%	20.0%	17.2%	18.8%	20.7%
Band 4	0.0%	0.0%	0.0%	0.0%	0.0%
Band 5	8.0%	8.7%	9.7%	8.8%	10.2%
Band 6	0.3%	0.8%	0.6%	0.3%	0.3%

Table B10: IR Analyses of Feedstocks

Group	CGOD1	CGOD2	CGOD3	CGOD4
Average Areas (*10³)				
Sulfoxide	2.298	2.976	3.688	1.433
Amide	6.150	3.294	1.151	0.379
Ketone		2.398	3.995	4.673
Carbox.	25.270	0.859	7.674	5.531
Carbazole	5.993	2.883	1.851	5.749
Phenol	1.800	3.287	1.355	0.358
Concentrations (mol/100 g)				
Sulfoxide	0.0024	0.0034	0.0036	0.0014
Amide	0.0026	0.0015	0.0005	0.0002
Ketone		0.0023	0.0034	0.0040
Carbox.	0.0134	0.0005	0.0038	0.0028
Carbazole	0.0109	0.0056	0.0031	0.0098
Phenol	0.0046	0.0090	0.0032	0.0009

Group	CGOD5	CGOD6	CGOD7
Average Areas (*10³)			
Sulfoxide	3.717	8.474	12.030
Amide	1.061	2.578	1.002
Ketone	4.031	4.347	2.535
Carbox.	8.871	9.440	4.970
Carbazole	9.631	12.040	9.731
Phenol	0.720	1.390	1.927
Concentrations (mol/100 g)			
Sulfoxide	0.0044	0.0092	0.0144
Amide	0.0005	0.0011	0.0005
Ketone	0.0041	0.0040	0.0026
Carbox.	0.0052	0.0051	0.0030
Carbazole	0.0194	0.0224	0.0200
Phenol	0.0020	0.0036	0.0055

Table B11: IR Analyses of Products

Group	MG–32	MG–33	MG–34	MG–35	MG–36
Average Areas (*10³)					
Sulfoxide	1.050	1.007	0.936	0.803	1.049
Concentrations (mol/100 g)					
Sulfoxide	0.0012	0.0010	0.0012	0.0009	0.0011

Sample	MG–37	MG–38	MG–39	MG–40	MG–41
Average Areas (*10³)					
Sulfoxide	1.849	4.396	3.440	3.501	3.239
Carbox.	2.511				
Carbazole	2.884	18.515	18.571	16.815	20.863
Phenol	2.301	3.371	2.125	2.744	2.216
Concentrations (mol/100 g)					
Sulfoxide	0.0021	0.0041	0.0037	0.0035	0.0033
Carbox.	0.0014				
Carbazole	0.0056	0.0297	0.0341	0.0288	0.0360
Phenol	0.0063	0.0076	0.0055	0.0066	0.0054

Table B12: Nitrogen Titration Analyses (Concentrations in mol/100 g)

Sample	V_{np} (μL)	Concentration
CGOD1	60	0.00368
CGOD2	82	0.00456
CGOD3	100	0.00535
CGOD4	135	0.00744
CGOD5	115	0.00670
CGOD6	155	0.00933
CGOD7	210	0.01345

Table B13: Nitrogen Titration Analyses (Concentrations in mol/100 g)

Sample	V_{np} (μL)	Concentration
MG–32	0	0.00000
MG–33	12	0.00068
MG–34	10	0.00057
MG–35	5	0.00031
MG–36	14	0.00086
MG–37	35	0.00212
MG–38	130	0.00747
MG–39	130	0.00763
MG–40	105	0.00618
MG–41	150	0.00938

Table B14: Structural Groups

Aromatic Structures

Benzene	
Phenanthrene	
Biphenyl Bridge	•———•

Aliphatic Structures

α–carbon	•–CH_2–o + •–CH_3
β–methyl	x–CH_3
γ–methyl	o–CH_3
Chain methylene	o–CH_2–o
Chain methyne	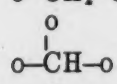
Naphthenic methyne	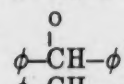
Naphthenic methyl	ϕ–CH_3
Naphthenic methylene	ϕ–CH_2–ϕ

Heteroatomic Structures

Benzothiophene	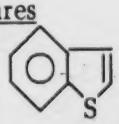	Indole	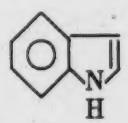
Sulfoxide	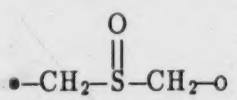	Amide	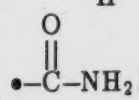
Benzofuran	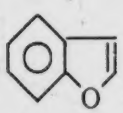	Quinoline	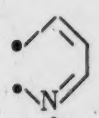
Ketone	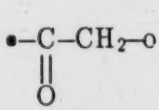	N–subst. Indole	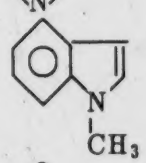
Arom. hydroxyl	•–OH	Carboxylic acid	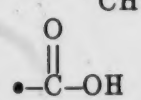

Legend

o–	bound to alkyl carbon
x–	bound to α–carbon
•–	bound to aromatic carbon
ϕ–	bound to α or naphthenic carbon

Table B15: Structural Group Analysis of Feedstocks (concentration in mol/100 g)

Group	CGOD1	CGOD2	CGOD3	CGOD4
Aromatic				
Benzene	0.202	0.150	0.141	0.054
Phenanth.	0.0	0.0	0.0	0.045
Biphenyl	0.0	0.012	0.136	0.0
Aliphatic				
α–Carbon	0.998	0.858	0.753	0.873
β–CH_3	0.205	0.168	0.154	0.115
γ–CH_3	0.372	0.450	0.458	0.313
o–CH_2–o	0.673	0.546	0.539	0.482
o–CH–o	0.113	0.110	0.175	0.090
ϕ–CH_3	0.420	0.578	0.355	0.442
ϕ–CH_2–ϕ	0.891	0.975	0.967	1.026
ϕ–CH–ϕ	1.209	1.229	1.452	0.990
Heteroatomic				
Bthiophene	0.103	0.102	0.107	0.133
Sulfoxide	0.002	0.003	0.004	0.001
Benzofuran	0.014	0.045	0.049	0.032
Hydroxyl	0.005	0.009	0.003	0.001
Ketone	0.0	0.002	0.003	0.004
Carboxylic	0.013	0.001	0.004	0.003
Amide	0.003	0.001	0.001	0.0
Indole	0.0	0.004	0.003	0.010
Quinoline	0.003	0.004	0.005	0.007
N–Sub Ind.	0.0	0.0	0.005	0.007

Table B15: Structural Group Analysis of Feedstocks (cont.)

Group	CGOD5	CGOD6	CGOD7
Aromatic			
Benzene	0.053	0.0	0.062
Phenanth.	0.034	0.066	0.057
Biphenyl	0.084	0.017	0.212
Aliphatic			
α–Carbon	0.835	0.819	1.017
β–CH_3	0.147	0.119	0.137
γ–CH_3	0.317	0.269	0.190
o–CH_2–o	0.422	0.564	0.610
o–CH–o	0.094	0.120	0.313
ϕ–CH_3	0.384	0.376	0.188
ϕ–CH_2–ϕ	1.058	0.896	0.468
ϕ–CH–ϕ	1.077	0.850	0.796
Heteroatomic			
Bthiophene	0.140	0.147	0.148
Sulfoxide	0.004	0.009	0.014
Benzofuran	0.060	0.063	0.077
Hydroxyl	0.002	0.004	0.006
Ketone	0.004	0.004	0.003
Carboxylic	0.005	0.005	0.003
Amide	0.001	0.001	0.001
Indole	0.019	0.022	0.020
Quinoline	0.007	0.009	0.014
N–Sub Ind.	0.008	0.013	0.011

Table B16: Structural Group Analysis of Products (concentration in mol/100 g)

Group	MG–32	MG–33	MG–34	MG–35	MG–36
Aromatic					
Benzene	0.189	0.210	0.206	0.236	0.209
Phenanth.	0.0	0.0	0.0	0.0	0.0
Biphenyl	0.0	0.001	0.012	0.0	0.082
Aliphatic					
α–Carbon	0.656	0.754	0.607	0.832	0.666
β–CH_3	0.102	0.143	0.113	0.126	0.134
γ–CH_3	0.720	0.696	0.646	0.572	0.606
o–CH_2–o	1.044	0.730	0.904	0.904	0.656
o–CH–o	0.298	0.150	0.267	0.269	0.195
φ–CH_3	0.499	0.369	0.600	0.490	0.419
φ–CH_2–φ	1.420	1.485	1.360	1.229	1.310
φ–CH–φ	1.137	1.210	1.174	1.205	1.534
Heteroatomic					
Bthiophene	0.004	0.014	0.006	0.004	0.015
Sulfoxide	0.0	0.001	0.001	0.001	0.001
Benzofuran	0.020	0.035	0.030	0.024	0.040
Quinoline	0.0	0.001	0.001	0.0	0.001
N–Sub Ind.	0.0	0.001	0.0	0.001	0.003

Group	MG–37	MG–38	MG–39	MG–40	MG–41
Aromatic					
Benzene	0.229	0.144	0.257	0.300	0.270
Phenanth.	0.016	0.040	0.026	0.016	0.015
Biphenyl	0.220	0.137	0.361	0.252	0.197
Aliphatic					
α–Carbon	0.681	0.910	0.718	0.872	0.922
β–CH_3	0.144	0.129	0.136	0.118	0.120
γ–CH_3	0.486	0.399	0.551	0.511	0.458
o–CH_2–o	0.617	0.650	1.029	0.746	0.731
o–CH–o	0.178	0.143	0.130	0.107	0.120
φ–CH_3	0.399	0.350	0.424	0.352	0.327
φ–CH_2–φ	1.157	1.050	0.891	1.277	0.943
φ–CH–φ	1.283	0.896	0.424	0.679	0.896
Heteroatomic					
Bthiophene	0.030	0.084	0.072	0.044	0.065
Sulfoxide	0.002	0.004	0.004	0.004	0.003
Benzofuran	0.041	0.041	0.028	0.004	0.016
Hydroxyl	0.006	0.008	0.006	0.007	0.005
Carboxylic	0.001				
Indole	0.006	0.021	0.019	0.017	0.022
Quinoline	0.002	0.007	0.008	0.006	0.009
N–Sub Ind.	0.006	0.001	0.000	0.001	0.000

Table B17: Molecular Parameters for Feedstocks

Parameter	CGOD1	CGOD2	CGOD3	CGOD4
Mean Side Chain	8.6	7.4	7.4	8.1
Average Ring # 1	1.36	1.49	1.53	1.95
Average Ring # 2	1.16	1.26	1.88	1.54
Mean Ring Number	1.26	1.38	1.70	1.75

Parameter	CGOD5	CGOD6	CGOD7
Mean Side Chain	7.7	9.2	11.4
Average Ring # 1	1.92	2.18	1.95
Average Ring # 2	1.88	1.78	2.64
Mean Ring Number	1.90	1.98	2.30

Table B18: Molecular Parameters for Products

Parameter	MG–32	MG–33	MG–34	MG–35	MG–36
M.S.C.L.	7.9	7.1	7.8	8.2	7.2
Avg.Ring#1	1.11	1.19	1.15	1.11	1.21
Avg.Ring#2	1.05	1.09	1.11	1.05	1.45
Mean Ring#	1.08	1.14	1.13	1.08	1.33

Parameter	MG–37	MG–38	MG–39	MG–40	MG–41
M.S.C.L.	7.5	8.3	9.0	7.9	8.2
Avg.Ring#1	1.35	1.67	1.45	1.25	1.34
Avg.Ring#2	2.37	2.04	3.07	2.27	1.93
Mean Ring#	1.86	1.86	2.26	1.76	1.64

Appendix C: Properties of Feedstocks and Products

Table C1: Original Class Separation of Feedstocks

Table C2: Normalized Class Separation of Feedstocks

Table C3: Specific Gravities of Feedstocks

Table C4: Specific Gravities of Products

Table C5: SDA Summaries of Feedstocks

Table C6: SDA Summaries of Products

Table C7: Molecular Weight Estimation

Table C8: Carbon–Carbon Bond Estimates for Feedstocks

Table C9: Carbon–Carbon Bond Estimates for Products

This section contains the tabulations for analyses of class separation, specific gravity, simulated distillation analysis (boiling distribution), class separation, estimates of molecular weights, and estimates of the average number of carbon–carbon bonds per molecule. The methods for obtaining these values are given in Chapter 3. The data for SCGO, the whole oil, will be included with the feedstock data for comparison.

The original and normalized data for class separation are shown in Tables C1 and C2. The original data show the loss of very light material or gain of solvents, leading to totals slightly smaller or larger than 100%. The specific gravities are shown in Tables C3 and C4 at 23°C and at the standard condition of 15°C (calculated from the raw data at 23°C using equation C.1).

$$\rho_{15} = \sqrt{\rho_{23} - 0.0011 \cdot (15-23)} \qquad \text{C.1}$$

The summaries of simulated distillation analysis (Tables C5 and C6) are calculated by summation from the full SDA data set, with linear interpolation near the endpoints. The values are tabulated as volume % of oil boiling within 50°C ranges. A sample full SDA data set is shown in Chapter 3, where the SDA procedure is described in greater depth.

The molecular weights (Table C7) shown are calculated in the three fashions discussed in Chapter 3. The first set of seventeen points was calculated from the Winn equation (equation C.2) with the normal published parameters, while the second set (11 points) was calculated by vapour pressure osmometry in the Microanalytical Laboratory in the Department of Chemistry.

$$\text{Winn Correlation: } MW = a \cdot T_b^{\alpha} \cdot \rho^{\beta} \qquad \text{C.2}$$

The third set was calculated using the recorrelated Winn equation. The parameters for both correlations are shown here. Both correlations use the average boiling point (K) and the specific gravity (15°C).

Old Parameters	New Parameters
$a = 5.805*10^{-5}$	$a = 2.41*10^{-6} \pm 9*10^{-8}$
$\alpha = 2.3776$	$\alpha = 2.847 \pm 0.30$
$\beta = -0.9371$	$\beta = -2.130 \pm 0.69$

The estimates for the average number of carbon–carbon bonds per molecule were calculated in the following manner.

1) Calculate the molar carbon to oil ratio (n_c) using data from elemental analysis and molecular weight estimation.

$$n_c = \frac{(AMW)\cdot(C)}{12}$$

2) Calculate the carbon valency (V), or total number of carbon bonding sites.

$$V = 4 \cdot n_c$$

3) Calculate the number of carbon sites available for carbon–carbon bonding (ABS) by removing the sites used by hydrogen, sulfur, nitrogen, and oxygen.

$$ABS = V - n_h - 2\cdot n_s - 2\cdot n_o - 2\cdot n_n$$

There is some error due to the heteroatoms, as there may be one, two, or three heteroatom–carbon bonds, but the error is small due to the low content of heteroatoms in the oil. A factor of two is used for simplicity and as an average value.

4) Calculate the actual number of carbon–carbon bonds (moles bonds per mole oil), accounting for the fraction of carbon that is aromatic (aromatic bonds use 1.5 bonding sites while aliphatic bonds use 1 bonding site). It is assumed that the amount of carbon–carbon double bonds is negligible.

$$NB = ABS \cdot (\tfrac{1}{2} - \tfrac{1}{6} \cdot f_{ar})$$

Here NB is the actual average number of carbon–carbon bonds per molecule, or the moles of carbon–carbon bonds per mole of oil, and f_{ar} is the fraction of carbon that is aromatic (determined from ^{13}C NMR).

The values for carbon to oil ratio (n_c), hydrogen to oil ratio (n_h), sulfur to oil ratio (n_s), oxygen to oil ratio (n_o), nitrogen to oil ratio (n_n), and average number of carbon–carbon bonds per molecule (NB) are shown in Tables C8 and C9. Table C9 also gives the percent reduction in the average number of carbon–carbon bonds per molecule for each product, setting values of less than 1.5 % reduction to 0 (to eliminate negative reductions due to fluctuating error).

As an illustration of the method, consider benzothiophene with a butyl chain attached adjacent to the sulfur atom (2–butyl benzothiophene).

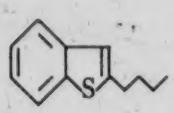

This molecule has a molecular formula of $C_{12}H_{14}S$, and therefore has a n_c value of 12, an n_h value of 14, and an n_s value of 1. Using the methodology outlined, the valency is V = 48, and the number of available carbon–carbon bonding sites is 48 − 14 − 2 = 32. Given an aromatic carbon fraction of $f_{ar} = \frac{2}{3}$ (8 aromatic and 4 aliphatic carbon atoms), the total number of carbon–carbon bonds is $32 \cdot (\frac{1}{2} - \frac{1}{6} \cdot \frac{2}{3})$, or 12.44. As we are dealing with a single molecule, partial bonds are not allowed, and the actual number of carbon–carbon bonds must be rounded to 12, which is the actual number of bonds. In dealing with an oil sample, the number of carbon-carbon bonds would not be rounded to a whole number, as a wide variety of molecules are present and it is only the average structure information that is of interest.

Table C1: Class Separation of the Feedstocks — Original

Fraction	SCGO	CGOD1	CGOD2	CGOD3
Saturates	24.18%	47.27%	44.45%	41.43%
Aromatics	21.37	23.78	29.22	17.90
Resins	49.82	20.05	23.28	39.57
Asphaltenes	0.14	0.0	0.0	0.0
Total	95.51%	91.10%	96.95%	98.90%

Fraction	CGOD4	CGOD5	CGOD6	CGOD7
Saturates	29.78%	26.33%	14.60%	3.71%
Aromatics	16.02	11.39	10.40	3.98
Resins	54.33	65.29	78.20	70.05
Asphaltenes	0.0	0.0	0.0	25.69
Total	100.13%	103.01%	103.20%	103.43%

Table C2: Class Separation of the Feedstocks — Normalized

Fraction	SCGO	CGOD1	CGOD2	CGOD3
Saturates	25.32%	51.89%	45.85%	41.89%
Aromatics	22.37	26.10	30.14	18.10
Resins	52.16	22.01	24.01	40.01
Asphaltenes	0.15	0.0	0.0	0.0

Fraction	CGOD4	CGOD5	CGOD6	CGOD7
Saturates	29.74%	25.56%	14.15%	3.59%
Aromatics	16.00	11.06	10.08	3.85
Resins	54.26	63.38	75.78	67.73
Asphaltenes	0.0	0.0	0.0	24.84

Table C3: Feedstock Specific Gravity

Sample	S.G. (23°C)	S.G. (15°C)
SCGO	0.95729	0.98290
CGOD1	0.90740	0.91224
CGOD2	0.92622	0.93096
CGOD3	0.95208	0.95669
CGOD4	0.98961	0.99405
CGOD5	1.01292	1.01725
CGOD6	1.03570	1.03994
CGOD7	1.18375	1.19255

Table C4: Product Specific Gravity

Sample	S.G. (23°C)	S.G. (15°C)
MG–32	0.84980	0.85407
MG–33	0.88107	0.88605
MG–34	0.87170	0.87673
MG–35	0.86258	0.86767
MG–36	0.89759	0.90248
MG–37	0.93648	0.94117
MG–38	0.98109	0.98556
MG–39	0.97273	0.97724
MG–40	0.94355	0.94820
MG–41	0.96865	0.97318

Table C5: Summary of Simulated Distillation Analysis — Feedstocks (Volume % of Oil Boiling Within Temperature Range)

Temp (°C)	SCGO	CGOD1	CGOD2	CGOD3
Nominal Range		250–300	300–350	350–400
0 – 250	3.1%	17.6%	1.6%	0.6%
250–300	10.7	74.8	34.9	3.0
300–350	19.0	5.7	60.4	42.2
350–400	23.6	0.7	1.3	47.9
400–450	21.4	0.5	0.7	4.4
450–500	15.0	0.3	0.6	0.9
500–550	6.2	0.2	0.4	0.7
> 550	1.0	0.0	0.1	0.2
T_b (°C)	392.4	278.0	314.2	360.0

Temp (°C)	CGOD4	CGOD5	CGOD6
Nominal	400–450	450–500	500–550
0 – 250	0.3%	0.0%	0.0%
250–300	0.0	0.0	0.0
300–350	3.1	0.0	0.0
350–400	33.0	0.7	0.0
400–450	45.6	23.2	0.0
450–500	15.2	53.9	14.3
500–550	2.5	19.2	58.6
> 550	0.3	3.0	27.1
T_b (°C)	421.0	481.4	539.1

Table C6: Summary of Simulated Distillation Analysis — Products (Volume % of Oil Boiling Within Temperature Range)

Temp (°C)	MG–32	MG–33	MG–34	MG–35	MG–36
0 – 250	45.8%	17.3%	22.4%	31.3%	9.8%
250 – 300	48.8	40.0	38.1	36.1	16.9
300 – 350	3.7	39.8	37.6	30.5	40.1
350 – 400	0.6	1.4	1.1	1.2	28.4
400 – 450	0.5	0.7	0.4	0.4	3.5
450 – 500	0.3	0.6	0.4	0.3	0.7
500 – 550	0.1	0.2	.1	0.1	0.4
> 550	0.0	0.0	0.0	0.0	0.1
T_b (°C)	254.9	294.0	285.9	274.5	329.9

Temp (°C)	MG–37	MG–38	MG–39	MG–40	MG–41
0 – 250	6.4%	2.4%	8.9%	16.7%	13.1%
250 – 300	6.2	1.4	3.7	6.5	5.5
300 – 350	15.0	2.8	5.1	8.1	6.4
350 – 400	31.7	7.6	9.6	12.6	8.7
400 – 450	30.6	27.1	25.8	23.9	11.8
450 – 500	8.5	43.2	35.3	24.7	20.9
500 – 550	1.3	13.8	10.4	6.6	27.3
> 550	0.2	1.7	1.2	0.9	6.3
T_b (°C)	381.5	454.3	423.2	385.4	426.4

Table C7: Molecular Weight Estimates

Sample	AMW, Winn	AMW, V.P.O.	AMW, Recorrelated
SCGO	303		270
CGOD1	208	183	187
CGOD2	238	207	214
CGOD3	277	256	250
CGOD4	333	308	300
CGOD5	397	363	362
CGOD6	463	407	425
CGOD7		653	

Sample	AMW, Winn	AMW, V.P.O.	AMW, Recorrelated
MG–32	200	194	190
MG–33	229		215
MG–34	224		211
MG–35	215		204
MG–36	261	240	247
MG–37	305	282	285
MG–38	375		349
MG–39	341	332	313
MG–40	307		285
MG–41	346		320

Table C8: Carbon–Carbon Bond Estimates for Feedstocks

Parameter	CGOD1	CGOD2	CGOD3	CGOD4	CGOD5	CGOD6	CGOD7
n_c	13.20	15.07	17.61	20.95	25.30	29.53	45.80
n_h	20.37	23.25	26.17	29.70	34.77	39.89	53.19
n_s	0.20	0.22	0.28	0.40	0.52	0.66	1.06
n_n	0.01	0.02	0.03	0.07	0.13	0.19	0.30
n_o	0.09	0.13	0.17	0.22	0.29	0.39	0.70
NB	14.0	16.1	19.3	22.9	27.8	32.3	52.9

Table C9: Carbon–Carbon Bond Estimates for Products

Parameter	MG–32	MG–33	MG–34	MG–35	MG–36
n_c	13.68	15.48	15.28	14.84	17.88
n_h	24.64	26.54	26.67	24.35	29.09
n_s	0.01	0.03	0.02	0.01	0.04
n_n	0.00	0.00	0.00	0.00	0.01
n_o	0.04	0.08	0.07	0.05	0.10
NB	14.1	16.1	15.9	16.2	19.3
% Breakage	0.0	0.0	0.0	0.0	0.0

Parameter	MG–37	MG–38	MG–39	MG–40	MG–41
n_c	20.81	25.01	22.40	20.81	23.32
n_h	31.39	35.11	32.39	30.99	33.27
n_s	0.09	0.31	0.24	0.14	0.22
n_n	0.04	0.10	0.08	0.07	0.10
n_o	0.15	0.19	0.12	0.04	0.08
NB	23.0	27.9	24.6	22.8	25.6
% Breakage	0.0	0.0	11.5	18.0	20.7

Appendix D: Kinetic Analysis

Table D1: Summary of Pseudo–First–Order Rate Constants

Table D2: Summary of Apparent Arrhenius Parameters

Table D3: Estimates of Properties at Reactor Conditions

Table D4: Intrinsic Rate Constants for HDS

Table D5: Intrinsic Rate Constants for HDN

Table D6: Intrinsic Arrhenius Parameters

Table D7: Rate Constants for Aromatic Carbon Conversion

Table D8: Aromatic Carbon/Heteroatom Selectivity

The calculations and tabulations for the kinetic analyses performed are contained in this appendix. The observed rate constants and apparent Arrhenius parameters will be covered, followed by calculations of density and viscosity at reactor conditions. Given these values, the diffusivity values will be calculated, and used to calculate intrinsic rate constants, Thiele parameter values, and effectiveness factors. The intrinsic rate constants will be used to calculate intrinsic Arrhenius parameters.

Table D1 tabulates the observed pseudo–first–order rate constants for HDS, HDN, pitch conversion, and gas formation for each run. These are summarized from the data sheets in Appendix A, and are given in units of mL/(s·kg catalyst). The regressions for the apparent Arrhenius parameters for feedstocks CGOD2 and CGOD5 are shown in Table D2. The estimates for density, viscosity, and diffusivity at reactor conditions for the feedstocks are shown in Table D3, with the diffusivity calculated by the Wilke–Chang and Scheibel equations (Perry *et al.*, 1984). The final diffusivity value is the average molecular diffusivity. The densities and viscosities were calculated as described in Chapter 3. Using the tortuosity equation (Satterfield, 1980) for estimating effective diffusivity, the ratio of effective diffusivity to molecular diffusivity was set at 0.1 for all runs, to allow calculation of the intrinsic rate constants, effectiveness factors, and Thiele parameters as follows (Fogler, 1986):

$$\phi^2 = R^2 \cdot \left[\frac{\hat{k}_i \cdot \rho_c \cdot S_a}{\mathscr{D}_{eff}} \right] \qquad \text{D.1}$$

$$\eta = \frac{3}{\phi^2} \cdot (\phi \cdot \coth\phi - 1) \qquad \text{D.2}$$

$$\hat{k}_{obs} = \hat{k}_i \cdot \eta \qquad \text{D.3}$$

where ϕ is the Thiele parameter, η is the effectiveness factor, ρ and S_a refer to the density (kg/m^3) and specific surface area (m^2/kg) of the catalyst, $\hat{k}_{obs}$ and $\hat{k}_i$ are the observed and intrinsic rate constants (units of m/s, $\hat{k} = 10^{-6} \cdot k/S_a$, k in units of $mL/s \cdot kg$ catalyst), and $\mathscr{D}_{eff}$ is the effective diffusivity (m^2/s). These equations can be condensed into one non–linear equation as a function of I:

$$k_{obs} = -\frac{3 \cdot \mathscr{D}_{eff}}{R^2 \cdot \rho \cdot S_a} \cdot \left[R \cdot I \cdot \coth(R \cdot I) - 1 \right] \qquad D.4$$

$$I = \left[\frac{\hat{k}_i \cdot \rho \cdot S_a}{\mathscr{D}_{eff}} \right]^{\frac{1}{2}} \qquad D.5$$

This equation was solved iteratively to find the value of $\hat{k}_i$ corresponding to the effective diffusivity used. The Thiele parameter and effectiveness factors were then calculated from the value of $\hat{k}_i$.

Given values of $\hat{k}_i$ (or k_i) for each run, the intrinsic Arrhenius parameters for the catalytic runs may be calculated. The intrinsic rate constants for HDS and HDN are listed in Tables D4 and D5, along with the effectiveness factors and Thiele parameters. The intrinsic Arrhenius parameters for HDS and HDN are listed in Table D6.

The values of the pseudo–first–order rate constants for aromatic carbon conversion are given in Table D7. Values for the selectivity of aromatic carbon hydrogenation over heteroatom removal are given in Table D8. These values relate the moles of aromatic carbon removed to the moles of heteroatoms removed, and indicate the degree at which aromatic carbon hydrogenation is proceeding without heteroatom removal. Due to the natures of the molecules, the ratio should be higher, up to approximately 4, for light fractions with no aromatic carbon hydrogenation. Heavy fractions would give ratios between 0 and 2 at optimal

selectivity. Ratios substantially higher than these indicate hydrogenation of non-beteroatomic aromatic compounds. In both Tables D7 and D8, the product flowrate for run MG–41 has been adjusted by –10% (1.889 to 1.709) as the material balance was observed to be 110% (M_{out}/M_{in}) and the aromatic carbon conversion was negative due to the larger product flowrate.

Table D2: Summary of Apparent Arrhenius Parameters

Reaction	ln(A)	Std. Err.	$E_{a,app}$	Std. Err.	r^2
CGOD2					
HDS	23.236	0.160	108.9	21.3	0.963
HDN	16.903	0.175	77.9	23.3	0.918
Gas Form.	22.532	0.160	144.9	21.3	0.979
CGOD5					
HDS	27.958	0.028	149.2	5.0	0.999
HDN	19.610	0.077	108.8	14.0	0.984
Gas Form.	24.581	0.005	153.4	1.0	1.000
Pitch	41.903	0.392	238.7	71.0	0.919

Table D3: Estimates of Oil Properties at Reactor Conditions

Run	Density (kg/m^3)	Viscosity (10^4 Pa·s)	$\mathscr{D}^{\circ}_{ac}$	$\mathscr{D}^{\circ}$ (10^9 m^2/s)	$\mathscr{D}^{\circ}_{avg}$
MG–32	768.62	4.385	5.73	6.22	5.98
MG–33	783.67	5.961	4.09	4.27	4.18
MG–34	781.71	5.721	4.38	4.58	4.48
MG–35	782.29	5.592	4.62	4.83	4.72
MG–36	802.58	8.824	2.84	2.85	2.84
MG–37	832.30	17.686	1.42	1.35	1.39
MG–38	849.55	29.891	0.830	0.751	0.791
MG–39	846.00	28.047	0.897	0.813	0.855
MG–40	840.16	25.272	1.02	0.925	0.972
MG–41					0.432†

† extrapolated based on regression of $\ln(\mathscr{D}^{\circ}_{400})$ vs. T

Table D4: Intrinsic Rate Constants for HDS at Reaction Temperature

Run	k_{obs}	k_i	η	ϕ
MG–32	93.65	268.6	0.348	7.47
MG–33	22.51	34.6	0.646	3.21
MG–34	49.59	112.2	0.442	5.58
MG–35	71.37	199.5	0.357	7.25
MG–36	22.36	41.6	0.540	4.25
MG–37	11.90	23.0	0.516	4.54
MG–38	3.02	4.15	0.730	2.55
MG–39	4.50	6.91	0.652	3.16
MG–40	9.53	20.2	0.476	5.05
MG–41	4.66	10.4	0.449	5.46

Table D5: Intrinsic Rate Constants for HDN at Reaction Temperature

Run	k_{obs}	k_i	η	ϕ
MG–32			0	∞
MG–33	13.90	18.3	0.760	2.33
MG–34	17.21	23.4	0.729	2.56
MG–35	31.94	54.9	0.583	3.79
MG–36	11.94	16.9	0.708	2.71
MG–37	2.51	2.92	0.861	1.61
MG–38	0.98	1.09	0.902	1.30
MG–39	1.49	1.72	0.865	1.58
MG–40	2.31	2.82	0.821	1.89
MG–41	1.43	1.89	0.760	2.32

$\mathscr{D}_{eff}$ based on method of tortuosity/porosity, $\mathscr{D}_{eff}/\mathscr{D}^{\circ} = 0.1$

Table D6: Intrinsic Arrhenius Parameters for HDS and HDN

Reaction	ln(A)	Std. Err.	E_a	Std. Err.	r^2
CGOD2					
HDS	34.017	0.221	164.9	29.4	0.969
HDN	21.697	0.253	102.6	33.6	0.903
CGOD5					
HDS	38.360	0.066	205.3	12.0	0.997
HDN	21.885	0.082	120.9	14.9	0.985

Table D7: Pseudo–First–Order Rate Constants for Aromatic Carbon Conversion

Run	k_1 (mL/s·kg catalyst)
MG–32	3.535
MG–33	1.611
MG–34	2.343
MG–35	2.372
MG–36	1.040
MG–37	0.816
MG–38	0.357
MG–39	0.323
MG–40	0.518
MG–41	0.353†

† product flowrate adjusted by –10% to achieve 100% material balance (observed material balance 110%, negative aromatic carbon conversion)

Table D8: Aromatic Carbon/Heteroatom Selectivity

Run	C_{ar} Removed (g/min)	SON Removed (g/min)	Selectivity (C_{ar}/SON)
MG–32	0.0195	0.0020	9.56
MG–33	0.0118	0.0019	6.21
MG–34	0.0151	0.0021	7.25
MG–35	0.0151	0.0021	7.04
MG–36	0.0084	0.0020	4.13
MG–37	0.0087	0.0022	3.95
MG–38	0.0047	0.0018	2.62
MG–39	0.0043	0.0024	1.76
MG–40	0.0065	0.0033	2.01
MG–41	0.0049	0.0025	1.95†

† product flowrate adjusted by –10% to achieve 100% material balance (observed material balance 110%, negative aromatic carbon conversion)

Appendix E: Factor Analysis

Table E1: Rates of Reaction

Table E2: Correlation Matrix

Table E3: Rotated Factor Loadings

In the past, some of the more advanced techniques for analyzing data have not been used due to a lack of data: most statistical techniques are more reliable given a large amount of data. This appendix will describe the application of factor analysis to a small set of hydroprocessing data.

Factor analysis is a method whereby variables may be grouped based upon the changes seen between different cases. For example, if Variable A changes from 1 to 2 to 4 in three subsequent cases (or sets of data), while Variable B changes from 4 to 8 to 16 and Variable C changes from 7 to 2.5 to 14, it may be inferred from the changes in the variables that Variables A and B are related, while Variable C is not related to Variables A and B. Factor analysis groups these data based upon the correlation or covariance matrix, providing a set of output data indicating the degree of relationship between different variables. A number of different factors may be introduced, so that one may say that Variables A and B are related to Factor 1 while Variable C is related to Factor 2. The maximum number of factors is the number of variables in the data set. The meaning of the factors may be extracted by examining which groups are related to the factor and which are not. In general, a large amount of data is desired for any factor analysis; this ensures that the factors will have some statistical, and presumably meaningful, interpretation. A small amount of data (especially imprecise data) can lead to variables that are only related by random error, and thus can lead to meaningless factors. For a more extensive treatise on factor analysis, see an advanced statistics text, such as "Statistical Methods for Engineers" by R.H. McKuen (Prentice–Hall, 1985).

A set of data from catalytic hydroprocessing runs with Syncrude Coker Gas Oil using a Ni/Mo catalyst were examined and the structural group analysis and reactor data lumped into eight variables. The eight variables used in the statistical analysis were the rates of reaction for paraffinic methyl, β–methyl, naphthenic

carbon, aromatic carbon bound to heteroatoms, aromatic carbon bound to aromatic carbon (bridgehead), sulfur, methane formation, and pitch conversion. Variables that were excluded from the analysis due to negligible overall changes included α–carbon and normal aromatic carbon (aromatic carbon bound to two additional aromatic carbon atoms and one hydrogen atom). Five cases, or sets of data, were used, with runs at 400°C at three different flowrates, and one run each at 380°C and 420°C. The 380°C and 420°C runs and one of the 400°C runs were made at the same liquid flowrate. The reaction rates (mol/min·g cat) of the variables were used as data for a commercial statistics package with factor analysis capabilities (BMDP–79).

The reaction rates of the eight variables are shown in Table E1. All of the reaction rates except paraffinic methyl (γ–CH_3) and naphthenic carbon are positive for the five cases. The corresponding correlation matrix is shown in diagonal form in Table E2. In the correlation matrix, it may be noted that the cross–correlations between β–CH_3, pitch conversion, naphthenic carbon, and the two heteroatomic variables are all high (absolute value > 0.8) while the other entries in the correlation matrix are moderate to low. This indicates that these five groups are related. The rotated factor loadings are shown in Table E3, along with the percent of the total variance explained by each factor. The rotated factor loadings show the predictor–criterion correlation (or correlation between the variable and the factor). In this table, the factor loadings have been simplified by setting any factor loading with an absolute value less than 0.25 to 0, setting any factor loading with an absolute value greater than 0.8 to 1 (or –1). As well, factor loadings between 0.4 and 0.6 have been set to 0.5. Other values have been rounded to the nearest 0.1. This procedure allows investigation of the inter–relationships while eliminating conclusions based on insignificant changes in the factor loadings. Only three factors have been selected here (up to 8 could have been chosen) as the first three factors

explain 58%, 21%, and 15% of the total variance, respectively, for a total of 94%, while the fourth factor only explains another 5% of the total variance.

Examining the first factor, we see that it is highly correlated with β–CH_3, pitch conversion, naphthenic carbon, and the heteroatomic variables. The second factor seems correlated with methane production, and to a lesser degree, pitch conversion and the disappearance of bridgehead carbon. The third factor is also related to the removal of bridgehead carbon, but more strongly to the disappearance of γ–CH_3.

If one examines the first factor, the most apparent item is that β–CH_3 disappearance, pitch conversion, naphthenic carbon appearance, and heteroatom disappearance all have a factor loading of 1. If we examine the kinds of reactions that are known to take place, catalytic hydrogenation and heteroatom removal would cause a decrease in the sulfur content and in the amount of aromatic carbon bound to heteroatoms. For the disappearance of naphthenic carbon, the factor loading is –1; therefore, the factor is related to the appearance of naphthenic carbon. The gain in naphthenic carbon could be explained by the hydrogenation of condensed aromatic structures. At the low temperatures used, the pitch conversion is undoubtedly due, at least in part, to catalytic reactions such as HDS and HDN. The loss of β–CH_3 could, theoretically, be due to HDS of structures such as benzothiophene which are substituted by two-carbon chains adjacent to the sulfur molecule. It appears that Factor 1 may be related to the catalytic hydroprocessing reactions occurring.

Factor 2, having a high loading on methane production and lower loadings on bridgehead carbon and pitch conversion, may be related to thermal processes. Gas production is known to be a primarily thermal reaction at all temperatures, as the light paraffins can only be produced by thermal rupture of the carbon–carbon bonds. Pitch conversion also has a thermal component, although this component

may be small at low temperatures. Bridgehead carbon conversion is due to two mechanisms: the hydrogenation of condensed aromatic species and the thermal rupture of ring bonds in condensed aromatic species. It is unlikely that the thermal ring rupture is significant at this temperature, so it appears that Factor 2 is not well–represented by thermal reactions solely. A factor should be represented by a reaction or set of reactions, although the likelihood of factors other than Factor 1 being well–represented by a single class of reactions is remote. Two reactions may combine to be interpreted as a single factor if they affect primarily the same groups.

Factor 3 in this study is related primarily to γ–CH_3. This is because the rate of appearance of γ–CH_3 increases substantially from 380°C to 400°C, but then decreases as the temperature is increased further to 420°C. This trend is mirrored slightly in bridgehead carbon, which is the other variable correlated with Factor 3.

With such a limited data set, attention must be paid to data that appear invalid. One bad datum in such a small set of data can lead to significant changes in the resultant factor analysis. For example, if we consider that the reaction rate for γ–CH_3 for Case 2 may be incorrect, and perhaps should be on the order of –0.25, we would see a shift in the factor analysis for γ–CH_3 from Factor 3 to Factor 1. This would indicate that the change in γ–CH_3 is related to the catalytic reactions, and is not isolated. If we also considered the reaction rate for bridgehead carbon for Case 4 to be an outlier, then Factor 3 would become insignificant and the bridgehead carbon would become heavily loaded on Factor 1, indicating a catalytic reaction. This result would give us two significant factors, of which the dominant factor would represent catalytic reactions and the second factor would represent thermal reactions.

Factor analysis provides a method of grouping variables according to rate of change. It provides a statistical basis for what has long been done by intuition — the analysis of sets of data for trends among the variables. Although of greatest use

and significance when large sets of data are available, even small sets can be used to investigate major trends, particularly for experiments with large numbers of measurements. The factors calculated for hydroprocessing data may be related to a single reaction or to more than one reaction. In general, factors that explain a large degree of variance likely represent a single reaction or class of reactions, while the interpretation of less significant factors may be complicated by the relationship to more than one class of reactions. In this study, the first factor was seen to represent general catalytic reactions reasonably well, while thermal reactions undoubtedly had an effect on the second factor. The second factor may also have a relationship with some other reactions, however, and also may be partly due to error in the data. When using a small set of data such as this one, special care must be taken in interpreting the factor loadings, as large errors in factor interpretation or in the significance of the interpretation may result from slight inaccuracies in the data.

Table E1: Reaction Rates

Variable	Case 1	Case 2	Case 3	Case 4	Case 5
T (C)	380	400	400	400	420
Q (mL/min)	1.66	1.67	2.40	3.13	1.66
γ–CH_3	–0.241	–0.392	–0.309	–0.349	–0.252
β–CH_3	0.187	0.171	0.257	0.324	0.145
Naphth. C	–1.108	–1.299	–1.688	–2.374	–1.285
C_{ar}–(ONS)	0.544	0.570	0.736	0.863	0.640
C_{ar}–$(C_{ar})_3$	0.420	0.537	0.558	0.430	0.525
Sulfur	0.208	0.223	0.289	0.336	0.250
C_1 (*100)	0.075	0.181	0.220	0.252	0.437
Pitch (g/min)	0.256	0.321	0.347	0.459	0.391

Table E2: Correlation Matrix

	C_1	γ–CH_3	β–CH_3	Pitch	Naph. C	C_{ar}–ONS	C_{ar}–C_{ar}	S
C_1	1							
γ–CH_3	+0.131	1						
β–CH_3	–0.157	–0.354	1					
Pitch	+0.668	–0.309	+0.575	1				
Naph. C	–0.159	+0.442	–0.931	–0.826	1			
C_{ar}–ONS	+0.315	–0.290	+0.888	+0.863	–0.970	1		
C_{ar}–C_{ar}	+0.405	–0.260	–0.336	–0.010	+0.232	–0.120	1	
Sulfur	+0.334	–0.307	+0.877	+0.869	–0.965	+0.999	–0.080	1

Legend:

C_1	rate of appearance of methane product (mol/min.g cat * 100)
γ–CH_3	rate of disappearance of paraffinic methyl (mol/min.g cat)
β–CH_3	rate of disappearance of β–methyl
Pitch	rate of disappearance of pitch fraction (g/min)
Naph. C	rate of disappearance of naphthenic carbon
C_{ar}–ONS	rate of disappearance of aromatic carbon bound to heteroatoms
C_{ar}–C_{ar}	rate of disappearance of aromatic bridgehead carbon
Sulfur	rate of disappearance of sulfur

Table E3: Rotated Factor Loadings

Variable	Factor 1	Factor 2	Factor 3
C_1	0	1	0
γ–CH_3	–0.3	0	1
β–CH_3	1	–0.3	0
Pitch	1	0.5	0
Naph. C.	–1	0	0
Car–ONS	1	0	0
Car–Car	–0.3	0.6	–0.6
Sulfur	1	0	0
% Variance Explained	58	21	15

END

26/10/90

FIN